

**SKELETAL GROWTH RING MICROANALYSIS AND GROWTH RATES IN
SEA PENS FROM THE LAURENTIAN CHANNEL MPA, NEWFOUNDLAND**

By Krista Greeley

Thesis submitted to the School of Graduate Studies in partial fulfillment of the

requirements for the degree of

MSc in Environmental Science

Faculty of Sciences

Memorial University of Newfoundland

January 2022

St. John's Newfoundland and Labrador

Abstract

Valuable information can be obtained through sea pen skeletons due to their high longevities and their annually deposited growth rings. Using Scanning Electron Microscopy with Energy Dispersive X-Ray Analysis (SEM-EDX), elemental microanalyses were performed on sea pen skeletons to understand the physical basis of their growth rings. Here, the elemental composition and structure of growth bands in *Anthoptilum grandiflorum*, *Anthoptilum murrayi*, *Pennatula aculeata*, *Funiculina quadrangularis*, *Protoptilum carpenteri*, and *Kophobelemnion stelliferum* are shown. Samples were collected using the remotely operated vehicle (ROV) ROPOS in 2017 from the Laurentian Channel marine protected area (MPA) at depths of 400-600 m. Cross-sections of the axes were examined using SEM-EDX, presenting minor element variations within each growth ring (light: 2.64 cps Mg, 47.5 cps Ca; dark: Mg 2.25 cps, Ca 51.2 cps). The data suggests primary differences include large, abundant voids in dark growth rings, and fewer smaller voids in the light growth rings.

Acknowledgments

This thesis would not have been possible without the help and support of my co-supervisors Evan Edinger and Graham Layne who expressed unwavering patience for me as I translated my knowledge as a geologist into marine biology and geochemistry. I am extremely grateful to have had the opportunity to explore my passion for corals, paving the way towards a future career where I can work closely to protect them. I appreciate all the time and help made available to me by my committee member Bárbara de Moura Neves who never failed to bring excitement and passion into my project. I would also like to thank those from the CREAT Network team (Memorial University of Newfoundland) who helped me complete the analytical portion of my project. David Grant and Dylan Goudie were always incredibly helpful with the SEM, providing substantial insight into different applicable analysis techniques. Glenn Piercey helped me with SIMS work for possible trace element analyses, and Wanda Aylward helped with the XRD analyses.

I am extremely grateful for Heather Penny and Andrés Beita who saved me from spending an absurd amount of time coding by helping me with R-Studio. I thank Pam Murphy and Dominique Lavers in Geography for all the help involving my funding and exhausting amounts of paperwork. To one of my closest friends on the island, Marion Boulard, for the support and incredible amount of help both as a friend and as a colleague. I would not have enjoyed my time in Newfoundland as much as I did without her.

This research was funded and made possible during my M.Sc. at Memorial University of Newfoundland by the Canadian Healthy Oceans Network (CHONe). The NSERC CHONe II Strategic Research Program is developing new conservation strategies

for Canada's changing oceans by partnering Canadian university researchers and government scientists. Major funding is provided by the Natural Sciences and Engineering Research Council of Canada (NSERC) in partnership with Fisheries and Oceans Canada and other government agencies; INREST (representing the Port of Sept-Îles and City of Sept-Îles); and ENGOs. and by the Natural Sciences and Engineering Research Council of Canada (NSERC).

Table of Contents

Abstract	ii
Acknowledgments.....	iii
Table of Contents	v
List of figures	viii
List of tables.....	xvi
Abbreviations	xviii
Co-authorship Statement.....	xix
Thesis impact statement	xx
Appendices	xxi
1. Introduction	1-1
1.1 Sea pens (order Pennatulacea)	1-3
1.1.1 Sea pen skeletal growth.....	1-4
1.1.2 Growth rates and age determination in sea pens	1-5
1.1.3 Conservation of sea pens	1-6
1.2 Thesis objectives and chapter structure.....	1-8
1.3 References	1-10
2. Scanning electron microscope observations on the structure and composition in six sea pen species	2-1
Abstract	2-1
2.1 Introduction.....	2-1
2.2 Materials and Methods.....	2-3
2.2.1 Study area and sampling	2-3

2.2.2	Sampling and identification	2-8
2.2.3	Growth ring microanalysis via SEM-EDX	2-13
2.2.4	Skeletal composition via XRD	2-14
2.3	Results	2-15
2.3.1	Growth ring characteristics.....	2-15
2.3.2	Characteristics in the center of the axis	2-27
2.3.3	Growth ring microanalysis via SEM-EDX	2-33
2.4	Discussion	2-39
2.4.1	Growth band characteristics	2-39
2.4.2	Growth band elemental analysis.....	2-41
2.5	Conclusions.....	2-42
2.6	References.....	2-44
3.	Colony metrics, ages and growth rates of six sea pen species collected from the Laurentian Channel Marine Protected Area, Atlantic Canada.....	3-1
	Abstract	3-1
3.1	Introduction.....	3-1
3.2	Material and methods.....	3-4
3.2.1	Collection and measurements.....	3-4
3.2.2	Ring counting methods.....	3-8
3.2.3	Growth curve analysis.....	3-10
3.3.	Results.....	3-10
3.3.1	Colony metrics.....	3-10
3.3.2	Colony and axis metrics in relation to colony length.....	3-11
3.3.3	Estimated longevity and growth rates.....	3-16

3.3.4 Age estimation from colony size.....	3-23
3.4. Discussion.....	3-31
3.4.1 Colony metrics.....	3-31
3.4.2 Longevity and growth rates.....	3-32
3.4.3 Age estimation from colony size.....	3-34
3.5 Conclusions	3-35
3.6 References.....	3-36
4. General conclusions	4-1
4.1 Growth band characteristics.....	4-1
4.2 Growth band elemental analysis	4-1
4.3 Colony metrics, age, growth rates and longevity.....	4-2
4.4 Future work	4-4
4.5 References.....	4-5

List of figures

- Figure 2-1. Image of an *Anthoptilum* sp. colony showing the peduncle (indicated by yellow brackets) and the rachis (remaining portion of the colony) (A) and its axis (B)2-3
- Figure 2-2. In-situ ROV image of a sea pen field taken in the Laurentian Channel MPA during the ROPOS 2017 cruise.....2-5
- Figure 2-3. Bathymetric map of the MPA within the Laurentian Channel and its zones (1a, 1b, 2a, 2b). Map generated and extracted from ArcGIS 1.0.....2-6
- Figure 2-4. Bathymetric map of the MPA within the Laurentian Channel, the station numbers and the locations of the species collected for this study (indicated by colored circles). *Anthoptilum* spp. is indicated by the blue circles, *P. aculeata* is indicated by the red circles, *F. quadrangularis* is indicated by the green circles, *P. carpenteri* is indicated by the orange circles, and *K. stelliferum* is indicated by the yellow circles. *F. quadrangularis* samples collected outside of the MPA in 2007 are indicated by a purple circle, and in 2009 a black circle. On the right is the location of the MPA. Map generated and extracted from ArcGIS 1.0..... 2-7
- Figure 2-5. Images showing several sea pen species in situ A-E: A) *Anthoptilum* sp., B) *Pennatula aculeata*, C) *Funiculina quadrangularis*, D) *Protoptilum carpenteri*, E) *Kophobelemnon stelliferum*, their whole colonies (F-J), and their cross sections under SEM (K-O), respectively. Tape measurements are in cm.....2-12
- Figure 2-6. Thickest point in *Anthoptilum* sp. (indicated by a yellow arrow) and an Isomet saw (A), cut thin sections placed in metal rings for SEM-BSE imaging (B). Scale bar: 1.5 cm.....2-14

Figure 2-7. X-ray diffraction analysis for the carbonate portion of the skeleton in (A) *Anthoptilum grandiflorum*, (B) *Pennatula aculeata*, (C) *Funiculina quadrangularis*, (D) *Kophobelemnon stelliferum*, and (E) *Protoptilum carpenteri*.....2-17

Figure 2-8. A-G) SEM-BSE images of cross sections taken from the axis of several sea pen species with high magnification images of their growth rings: (A) *Anthoptilum grandiflorum*, (B) *Anthoptilum murrayi*, (C) *Pennatula aculeata*, (D) juvenile *Funiculina quadrangularis*, (E) adult *Funiculina quadrangularis*, (F) *Protoptilum carpenteri*, (G) *Kophobelemnon stelliferum*.....2-18

Figure 2-9 SEM-BSE images of the light and dark growth rings found in: (A) *Anthoptilum grandiflorum*, (B) *Pennatula aculeata*, (C) *Funiculina quadrangularis*, (D) *Protoptilum carpenteri*, (E) *Kophobelemnon stelliferum*.....2-19

Figure 2-10. Image of a colony of *Anthoptilum* sp. (sample # R2038-8) (right), (A) its cross sections taken at 30 cm in the rachis, (B) at 12 cm in the rachis above the peduncle, (C) and at the transition point between the end of the peduncle and the beginning of the rachis (location of cross sections indicated by yellow arrows). Cross sections were imaged under SEM-BSE.....2-20

Figure 2-11. Image of a colony of *Pennatula aculeata* (sample # R2038-18) (right), (A) its cross sections taken at 10 cm in the rachis, (B) and at the transition point between the end of the peduncle and the beginning of the rachis (location of cross sections indicated by yellow arrows). Cross sections were imaged under SEM-BSE.....2-21

Figure 2-12. Image of a colony of *Funiculina quadrangularis* from within the Laurentian Channel MPA (sample # 231) (right), (A) its cross sections taken at 8 cm in the rachis, (B) and at the transition point between the end of the peduncle and beginning of the rachis (location of cross sections indicated by yellow arrows). Cross sections were taken

under SEM-BSE.....2-22

Figure 2-13. Image of *Protoptilum carpenteri* colony (left), (A) its cross sections taken at 20 cm in the rachis, (B) and at the transition point between the end of the peduncle and the beginning of the rachis (bottom) (location of cross sections indicated by yellow arrows).
*Images were not altered and were taken with SEM-BSE.....2-23

Figure 2-14. Image of a *Kophobelemnon stelliferum* colony (right), (A) its cross sections taken at 8 cm in the rachis, (B) and at the transition point between the end of the peduncle and beginning of the rachis (bottom) (location of cross sections indicated by yellow arrows).
Cross sections were taken under SEM-BSE.....2-24

Figure 2-15. 200 μm SEM-BSE image of the growth ring increments in a cross section of *Anthoptilum* sp. showing the thicker banding in the beginning of growth, thinner banding in the middle of growth, and thicker banding towards the end of growth (indicated by the yellow markings). Also shown are the thinner growth rings observed in between the thicker growth rings (indicated by the yellow arrow) (sample R2041-22)2-25

Figure 2-16. SEM-BSE images of the unidentified features within the growth rings of each species (indicated by yellow circles): (A) *Anthoptilum grandiflorum*, (B) *Pennatula aculeata*, (C) *Funiculina quadrangularis*, (D) *Protoptilum carpenteri*, and (E) *Kophobelemnon stelliferum*.....2-26

Figure 2-17. SEM-BSE images of cross sections taken in the rachis of: (A) *Anthoptilum grandiflorum* (sample # R2041-23), (B) *Anthoptilum murrayi* (sample # R2041-30), and (C) *Anthoptilum* sp. (sample # R2038-6). Highlighted are the elongated, light-colored centers and the rounded center (yellow rectangle), and the cracks present (yellow arrows).....2-28

Figure 2-18. SEM-BSE images of the centers observed in: (A) *Anthoptilum grandiflorum*, (B)

Pennatula aculeata, (C) juvenile *Funiculina quadrangularis*, (D) adult *Funiculina quadrangularis*, (E) *Protoptilum carpenteri*, and (F) *Kophoblemnon stelliferum*.....2-29

Figure 2-19. (A) 200 μm SEM-BSE image of the center in a colony of *Protoptilum carpenteri*, (B) 20 μm SEM-BSE image of a large hole in the center (sample # R2039-3), (C) 20 μm SEM-BSE image of the tiny burrowed-like hole in the center, (D) 3 μm SEM-BSE of the tiny hole.....2-30

Figure 2-20. (A) 40 μm SEM-BSE image of the center in a colony of *Kophoblemnon stelliferum* showing the tiny black spots, rounded features, and cracks, (B) 5 μm SEM-BSE image of the rounded features found in the center (indicated by yellow arrow).....2-31

Figure 2-21. (A) SEM image showing the EDX spots taken in the center of a colony of *Kophoblemnon stelliferum*, (B) graph showing the elements in counts per second (cps) in the light spots, (C) graph showing the calcium present in counts per second (cps) in the light spots. Element composition in the center of the axis was similar across all species.....2-32

Figure 2-22. (A) Example of the EDX spots chosen in the dark and light growth rings within a colony of *Anthoptilum grandiflorum*, (B) bar graph showing the average counts per second (cps) for Mg/Ca detected in light and dark growth rings in each species.....2-36

Figure 2-23. (A) SEM-EDX spot analysis (spot locations are represented by the “+”) taken in a colony of *Anthoptilum murrayi* (sample # R2041-30), (B) a bar graph showing the differences in counts per second of each element between the light unidentified feature (spot 1) and the dark feature (spot 2), (C) bar graph showing the differences in calcium counts per second between spot 1 and 2. Error bars are shown as standard error.....2-37

Figure 3-1. Bathymetric map of the boundaries within the Laurentian Channel MPA, the stations

numbers from which sea pen samples were collected from for this study in 2017, and the locations of those samples collected for this study in 2017 (indicated by colored circles). *Anthoptilum* spp. samples collected are indicated by the blue circles, *P. aculeata* samples collected are indicated by the red circles, *F. quadrangularis* samples collected are indicated by the green circles, *P. carpenteri* samples collected are indicated by the orange circles, and *K. stelliferum* samples collected are indicated by the yellow circles. *F. quadrangularis* samples collected just outside of the MPA in 2007 during a DFO multispecies trawl survey are indicated by a purple circle, and *F. quadrangularis* samples collected further outside of the MPA in 2009 during a DFO multispecies trawl survey are indicated by a black circle. The location of the MPA is shown on the bottom right.....3-7

Figure 3-2. SEM-BSE image of the cross section in *Pennatula aculeata* (sample R2035-341) showing the thinner growth rings combining into a single, thicker growth ring that was used to represent one year (indicated by yellow arrow)3-9

Figure 3-3. Bar graph showing the total length (cm) for 23 *Anthoptilum* spp., 20 *Pennatula aculeata*, 19 *Funiculina quadrangularis*, 3 *Protoptilum carpenteri*, and 5 *Kophobelemnon stelliferum*. Error bars are shown as standard error..... 3-11

Figure 3-4. Images of *Anthoptilum* spp. showing differences in polyp densities in two colonies with the same height (28 cm) (A, B), and a juvenile colony with very few polyps and flesh (C). Scale bar 3.5 cm.....3-13

Figure 3-5. Image of the *Funiculina quadrangularis* collected from the Laurentian Channel MPA in 2017 (A), image of the *Funiculina quadrangularis* collected in 2007 in the Laurentian Channel MPA (B), image of the *Funiculina quadrangularis* collected in 2009 outside of the Laurentian Channel. Scale bar: 3.5 cm.....3-13

Figure 3-6. Peduncle length in relation to colony length in: (A) *Anthoptilum* spp., (B) *Pennatula aculeata*, and (C) *Funiculina quadrangularis*. Axis diameter in relation to colony length in: (D) *Anthoptilum* spp., (E) *Pennatula aculeata*, and (F) *Funiculina quadrangularis*. Wet weight in relation to colony length in: (G) *Anthoptilum* spp., (H) *Pennatula aculeata*, and (I) *Funiculina quadrangularis*.....3-14

Figure 3-7. Peduncle length in relation to colony length in: (A) *Protoptilum carpenteri*, (B) *Kophobelemnon stelliferum*. Axis diameter in relation to colony length in: (C) *Protoptilum carpenteri*, (D) *Kophobelemnon stelliferum*. Wet weight in relation to colony length in: (E) *Protoptilum carpenteri*, (F) *Kophobelemnon stelliferum*.....3-15

Figure 3-8. (A) 100 µm SEM-BSE image of the growth rings within a colony of *Anthoptilum* sp. showing the ring counting methods for “major rings” (indicated by red lines), and “all rings” (indicated by yellow dots). (B) Logistic graphs showing the relationship between: major rings and colony length, (C) all rings and colony length. Each point represents a single colony, and error bars are shown as standard error.....3-17

Figure 3-9. (A) 200 µm SEM-BSE image of the growth rings within a colony of *Protoptilum carpenteri* showing the ring counting methods for “major rings” (indicated by red lines), and “all rings” (indicated by yellow dots). (B) Graphs showing the relationship between: major rings and colony length, (C) all rings and colony length.....3-18

Figure 3-10. (A) 100 µm SEM-BSE image of the growth rings within a colony of *Funiculina quadrangularis* showing the ring counting methods for “major rings” (indicated by red lines), and “all rings” (indicated by yellow dots). (B) Logistic graphs showing the relationship between: major rings and colony length, (C) all rings and colony length. Each point represents a single colony.....3-19

Figure 3-11. (A) 200 µm SEM-BSE image of the growth rings within a colony of *Protoptilum*

carpenteri showing the ring counting methods for “major rings” (indicated by red lines), and “all rings” (indicated by yellow dots). (B) Graphs showing the relationship between: major rings and colony length, (C) all rings and colony length. Each point represents a single colony.....3-20

Figure 3-12. (A) 100 μm SEM-BSE image of the growth rings within a colony of *Kophobelemnon stelliferum* showing the ring counting methods for “major rings” (indicated by red lines), and “all rings” (indicated by yellow dots). (B) Logistic graphs showing the relationship between: major rings and colony length, (C) all rings and colony length. Each point represents a single colony.....3-21

Figure 3-13. Gompertz relationships for *Anthoptilum* spp. between (A) colony length and major rings, and (B) colony length and all rings; For *P. aculeata* between (C) colony length and major rings, and (D) colony length and all rings; For *F. quadrangularis* between (E) colony length and major rings, and (F) colony length and all rings. Relationships produced using the equation: $Length = Linf * \exp(\rho * \exp(-k * Rings))$ at a 95% confidence interval.....3-22

Figure 3-14. Thickness (μm) of each major couplet (indicated by the yellow line) in a colony of *Anthoptilum* spp. (sample # R2041-22). Number of rings and their thicknesses are shown in the adjacent table. Thickness measured with ImageJ software to the nearest μm.....3-25

Figure 3-15. Thickness (μm) of each major couplet (indicated by the yellow line) in a colony of *Pennatula aculeata* (sample # R2042-13). Number of rings and their thicknesses are shown in the adjacent table. Thickness measured with ImageJ software.....3-26

Figure 3-16. Thickness (μm) of each major couplet (indicated by the yellow line) in a colony of *Funiculina quadrangularis* (sample # R2038-4). Number of rings and their thicknesses are shown in the adjacent table. Thickness measured with ImageJ software.....3-27

Figure 3-17. Thickness (μm) of each major couplet (indicated by the yellow line) in a colony of *Protoptilum carpenteri* (sample # R2039-3). Number of rings and their thicknesses are shown in the adjacent table. Thickness measured with ImageJ software.....3-28

Figure 3-18. Thickness (μm) of each major couplet (indicated by the yellow line) in a colony of *Kophobelemnon stelliferum* (sample # R2041-28). Number of rings and their thicknesses are shown in the adjacent table. Thickness measured with ImageJ software.....3-29

Figure 4-1. Bar graphs showing (A) radial growth rates, and (B) linear growth rates for *Anthoptilum* spp., *P. aculeata*, *F. quadrangularis*, and *K. stelliferum* from this study, and *U. encrinus*, *H. finmarchica*, and *H. willemoesi* from previous studies.....4-3

List of tables

Table 1-1. Groups of deep-sea corals found off Atlantic Canada, their common species, and their skeletal composition (Packer et al., 2020)	1-1
Table 1-2. Average proportion of carbonate, organic, and water composition in the axis of sea pens <i>Umbellula encrinus</i> and <i>Anthoptilum grandiflorum</i> (Neves et al., 2018b)	1-3
Table 2-1 List of the species and number of samples collected from the Laurentian Channel MPA during the ROPOS cruise in 2017.....	2-9
Table 2-2. Sample ID, latitude, longitude, and species collected from the Laurentian Channel MPA. Only 5 samples of <i>Funiculina quadrangularis</i> were collected from the MPA, and 14 were collected during the DFO multispecies trawl survey in 2007 and 2009 (Trawl)	2-10
Table 2-3. Detection limit of each element measured in SEM-EDX spot analyses.....	2-34
Table 2-4. SEM-EDX spot analysis taken in the light and dark rings in all colonies for each species (<i>Anthoptilum</i> spp., <i>Pennatula aculeata</i> , <i>Funiculina quadrangularis</i> , <i>Protoptilum carpenteri</i> , and <i>Kophobelemnion stelliferum</i>) showing major elements present in average counts per second (cps). Error is in standard deviation.....	2-34
Table 2-5. SEM-EDX spot analysis taken in the light and dark rings of all colonies of <i>Anthoptilum</i> spp., <i>Pennatula aculeata</i> , <i>Funiculina quadrangularis</i> , <i>Protoptilum carpenteri</i> , and <i>Kophobelemnion stelliferum</i> showing the average major elements against calcium ratio counts.....	2-35
Table 3-1 Sample ID, latitude, longitude, and species collected from the Laurentian Channel MPA. Only 5 samples of <i>Funiculina quadrangularis</i> were collected from the MPA, and 14 were collected during the DFO multispecies trawl survey in 2007 and 2009 (Trawl)	3-5

Table 3-2. List per species showing the range of major rings counted, the range of all rings counted, the radial growth rates determined from counting major rings, the radial growth rates determined from counting all rings, the linear growth rates determined from counting major rings, the linear growth rates determined from counting all rings, and the maximum cut-off from which age can be estimated based on size as shown from the Gompertz growth pattern. Sample sizes for each species included 23 *Anthoptilum* spp., 20 *Pennatula aculeata*, 19 *Funiculina quadrangularis*, 3 *Protoptilum carpenteri*, and 5 *Kophobelemnon stelliferum* individuals. Standard error was calculated from these values.....3-24

Table 3-3. Summary of sea pen species analyzed showing their sample location, age range, radial growth rates and linear growth rates.....3-30

Abbreviations

DFO – Fisheries and Oceans Canada

EDX – Energy Dispersive X-Ray

GLM – General Linear Model

POC – Particulate Organic Carbon

DIC – Dissolved Inorganic Carbon

ROPOS – Remotely Operated Platform for Ocean Sciences

ROV – Remotely Operated Vehicle

SEM – Scanning Electron Microscope

VME – Vulnerable Marine Ecosystem

XRD – X-Ray Diffraction

Co-authorship Statement

This thesis was written by me, Krista Greeley. I had guidance from my co-supervisors Evan Edinger and Graham Layne as well as from my committee member Bárbara de Moura Neves who collected the samples I analyzed. I am the lead author in the contributions that arise from this thesis. Dr. Evan Edinger and Dr. Bárbara de Moura Neves edited chapters 1-4, and Dr. Graham Layne edited and aided with technical terms in chapter 2 involving the geochemical analyses used. Chapters 2 and 3 are intended for publication and were co-authored by Dr. Evan Edinger, Dr. Bárbara de Moura Neves, and Dr. Graham Layne.

Thesis Impact Statement: COVID-19

Prior to COVID-19, additional analyses regarding the elemental composition and aging of my sea pen samples were possible but not necessary. My methodology included SEM-EDX analyses to better understand the elemental composition of sea pen growth rings as well as measurements on sea pen colony metrics and age. I conducted a majority of my work in the lab and benefited from meeting with my advisors in person. Overall, I had enough data to finish this thesis before COVID-19 rapidly spread throughout Canada, and I was able to return home to Boston, MA before any lockdowns. However, due to COVID-19, communication with my advisors and committee members was drastically reduced, and edits on my thesis took twice as long.

Appendices

Appendix 2-1. Image of a *Funiculina quadrangularis* colony showing its flexible axis

(sample #231)2-49

1. Introduction

Deep-sea corals have the potential to be valuable archives of ocean environments. Corals are cnidarians with a calcium carbonate and/or proteinaceous skeleton, characterized as either Anthozoa (Octocorallia or Hexacorallia) or as Hydrozoa (Hydrocorals) (Cairns et al., 2007) (Fig. 1-1). Around Atlantic Canada, deep-sea cnidarians such as scleractinians (stony coral), gorgonians, antipatharians (black coral) and sea pens are common. To protect these deep-sea corals, a marine protected area (MPA) was established within the Laurentian Channel in 2019 with the primary objective of protecting large aggregations of sea pens that reside there. These sea pen fields provide significant habitats for several marine species and have also been characterized as vulnerable marine ecosystems (VMEs) due to their slow growth and recovery rates (Murillo et al., 2018; Neves et al., 2018a,b; Baillon et al., 2012; Neves et al., 2015; dfo-mpo.gc.ca).

Table 1-1. Groups of deep-sea corals found off Atlantic Canada, their common species, and their skeletal composition (Packer et al., 2020).

Phylum	Class	Subclass	Order	Informal Name	Skeletal Composition
Cnidaria	Anthozoa	Hexacorallia	Scleractinia	Stony corals	Aragonite
		Octocorallia	Antipatharia	Black corals	Protein
			Gorgoniidae	Sea fans	Carbonate and protein
	Hydrozoa	Hydroidolina	Pennatulacea	Sea pens	Carbonate and protein
			Stylasteridae	Stylasterids	Aragonite

Thus far, studies on skeletal growth and composition of deep-sea corals in the region have focused on gorgonians, scleractinians, and most recently on pennatulaceans (Murillo et al., 2018; Neves et al., 2018a,b; Neves et al., 2015; Edinger & Sherwood 2012; Andrews et al., 2002). Neves et al., (2018b) determined the average proportion of axis components in

Umbellula encrinus and *Anthoptilum grandiflorum* to be primarily calcite and organics (Table 1-2). Understanding the elemental composition of deep-sea coral skeletons is essential to account for the mechanisms underlying the construction of its growth bands. Neves et al. (2015) examined the geochemistry in skeletons of sea pens *Halipteris finmarchica* and *Halipteris willemoesi*, and Neves et al. (2018a) examined the geochemistry in skeletons of *Umbellula encrinus*, identifying a connection between ring formation periodicity and trace elemental patterns including Sr/Ca, Mg/Ca, Na/Ca, and Ba/Ca. Correlating the number of growth ring occurrences to cyclical trace elemental patterns does not confirm annual periodicity but does confirm a relationship between the two. External factors such as temperature, salinity, seawater isotopic levels ($\rho^{18}\text{O}$) do not exhibit large fluctuations in the deep sea and thus contribute very minimally to skeletal growth (Adkins et al., 2003). Seasonal shifts in food availability do exhibit fluctuations due to the heterotrophic nature of sea pens, however the level of variability requires further research (Maier et al., 2020).

The minimal amount of research conducted on sea pens is due in part to complications utilizing radiometric dating techniques associated with their small axis diameters, young ages (under 50 years old), and in some cases porous nature (Neves et al. 2015). The only papers published thus far analyzing sea pen skeletons in this region are Murillo et al., (2018), Neves et al. (2018a, and 2018b, 2015), Wilson et al., (2002), and Birkeland (1974). Here, growth bands were analyzed within 6 sea pen species (*Anthoptilum grandiflorum*, *Anthoptilum murrayi*, *Pennatulula aculeata*, *Funiuclina quadrangularis*, *Protoptilum carpenteri* and *Kophobelemnion stelliferum*) collected from the Laurentian Channel MPA. High resolution micron-scale images and elemental microanalyses of the growth bands within each species were quantitatively measured from thick sections taken at the peduncle

and 3 cm above the peduncle to discern the differences in growth between the peduncle and the rachis. The objectives of this study were to identify the elemental composition of growth bands, establish the growth rates, ages and longevities in each species, and determine possible evidence for annual and sub-annual banding.

Table 1-2. Average proportion of carbonate, organic, and water composition in the axis of sea pens *Umbellula encrinus* and *Anthoptilum grandiflorum* (Neves et al., 2018b).

Species	Carbonate Composition (%)	Organic Composition (%)	Water Composition (%)
<i>U. encrinus</i>	71	24	5
<i>A. grandiflorum</i>	64.8	32.7	2.5

1.1 Sea pens (order Pennatulacea)

Sea pens (Octocorallia: Pennatulacea) can grow in areas of soft sediment and low energy (Baker et al., 2012; Edinger & Sherwood 2012; Williams 2011). In the Laurentian Channel, noticeably dense patches of sea pen fields are found below 200 m and create habitats for several marine species (Baillon et al., 2012). It is their wide distributions, slow growth and recovery rates, and preferences for muddy and sandy regions that make sea pens a priority for habitat analyses as they are highly vulnerable to anthropogenic disturbances. Sea pens are known to be the most biologically complex type of octocorals due to their polyp functions, colony formation, and colony integration (Baillon et al., 2015; Wilson 2002). The initial development of a sea pen begins with a single polyp or oozoid that generates a rachis consisting of additional polyps that grow as autozooids and siphonozooids (Wilson et al., 2002). Autozooids and mesenteries are used for food and reproduction purposes, while siphonozooids are used for water circulation in the colony (Baillon et al., 2015). Being active suspension feeders, sea pens anchor into soft sediment or can sometimes

attach onto rocky substrata by way of the peduncle found at the bottom of the skeleton (Baillon et al., 2015).

1.1.1 Sea pen skeletal growth

The skeletons of sea pen species consist of an axial rod that is composed of calcite and protein, encompassing growth rings that disclose the age of the individual sea pen (Neves et al., 2018a; Murillo et al., 2018; Neves et al., 2015; Wilson et al., 2002). Growth rings consist of alternating light and dark couplets that occur throughout the entire axis (Neves et al., 2018a,b; Murillo et al., 2018; Neves et al., 2015). In most sea pen species, the axis usually follows the entire colony length and ranges from 1-6 mm in diameter (Neves et al., 2015). The thickest region of the axis is located in the peduncle, while the thinnest region of the axis is located in the distal part of the rachis where the axis is most flexible to cope with strong currents (Neves et al., 2018a,b; Neves et al., 2015; Wilson et al., 2002). A variety of axis shapes and sizes have been documented in several species of sea pens as shown in *Halipterus willemoesi* (Wilson et al., 2002), *Halipterus finmarchica* (Neves et al., 2015), *Pennatula grandis* (Neves 2016), *Anthoptiljum grandiflorum* (Murillo et al., 2018), and in *Anthoptilum grandiflorum* and *Umbellula encrinus* by Neves et al., (2018b). *Anthoptilum grandiflorum* and *Anthoptilum murrayi* are known to have an axis up to 60 cm in length that is a “question mark shape” with a cross-sectional “elliptical” and/or “squared” shape at its base that becomes circular further up the rachis (Murillo et al., 2018; Neves et al., 2018b; Baillon et al., 2015; Pires et al., 2009; Thomson and Henderson 1906) *Pennatula grandis*, *Pennatula phosphorea* and *Pennatula aculeata* are known to have a short and straight axis up to 50 cm in length with a rounded shape at its base, squared-shape within its peduncle, and rounded further up its rachis (Neves et al., 2018b; Neves 2016; Musgrave 1909). *Funiculina quadrangularis* is known to have a long and very flexible axis that reaches up to

2 m in length with a squared base and a four-lobed shape further up the rachis (Wright et al., 2014). *Umbellula encrinus* is known to have a long axis (> 2 m) that consists of a very long stalk and a group of autozooids at the tip of the rachis with a four-lobed axial shape (Neves et al., 2018b), and *Kophobelemnion stelliferum* is known to have a short, straight axis that reaches up to 70 cm in length with no previous studies on the shape of its axis (Rice et al., 1992). The unique shape of each sea pen species' axis could be linked to morphological differences (i.e. polyp size) and/or environmental factors (i.e. primary productivity) since external factors such as temperature, food flux, pH, calcite saturation and salinity influence sea pen growth rates and where they are dispersed (Neves et al., 2018b; Baillon et al., 2015a; Wilson et al., 2002).

1.1.2 Growth rates and age determination in sea pens

Throughout the length of their axes, sea pens periodically lay down growth rings of dark and light couplets (Neves et al., 2018a,b; Murillo et al., 2018; Neves 2016; Neves et al., 2015). Annual periodicity has been confirmed in several deep-sea corals (Aranha et al., 2014; Sherwood & Edinger 2009; Sherwood et al., 2005a; Roark et al., 2005; Risk et al., 2002), but only in a few species of sea pens (Neves et al., 2018a; Wilson et al., 2002; Birkeland 1974). To determine the age and growth rates of sea pens, growth ring counting has been found to be a reliable method when assuming annual periodicity. However, based on the ambiguous pattern of growth rings, ring counting is not enough to confirm annual periodicity on its own (Murillo et al., 2018; Sherwood et al., 2005a). To further validate the interpreted age achieved from visually counting the number of rings, a bomb-¹⁴C method can be used in colonies that are believed to date back to the 1950s-70s. This method correlates the estimated age of the colony with the $\Delta^{14}\text{C}$ peak that resulted from nuclear testing in the 1950s and 60s. This method illustrates the ¹⁴C concentration in the ocean that

was utilized by coral skeletons. Deep-sea corals containing proteinaceous skeletons in the NW Atlantic have been found to utilize surface particulate matter, while deep-sea corals such as sea pens with primarily calcite skeletons utilize the inorganic carbon found at great depths (Neves et al., 2018a; Sherwood et al., 2008). Because of this, the proteinaceous deep-sea coral skeletons did not experience a delay (up to 20 years) in the intake of ^{14}C like deep-sea corals with calcite skeletons do (Neves et al., 2018a; Sherwood et al., 2008). Neves et al., (2018a) determined the ^{14}C spikes in *U. encrinus* were comparable to those found in gorgonians *K. grayi* and *P. resedaeformis*, two species in which annual periodicity was confirmed (Neves et al., 2018a; Sherwood et al., 2008). Because of this, Neves et al., (2018a) was able to prove annual periodicity in *U. encrinus*. If a colony is not old enough for this radiocarbon analysis, annual periodicity can be validated through trace element analyses of the growth bands via secondary ion mass spectrometry (SIMS) if the colony has a diameter larger than 1 mm. Neves et al., (2018a) and Neves et al., (2015) correlated the number of trace element ratio peaks such as Mg/Ca with the number of rings visually counted in sea pens *Umbellula encrinus* and *Halipteris finmarchica*. Not only did spikes in Mg/Ca ratios exist with each growth band occurrence, but spikes in other trace element ratios including Sr/Ca, Ba/Ca, and Na/Ca did as well. It is through this validation of growth ring periodicity that the ages, longevity, recovery rates, and vulnerability of sea pens can be established to provide proper protection measures.

1.1.3 Conservation of sea pens

Organisms like sea pens provide unique structures that other marine life can benefit from when requiring shelter, food, and nursery grounds on the deep-sea floor (Baillon et al., 2012; Buhl-Mortensen et al., 2010). Certain species of deep-sea corals, and very recently sea pens, have been discovered to have especially slow growth and recovery rates, being identified as

VME indicators (OSPAR 2004; mpatlas.org) Today, these species' habitats are consistently being exploited from fisheries and oil activities, taking decades or even centuries to recover (Da Ros et al., 2019). Thus far, several organizations globally have begun to implement proper management and protection for these ecosystems. In the Mediterranean, pennatulaceans were reported as VMEs and essential fish habitats (EFHs) by the European Commission which has aimed to establish MPAs to prevent bottom trawling and promote the sustainable use of marine resources (OSPAR 2004). Growing research in the Mediterranean has focused on the identification and mapping of VMEs, as well as understanding the long-term impacts of bottom trawling on these habitats. Along the Atlantic Ocean, Spain has contributed research on VMEs since 2005 to the Spanish Government, the Regional Fisheries Management Organizations, and to the European Union (Muños et al., 2012). The protection of VMEs in the high seas will be enforced by regional fisheries management organizations (RFMO's) for Areas Beyond National Jurisdiction (Da Ros et al., 2019; Muños et al., 2012).

In 2006, the Mid-Atlantic Fishery Management Council applied the Magnuson-Stevens Reauthorization Act for the United States to enhance international fisheries management organizations to protect deep-sea coral habitats threatened by fisheries activities, while in 2016 the Obama administration implemented the Northeast Canyons and Seamounts Marine National Monument in 2016 (B.P. Kinlan et al., 2020). In the Northwest Atlantic, the Department of Fisheries and Oceans Canada established the Davis Strait conservation area in addition to 15 other areas with the aim to protect benthic habitats (including sea pens) through bottom contact fisheries restrictions in the area (mpatlas.org). The Northwest fisheries organization (NAFO) has also prohibited bottom contact fisheries in several areas (Murillo et al., 2018).

Further collaboration is required between the different sectors that involve deep-sea fisheries such as mining industries and fisheries management organizations for these conservation plans to be effective. In Canada, the Canadian Healthy Oceans Network (CHONe) is collaborating with Fisheries and Oceans Canada (DFO) to monitor vulnerable deep-sea ecosystems such as sea pen fields in the Laurentian Channel. In 2019, a marine protected area (MPA) was established in the Laurentian Channel to protect these sea pen habitats as well as several other marine species including leatherback sea turtles, black dogfish, smooth skate, and porbeagle sharks from human activities (Muntoni et al., 2019; Renshaw 2019). Research within this MPA has also been carried out involving monitoring deep-sea coral population structure, coral-fish relationships, biochemistry, growth, species diversity, sensitivity to anthropogenic disturbances, and recovery times (Baillon et al. 2012; dfo-mpo.gc.ca). The results from chapters 2 and 3 (this study) will be provided to other CHONe researchers and students and to DFO for further understanding of sea pen growth and vulnerability. It is through this research and teamwork that effective protection measures can be established, reducing human-induced damage to these vulnerable ecosystems.

1.2 Thesis objectives and chapter structure

This study explores the skeletal axis of six sea pen species (*Anthoptilum grandiforum*, *Anthoptilum murrayi*, *Pennatula aculeata*, *Funiculina quadrangularis*, *Protoptilum carpenteri*, and *Kophobelemnion stelliferum*) through a sclerochronological and geochemical approach as well as their skeletal growth and colony metrics which can assist in age dating and establishing proper protection measures for these species. Specifically, chapter 2 is designed to investigate the structure and elemental composition of growth rings and understand the nature of growth ring formation. High resolution SEM images and

geochemical analyses via SEM-EDX were utilized to determine the structure and elemental composition of light and dark growth rings in the six sea pen species. These elemental analyses were implemented to demonstrate the physical structure of sea pen skeletal growth rings, as well as how and why they form. Accurate age-dating methods for deep-sea corals can be generated from this knowledge, aiding in the resolution of their recovery rates and thus their vulnerability to anthropogenic disturbances. Chapter 3 determines the colony metrics, ages, growth rates, and longevity of these sea pen species through post-collection examination and SEM imaging. Chapter 4 is the closing chapter that summarizes the results of the other chapters, their conclusions, and what can be improved for future studies that are analyzing sea pen skeletons.

1.3 References

- Neves B., Edinger E., Wareham V., 2018b. Morphology and composition of the internal axis in two morphologically contrasting deep-water sea pens (Cnidaria: Octocorallia). *Journal of Natural History*, 52:11-12, 659-685.
- Adkins J.F., Henderson G.M., Wang S.-L., O'Shea S, Mokadem F., 2004. Growth rates of deep-sea Scleractinia *Desmophyllum cristagalli* and *Enallopsammia rostrata*. *Earth and Planetary Science Letters* 227: 481-490.
- Andrews, A.H., Cordes E.E., Mahoney M.M., Munk K., Coale K.H, Cailliet G.M & Heifetz J., 2002. Age, growth and radiometric age validation of a deep-sea, habitat-forming gorgonian (*Primnoa resedaeformis*) from the Gulf of Alaska. *Hydrobiologia* 471: 101-110.
- Aranha, R., E. Edinger, G. Layne & G. Piercey, 2014. Growth rate variation and potential paleoceanographic proxies in *Primnoa pacifica*: Insights from high-resolution trace element microanalysis. *Deep Sea Research Part II: Topical Studies in Oceanography* 99: 213-226.
- Baco A., 2004. Exploration for Deep-Sea Corals on North Pacific Seamounts and Islands. *Oceanography* vol. 20, No. 4.
- Baillon, S., Hamel, J.-F., Wareham, V. E. and Mercier, A. 2012. Deep cold-water corals as nurseries for fish larvae. *Frontiers in Ecology and the Environment* 10: 351–356.
- Baillon S., English M., Hamel J-F., Mercier A., 2015. Comparative biometry and isotopy of three dominant pennatulacean corals in the Northwest Atlantic. *Acta Zoologica* 0: 1-19.

- Baker K.D., Wareham V.E., Snelgrove P.V.R., Haedrich R. L., Fifield D.A., Edinger E.N. & Gilkinson K.D., 2012. Distributional patterns of deep-sea coral assemblages in three submarine canyons off Newfoundland, Canada. *Marine Ecology Progress Series* 445: 235-249.
- Ballantyne L., 2018. An examination of the distribution, abundance, and habitat preferences of soft corals (Octocorallia: Alcyonacea) in offshore Nova Scotian waters. Dalhousie University, Halifax, NS.
- Bastari A., Pica D., Ferretti F., Micheli F., Cerrano C., 2018. Sea pens in the Mediterranean Sea: hábitat suitability and opportunities for ecosystem recovery. *ICES Journal of Marine Science*, 75(5), 1722-1732.
- Best B., 1988. Passive suspension feeding in a sea pen: Effects of ambient flow on volume flow rate and filtering efficiency. *Bio Bull* 175: 332-342.
- Birkeland C., 1974. Interactions between a sea pen and seven of its predators. *Ecological Monographs* 44(2):211.
- Breeze H., Fenton, D.G., 2007. Designing management measures to protect cold-water corals off Nova Scotia, Canada. *Bull. Mar. Sci.* 81 (Suppl. 1), 123-133.
- Buhl-Mortensen, P., Buhl-Mortensen L., Gorgon Jr D.C., 2005. Distribution of deep-water corals in Atlantic Canada. *International Coral Reef Symposium*, 1832-1848.
- Buhl-Mortensen, P., Buhl-Mortensen, L., 2018. Impacts of Bottom Trawling and Litter on the Seabed in Norwegian Waters. *Front. Mar. Sci.* 5:42. doi: 10.3389/fmars.2018.00042.

- Buhl-Mortensen, L., Vanreusel A., Gooday A.J., Levin L.A., Priede I.G., Buhl-Mortensen P., Gheerardyn, H., King N.K., Raes M., 2010. Biological structures as a source of habit heterogeneity and biodiversity on the deep ocean margins. *Marine Ecology* 31:21-50.
- Cairns S. D., 2007. Deep-water corals: An overview with special reference to diversity and distribution of deep-water Scleractinian corals. *Bulletin of Marine Science* 81(3): 311-322.
- Clippele L.H., Buhl-Mortensen P., Buhl-Mortensen L., 2015. Fauna associated with cold water gorgonians and sea pens. *Continental Shelf Research* 105:67-78.
- Da Ros Z., Dell'Anno A., Morato T, Sweetman A.K., Carreiro-Silva M., Smith C.J., Papadopoulou N., Corinaldesi C., Bianchelli S., Gambi C., Cimino R., Snelgrove P., Lee Van Dover., Danovaro R., 2019. The deep sea: The new frontier for ecological restoration. *Marine Policy* 108: 1-10.
- Department of Fisheries and Oceans [DFO], Canada, 2003. Gully Marine Protected Area regulations: regulatory impact analysis statement. *Canada Gaz Part I* 137: 3882-3905. <https://laws-lois.justice.gc.ca/eng/regulations/SOR-2019-105/page-1.html>.
- Department of Fisheries and Oceans [DFO], Canada, 2017. Laurentian Channel Proposed Marine Protected Area.
- Department of Fisheries and Oceans [DFO], Canada, 2019. List of Marine Refuges. <https://www.dfo-mpo.gc.ca/oceans/oeabcm-amcepz/refuges/index-eng.html>.
- Duineveld G.C.A., Lavaleye M.S.S., Berghuis E.M., 2004. Particle flux and food supply to a seamount cold-water coral community (Galicia Bank, NW Spain). *Mar. Ecol. Prog. Ser.* Vol. 277: 13-23.

- Druffel E.R.M., King L.L., Belostock R.A., Buesseler K.O., 1990. Growth rate of a deep-sea coral using ^{210}Pb and other isotopes. *Geochemica et Cosmochimica Acta* Vol. 54: 1493-1500.
- Edinger E., Baker K.D., Devillers R., Wareham V., 2007a. Coldwater corals off Newfoundland and Labrador: distribution and fisheries impacts. World Wildlife Fund (WWF) Toronto.
- Edinger E.N., Sherwood O.A., 2012. Applied taphonomy of gorgonian and antipatharian corals in Atlantic Canada: experimental decay rates, field observations, and implications for assessing fisheries damage to deep-sea coral habitats. *N. Jb. Geol. Paläont. Abh* 265: 199-218.
- Fisheries and Oceans Canada, 2019. Atlantic Zone Monitoring Program Website. Retrieved 26 November 2019 from Fisheries and Oceans Canada.
- Gagnon A., Adkins J., Fernandez D., Robinson L., 2007. Sr/Ca and Mg/Ca vital effects correlated with skeletal architecture in a Scleractinian deep-sea coral and the role of Rayleigh fractionation. *Earth and Planetary Science Letters*: Vol. 261(1-2), pp. 280-295.
- Gass S. E. and J. H. M. Willison. 2005. An assessment of the distribution of deep-sea corals in Atlantic Canada by using both scientific and local forms of knowledge. Pages 223–245 in A. Freiwald and J. M. Roberts, eds. *Cold-water corals and ecosystems*. Springer-Verlag, Heidelberg.
- Gordon D.C. Jr., Kenchington E.L.R., 2007. Deep-water corals in Atlantic Canada: A review of DFO research (2001-2003). *Proc. N.S. Inst. Sci.* Vol. 44, pp.27-50.

- Greathead C., González-Irusta J.M., Clarke J., Boulcott P., Weetman A., Wright P.J., 2015. Environmental requirements for three sea pen species : relevance to distribution and conservation. *Journal of Mar. Sci.*:72(2), 575-586.
- Grigg R.W., 1974. Growth ring periodicity in two gorgonian corals. *Ecology* Vol. 55: 876-881, No. 4.
- Heikoop J.M., Hickmott D.D., Risk M.J., Shearer C.K., Atudorei V., 2002. Potential climate signals from the deep-sea gorgonian coral *Primnoa resedaeformis*. *Hydrobiologia* 471:117-124.
- Kulka D.W., Templeman N., 2013. Distribution and habitat associations of selected demersal fish species in the Laurentian Channel and Laurentian Area of Interest (AOI). *DFO Can. Sci. Advis. Sec. Res. Doc. 2013/099*. v + 44 p.
- Lauria V., Garofalo G., Fiorentino F., Massi D., Milisenda G., Piraino S., Russo T., Gristina M., 2017. Species distribution models of two critically endangered deep-sea octocorals reveal fishing impacts on vulnerable marine ecosystems in central Mediterranean Sea. *Scientific Reports* 7:8049.
- Lewis S., Ramirez-Luna V., Templeman N., Simpson M.R., Gilkinson K., Lawson J.W., C. Miri and Collins R. 2016. A Framework for the Identification of Monitoring Indicators Protocols and Strategies for the Proposed Laurentian Channel Marine Protected Area (MPA). *DFO Can. Sci. Advis. Sec. Res. Doc. 2014/093*. v + 55 p.
- Marschal C., Garrabou J., Harmelin, J., Pichon, M., 2004. A new method for measuring growth and age in the precious red coral *Coallium rubrum* (L.). *Coral Reefs*. 23: 423-432.

- Muñoz P.D., Sayago-Gil M., Murillo F., Del Río J.L., López-Abellán L.J., Sacau M., Sarralde R., 2012. Actions taken by fishing Nations towards identification and protection of vulnerable marine ecosystems in the high seas: The Spanish case (Atlantic Ocean).
- Murillo F., Durán Muños P., Altuna A., Serrano A., 2011. Distribution of deep-water corals of the Flemish Cap, Flemish Pass, and the Grand Banks of Newfoundland (Northwest Atlantic Ocean): Interaction with fishing activities. *ICES Journal of Marine Science* 68:319-332.
- Murillo F.J, MacDonald B.W., Kenchington E., Campana S.E., Sainte-Marie B. & Sacau M., 2018. Morphometry and growth of sea pen species from dense habitats in the Gulf of St. Lawrence, eastern Canada. *Marine Biology Research*, 14:4, 366-382.
- Murillo F.J., Kenchington E., Beazley L., Lirette C., Knudby A., Guijarro J., Benoit H., Bourdages H., Sainte-Marie B., 2016. Distribution Modelling of Sea Pens, Sponges, Stalked Tunicates and Soft Corals from Research Vessel Survey Data in the Gulf of St. Lawrence for Use in the Identification of Significant Benthic Areas. *Can. Tech. Rep. Fish. Aquat. Sci.* 3170: vi + 132 p.
- Musgrave E.M., 1909. Experimental observations on the organs of circulation and powers of locomotion in pennatulids. *QJ Microsc Sci.* 54:443–482.
- Neves B.M., 2016. Growth in cold-water octocorals: rates, morphology and environmental controls[dissertation]. St. John's (NL): Memorial University of Newfoundland.

- Neves B., Edinger E., Layne G., Hayes V., 2015. Decadal longevity and slow growth rates in the deep-water sea pen *Halipterus finmarchica* (Sars, 1851) (Octocorallia: Pennatulacea): Implications for vulnerability and recovery from anthropogenic disturbance. *The International Journal of Aquatic Sciences, Hydrobiologia* 759: 147-170.
- Neves B., Edinger E., Wareham V., Layne G., 2018a. Size metrics, longevity, and growth rates in *Umbellula encrinus* (Cnidaria: Pennatulacea) from the Eastern Canadian Arctic. *Arctic Science* 4(4): 722-749.
- Neves B., Edinger E., Wareham V., 2018b. Morphology and composition of the internal axis in two morphologically contrasting deep-water sea pens (Cnidaria: Octocorallia). *J Nat Hist*, 52:11-12, 659-685.
- Packer D.B., Nizinski M.S., Cairns D.S., Hourigan T.F., 2020. Deep-Sea Coral Taxa in the U.S. Northeast Region: Depth and Geographical Distribution (v. 2020).
- Pires D.O., Castro C.B., Silva J.C., 2009. Reproductive biology of the deep-sea pennatulacean *Anthoptilum murrayi* (Cnidaria, Octocorallia). *Mar Ecol Prog Ser* 397:103-112.
- Puglise K.A., Brock J.R., McDonough II J.J., 2005. Cold-water corals and ecosystems. Springer-Verlag Berlin Heidelberg, pp 1129-1140.
- Renshaw S., 2019. Monitoring elasmobranchs in marine protected areas: A Canadian case study of the Laurentian Channel. Dalhousie University, Halifax, Nova Scotia.
- Risk M. J., J. M. Heikoop, M. G. Snow & R. Beukens, 2002. Lifespans and growth patterns of two deep-sea corals: *Primnoa resedaeformis* and *Desmophyllum cristagalli*. *Hydrobiologia* 471: 125–131.

- Roark, E. B., Guilderson, T. P., Dunbar, R. B., Fallon, S. J., and Mucciarone, D. A. (2009). Extreme longevity in proteinaceous deep-sea corals. *Proc. Natl. Acad. Sci. U.S.A.* 106, 5204–5208. doi: 10.1073/pnas.0810875106.
- Roberts M., Wheeler A., Friewald A., 2006. Reefs of the Deep: The Biology and Geology of Cold-Water Coral Ecosystems. *Science* Vol. 312.
- Roberts J.M., Wheeler A., Friewald A., Cairns S.D., 2009. Cold water corals: The biology and Geology of Deep-Sea Coral Habitats. *Cambridge University Press*.
- Robinson L., Adkins J., Frank N., Gagnon A., Prouty N., Roark B., Flierdt T., 2014. The geochemistry of deep-sea coral skeleton: A review of vital effects and applications for paleoceanography. *Deep-Sea Research II* 99: 184-198.
- Rollion-Bard C., Blamart D., Cuif J.-P., Juillet-Leclerc A., 2003. Microanalysis of C and O isotopes of azooxanthellate and zooxanthellate corals by ion microprobe. *Coral Reefs* 22:405-415.
- Sherwood, O., Heikoop, A., Sinclair, J.M., Scott, D.J., Shearer C., and Azetsu-Scott, K., 2005a. Skeletal Mg/Ca in *Primnoa resedaeformis*: relationship to temperature. Friewald A, Murray JM (eds) *Cold-water corals and ecosystems*. Springer, Berlin, p. 1061-1079.
- Sherwood O.A., Edinger E.N., Guilderson T.P., Ghaleb B., Risk M.J., and Scott D.B., 2008. Late Holocene radiocarbon variability in Northwest Atlantic slope waters. *Earth Planet. Sci. Lett.* 275(1-2): 146-153.
- Sherwood O.A., & E. N. Edinger, 2009. Ages and growth rates of some deep-sea gorgonian and anthipatharian corals of Newfoundland and Labrador. *Canadian Journal of Fisheries and Aquatic Sciences* 66: 142-152.

- Thomson J.A., Henderson W.D., 1906. An account of the alcyonarians collected by the Royal Indian Marine Survey Ship Investigator in the Indian Ocean: I. *The Alcyonarians of the Deep Sea*. Calcutta: Order of the Trustees of the Indian Museum.
- Wagner, H., Purser, A., Thomsen, L., Jesus, C. C., and Lundälv, T. (2011). Particulate organic matter fluxes and hydrodynamics at the tislér cold-water coral reef. *J. Mar. Syst.* 85, 19–29. doi: 10.1016/j.jmarsys.2010.11.003
- Wareham, V. E. & E. N. Edinger, 2007. Distribution of deep-sea corals in the Newfoundland and Labrador region, Northwest Atlantic Ocean. *Bulletin of Marine Science* 81: 289–313.
- Williams G., 2011. Global Diversity of Sea Pens (Cnidaria: Octocorallia: Pennatulacea). PLoS ONE 6: 1-11.
- Wilson M., Andrews A., Brown, A., Cordes E., 2002. Axial rod growth and age estimation of the sea pen, *Halopteris willemoesi* Kolliker. *Hydrobiologia* 471:133-142.
- Wright E., Kemp K., Rogers A., Yesson C., 2014. Genetic structure of the tall sea pen *Funiculina quadrangularis* in NW Scottish sea lochs. *Mar Eco* Vol 36:659-667.

2 Scanning electron microscope observations on the structure and composition of growth bands in six species of sea pens

Abstract

The purpose of this study is to fill existing knowledge gaps on the physical basis of growth rings in sea pens to establish accurate age-dating methods. The elemental composition and structure of growth rings in six sea pens species (*Anthoptilum grandiflorum*, *Anthoptilum murrayi*, *Pennatula aculeata*, *Funiculina quadrangularis*, *Protoptilum carpenteri*, and *Kophobelemnon stelliferum*) are presented and discussed. Samples were collected using the remotely operated vehicle (ROV) ROPOS in 2017 from the Laurentian Channel marine protected area (MPA) at depths of 400-600 m. Scanning Electron Microscopy with Energy Dispersive X-Ray Analysis (SEM-EDX) determined major element variations within each growth ring. The average intensities of characteristic X-ray lines for Mg and Ca (in counts per second (cps)) were comparable in the light and dark rings (light: 2.64 cps Mg, 47.5 cps Ca; dark: Mg 2.25 cps, Ca 51.2 cps). The results reflect comparable element concentrations in light and dark rings and suggests they do not differ significantly in composition.

2.1 Introduction

Deep-sea corals have the potential to be valuable archives of ocean environments. Understanding the elemental composition of deep-sea coral skeletons is essential to account for the mechanisms underlying the construction of its growth rings. One group of particular interest are sea pens. Sea pens are made up of a peduncle, rachis, and an internal axis composed of high magnesium calcite (Fig. 2-1). Neves et al. (2015)

examined the geochemistry in skeletons of sea pens *Halipteris finmarchica* and *Halipteris willemoesi*, and Neves et al. (2018a) the geochemistry in skeletons of *Umbellula encrinus*, to identify a connection between ring formation periodicity and trace elemental patterns including Sr/Ca, Mg/Ca, Na/Ca, and Ba/Ca. Correlating the number of growth ring occurrences to cyclical trace elemental patterns does not confirm annual periodicity but does confirm a relationship between the two factors. Seasonal shifts in the deep-sea could influence skeletal growth in deep-sea corals as food availability does exhibit fluctuations, however the level of variability requires further research (Maier et al., 2020).

Corresponding elemental analyses with the skeletal growth of deep-sea corals on a micrometer (μm) scale is accessible through high-resolution microbeam techniques, generating new interpretations for the mechanisms by which deep-sea corals construct their skeleton. The limited amount of research conducted on sea pens is due in part to complications utilizing dating techniques associated with their immensely small axis diameters, young ages, and in some cases, porous nature (Neves et al. 2015). Neves et al. (2018a, and 2018b, 2015), Murillo et al., (2018), Wilson et al., (2002), and Birkeland (1974) are the only papers published thus far analyzing sea pen skeletons. Here, growth bands were analyzed within 6 sea pen species (*Anthoptilum grandiflorum*, *Anthoptilum murrayi*, *Pennatula aculeata*, *Funiculina quadrangularis*, *Protoptilum carpenteri* and *Kophobelemnon stelliferum*) collected from the Laurentian Channel MPA. High resolution micron-scale images and elemental microanalyses of the growth bands within each species were quantitatively measured from thick sections taken at the peduncle and 3 cm above the peduncle to discern the differences in growth between the peduncle and the rachis. The objectives of this were to identify what major and minor growth rings are

composed of and to determine possible evidence for annual and sub-annual banding.

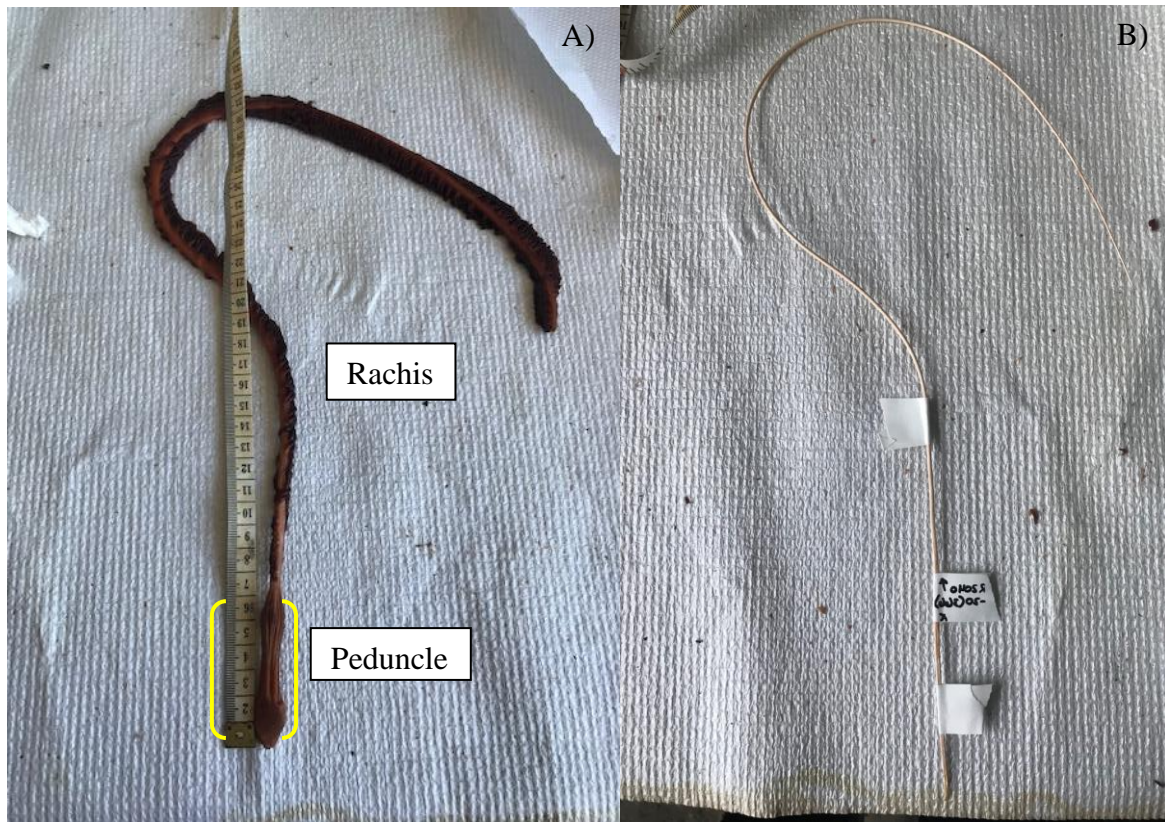


Figure 2-1. (A) Image of an *Anthoptilum* sp. colony showing the peduncle (indicated by yellow brackets) and the rachis (remaining portion of the colony), and (B) its axis.

2.2 Materials and Methods

2.2.1 Study area and sampling

The Laurentian Channel is an ecologically rich region southwest of Newfoundland and Labrador. The Laurentian Channel is a submarine trough with depth ranges from 400 m to 600 m and is 1200 km long found off the Southwest coast of Newfoundland and Labrador, encompassing sea pen meadows that are recognized as Vulnerable Marine Ecosystem indicators across the North Atlantic (Fig. 2-2). Within this channel, a marine protected area (MPA) was designated in 2019, preventing all fishing and new oil and gas exploration and production in this area (Fig. 2-3). The species collected for this

study and their locations are shown in Figure 2-4. Protecting these sea pen aggregations in the Laurentian Channel is one of the six conservation objectives described in the design of the Laurentian Channel MPA (dfo-mpo.gc.ca). Marine protected areas are established to protect marine ecosystems by regulating human activities such as fishing. This MPA consists of two zones where protection will be implemented: zone 1a/b and 2a/b. Activities that might destroy, damage or disturb existing habitats in these zones are banned, however some exceptions have been implemented for the two zones: 1) In zones 1a/b, vessels are permitted passage through the MPA given that no anchoring is used; 2) Fishing that is not commercial is permitted throughout the MPA given that it is established under the “Aboriginal Communal Fishing Licenses Regulations”; 3) In zones 2a/b, repair cables can be laid down and/or maintained as long as habitats are not destroyed in the MPA; 4) Public safety, national defense, national security, and responding law enforcement activities are permitted; and 5) Activities approved by the Minister. This area was recognized as an “area of interest” in 2010, limited to 12,000 km² (Kulka et al., 2013), and protection measures are being established for 10% of marine and coastal areas around Canada by 2020 (Fisheries and Oceans Canada, 2011). The protection of this region will enable research on sea pen population structure, longevity, and growth rates which are necessary for assessing their vulnerability to anthropogenic disturbances and their habitat recovery times.



Figure 2-2. In-situ ROV image of a sea pen field taken in the Laurentian Channel MPA during the ROPOS 2017 cruise.

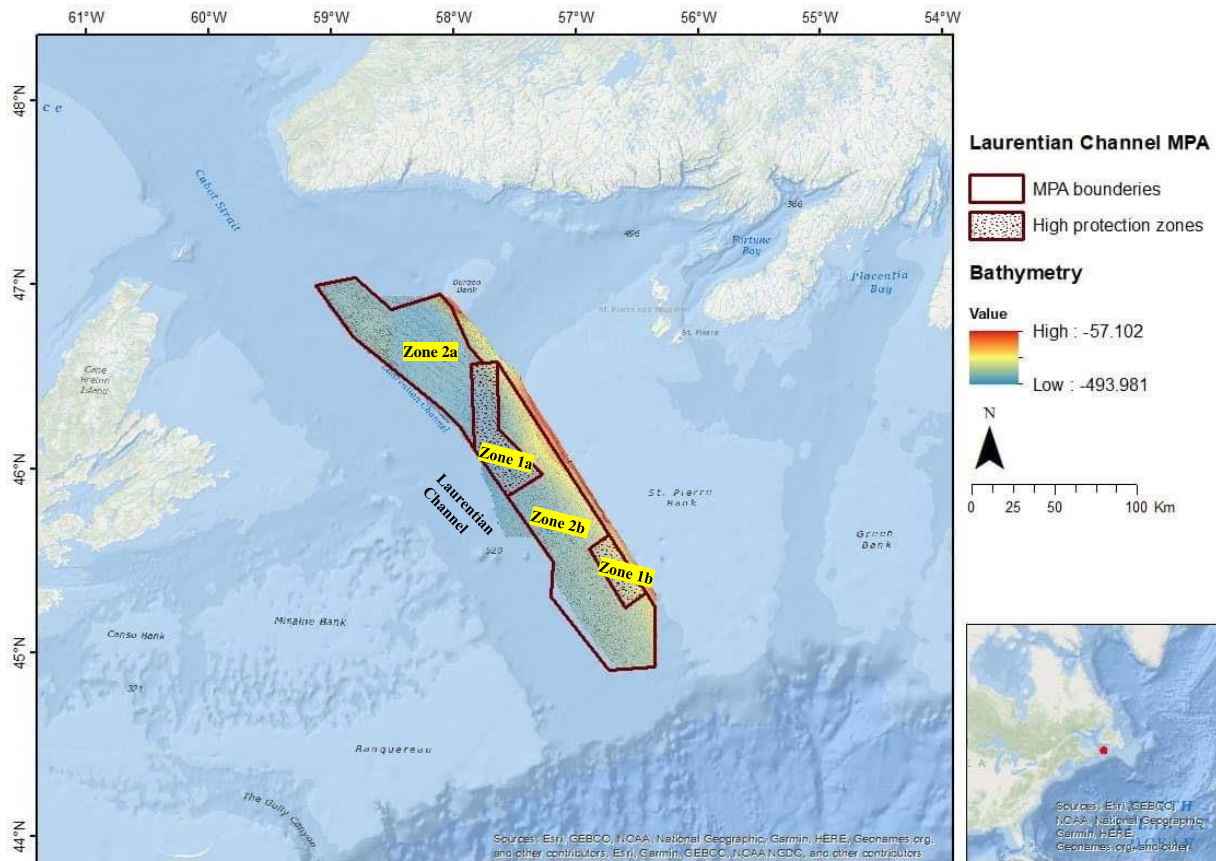


Figure 2-3. Bathymetric map of the MPA within the Laurentian Channel and its zones (1a, 1b, 2a, 2b).

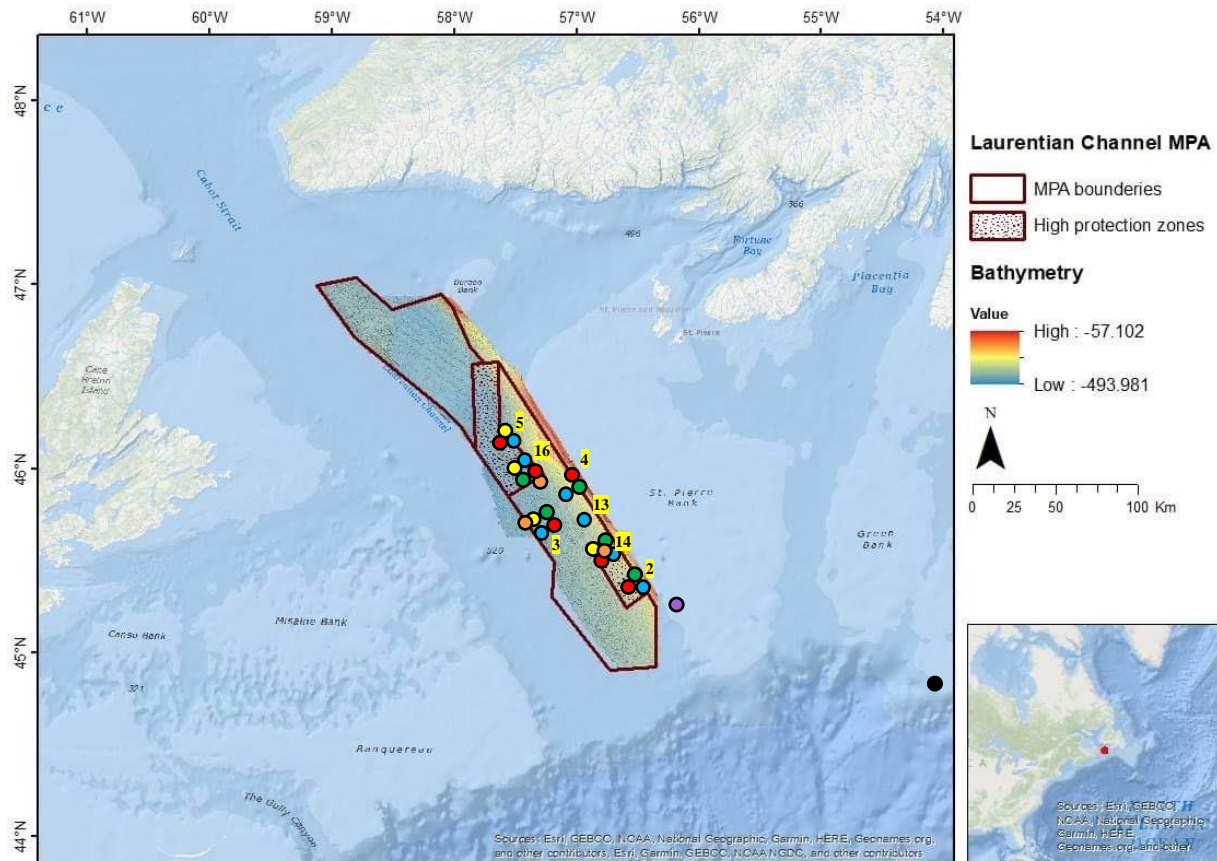


Figure 2-4. Bathymetric map of the MPA within the Laurentian Channel, the station numbers and the locations of the species collected for this study (indicated by colored circles). *Anthoptilum* spp. is indicated by the blue circles, *P. aculeata* is indicated by the red circles, *F. quadrangularis* is indicated by the green circles, *P. carpenteri* is indicated by the orange circles, and *K. stelliferum* is indicated by the yellow circles. *F. quadrangularis* samples collected outside of the MPA in 2007 are indicated by a purple circle, and in 2009 a black circle. On the right is the location of the MPA. Map generated and extracted from ArcGIS 1.0.

2.2.2 Sampling and identification

A total of 70 sea pen samples (Tables 2-1, 2-2) were collected for this study from the Laurentian Channel MPA, 23 of which were *Anthoptilum* spp. (14 *Anthoptilum* sp., 6 *Anthoptilum grandiflorum*, 3 *Anthoptilum murrayi*) (Figs. 2-5A), 20 *Pennatula aculeata* (Fig. 2-5B), 19 *Funiculina quadrangularis* (Figs. 2-5C), 3 *Protoptilum carpenteri* (Fig. 2-5D), and 5 *Kophobelemnon stelliferum* (Fig. 2-5E). Samples were collected using ROV manipulator arms, and video surveyed in September 2017 using the remotely operated vehicle (ROV) ROPOS during a joint CHONE DFO cruise in the Laurentian Channel. Samples were frozen at -20°C immediately after collection. In situ sizes were measured using the ROPOS lasers which are 10 cm apart. The depth range in which these samples were collected in the Laurentian Channel was 400-600 m with seawater consistently 6.2°C, a pH of 7.9, and salinity of 35 PSU. Among the 19 samples of *F. quadrangularis* collected, 14 were opportunistically collected during a DFO multispecies trawl survey within and just outside of the Laurentian Channel in similar conditions. To prepare the samples for this analysis a cross-section was taken using an Isomet® Low Speed Saw at the transition point where the peduncle ends, and polyp formation begins in the thickest part of the axis (Fig. 2-6). This cross section was then placed in aluminum rings 2.54 cm in diameter and embedded in epoxy (Epofix™ – Electron Microscopy Sciences). These rings were then polished using a Struers TegraPol 31 automated lapidary system. A thin carbon coating was applied before microanalysis. Spot analyses were conducted to identify the major elemental composition of light and dark rings and in the subsidiary anatomical features. The growth ring structure and the elemental composition within the axis of each skeleton

was analyzed using Scanning Electron Microscopy (SEM) (CREAIT MAF-Facility, Memorial University of Newfoundland) combining Back Scattering Electron imaging (BSE), and Energy Dispersive X-ray (EDX) analysis. SEM-BSE was used due to the micron-scale nature of these sea pen skeletons to achieve high-resolution images of growth rings and their detailed features. Secondary Electron Imaging (SEM-SEI) was used in some cases to examine the topography of the sample. EDX was applied to provide the qualitative elemental composition.

Table 2-1. List of the species and number of samples collected from the Laurentian Channel MPA during the ROPOS cruise in 2017.

Species	Total number of samples
<i>Anthoptilum</i> sp.	14
<i>Anthoptilum grandiflorum</i>	6
<i>Anthoptilum murrayi</i>	3
<i>Pennatula aculeata</i>	20
<i>Funiculina quadrangularis</i>	19
<i>Protoptilum carpenteri</i>	3
<i>Kophobelemnon stelliferum</i>	5

Table 2-2. Sample ID, latitude, longitude, and species collected from the Laurentian Channel MPA. Only five samples of *Funiculina quadrangularis* were collected from the MPA, and 14 were collected during the DFO multispecies trawl survey in 2007 and 2009 (trawl).

Sample	Latitude	Longitude	Species
R2040-20	N45° 56.4349'	W57° 22.5652'	<i>Anthoptilum sp.</i>
R2037-6	N46° 12.6467'	W57° 31.6492'	<i>Anthoptilum sp.</i>
R2041-29	N46° 8.6816'	W57° 31.4488'	<i>Anthoptilum sp.</i>
R2038-6	N45° 43.7405'	W56° 51.1618'	<i>Anthoptilum sp.</i>
R2040-21	N45° 56.1789'	W57° 22.17'	<i>Anthoptilum sp.</i>
R2040-19	N45° 56.3497'	W57° 21.9456'	<i>Anthoptilum sp.</i>
R2040-18	N45° 56.3544'	W57° 21.9494'	<i>Anthoptilum sp.</i>
R2040-8	N45° 56.3544'	W57° 21.9494'	<i>Anthoptilum sp.</i>
R2038-19	N45° 43.743'	W56° 51.1671'	<i>Anthoptilum sp.</i>
R2041-12	N46° 8.7352'	W57° 31.5191'	<i>Anthoptilum sp.</i>
R2041-29	N46° 8.6816'	W57° 31.4488'	<i>Anthoptilum sp.</i>
R2036-14	N45° 52.0306'	W56° 12.1854'	<i>Anthoptilum sp.</i>
R2041-27	N46° 8.6846'	W57° 31.4447'	<i>Anthoptilum grandiflorum</i>
R2038-8	N45° 43.739'	W56° 51.1804'	<i>Anthoptilum grandiflorum</i>
R2041-22	N46° 8.7175'	W57° 31.4636'	<i>Anthoptilum grandiflorum</i>
R2041-23	N46° 8.6911'	W57° 31.4474'	<i>Anthoptilum grandiflorum</i>
R2041-25	N46° 8.6845'	W57° 31.4448'	<i>Anthoptilum grandiflorum</i>
R2041-24	N46° 8.691'	W57° 31.4476'	<i>Anthoptilum grandiflorum</i>
R2041-30	N46° 8.6813'	W57° 31.449'	<i>Anthoptilum murrayi</i>
R2041-32	N46° 8.6066'	W57° 31.4365'	<i>Anthoptilum murrayi</i>
R2041-21	N46° 8.7176'	W57° 31.4633'	<i>Anthoptilum sp.</i>
R2038-10	N45° 43.7391'	W56° 51.178'	<i>Pennatula aculeata</i>
R2035 #341	N45° 31.8903'	W56° 39.9928'	<i>Pennatula aculeata</i>
R2035 #378	N45° 31.8818'	W56° 39.9933'	<i>Pennatula aculeata</i>
R2035 #349	N45° 31.88'	W56° 39.9875'	<i>Pennatula aculeata</i>
R2035 #308	N45° 31.9009'	W56° 40.0436'	<i>Pennatula aculeata</i>
R2042-8	N46° 5.6136'	W57° 14.6986'	<i>Pennatula aculeata</i>
R2042-26	N46° 5.1909'	W57° 15.6002'	<i>Pennatula aculeata</i>
R2038-5	N45° 43.7456'	W56° 51.1678'	<i>Pennatula aculeata</i>
R2038-12	N45° 43.7412'	W56° 51.1613'	<i>Pennatula aculeata</i>
R2042-10	N46° 5.6095'	W57° 14.6969'	<i>Pennatula aculeata</i>
R2038-21	N45° 43.739'	W56° 51.1786'	<i>Pennatula aculeata</i>
R2042-9	N46° 5.6095'	W57° 14.697'	<i>Pennatula aculeata</i>
R2042-25	N46° 5.2121'	W57° 15.5825'	<i>Pennatula aculeata</i>
R2035-400	N45° 31.9268'	W56° 40.0923'	<i>Funiculina quadrangularis</i>
R2038-16	N45° 43.7268'	W56° 51.1813'	<i>Funiculina quadrangularis</i>
R2038-4	N45° 43.7462'	W56° 51.1689'	<i>Funiculina quadrangularis</i>
R2038-15	N45° 43.7294'	W56° 51.18'	<i>Funiculina quadrangularis</i>
R2038-17	N45° 43.7273'	W56° 51.1806'	<i>Funiculina quadrangularis</i>
5256-1	N43° 43.8233'	W52° 52.5667'	<i>Funiculina quadrangularis</i> (Trawl)
5256-2	N43° 43.8233'	W52° 52.5667'	<i>Funiculina quadrangularis</i> (Trawl)
5256-3	N43° 43.8233'	W52° 52.5667'	<i>Funiculina quadrangularis</i> (Trawl)
5256-4	N43° 43.8233'	W52° 52.5667'	<i>Funiculina quadrangularis</i> (Trawl)
5256-5	N43° 43.8233'	W52° 52.5667'	<i>Funiculina quadrangularis</i> (Trawl)

5256-6	N43° 43.8233'	W52° 52.5667'	<i>Funiculina quadrangularis</i> (Trawl)
5256-7	N43° 43.8233'	W52° 52.5667'	<i>Funiculina quadrangularis</i> (Trawl)
5256-8	N43° 43.8233'	W52° 52.5667'	<i>Funiculina quadrangularis</i> (Trawl)
5256-9	N43° 43.8233'	W52° 52.5667'	<i>Funiculina quadrangularis</i> (Trawl)
3491-230	N45° 45.7250'	W56° 56.8883'	<i>Funiculina quadrangularis</i> (Trawl)
3491-231	N45° 45.7250'	W56° 56.8883'	<i>Funiculina quadrangularis</i> (Trawl)
3491-232	N45° 45.7250'	W56° 56.8883'	<i>Funiculina quadrangularis</i> (Trawl)
3491-233	N45° 45.7250'	W56° 56.8883'	<i>Funiculina quadrangularis</i> (Trawl)
3491-234	N45° 45.7250'	W56° 56.8883'	<i>Funiculina quadrangularis</i> (Trawl)
R2035-20	N45° 31.9502'	W56° 40.1694'	<i>Protoptilum carpenteri</i>
R2042-14	N46° 5.7308'	W57° 14.6101'	<i>Protoptilum carpenteri</i>
R2039-3	N45° 44.0621'	W56° 50.9827'	<i>Protoptilum carpenteri</i>
R2041-31	N46° 8.6704'	W57° 31.4459'	<i>Kophobelemnon stelliferum</i>
R2041-28	N46° 8.6815'	W57° 31.4491'	<i>Kophobelemnon stelliferum</i>
R2040-22	N45° 56.4377'	W57° 22.56'	<i>Kophobelemnon stelliferum</i>
R2041-26	N46° 8.6848'	W57° 31.4447'	<i>Kophobelemnon stelliferum</i>
R2041-36	N46° 8.4914'	W57° 31.5157'	<i>Kophobelemnon stelliferum</i>

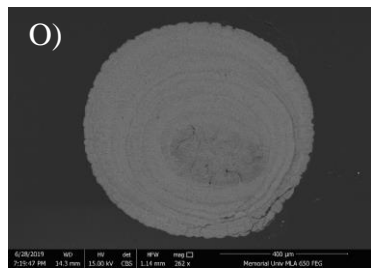
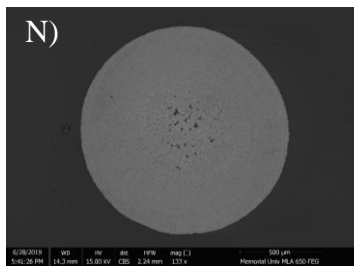
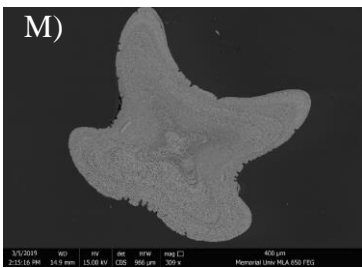
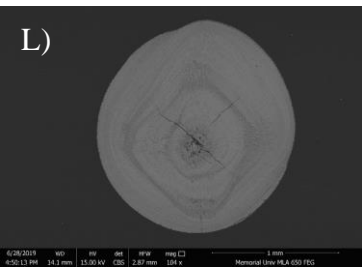
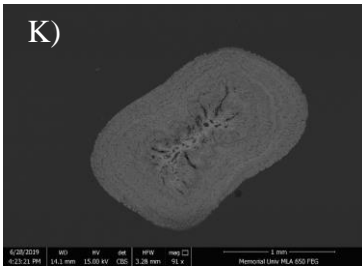
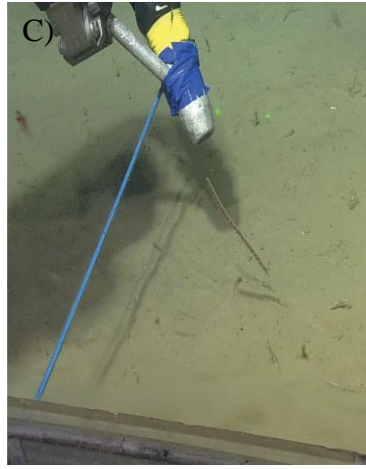


Figure 2-5. Images showing several sea pen species in situ A-E: A) *Anthoptilum* sp., B) *Pennatula aculeata*, C) *Funiculina quadrangularis*, D) *Protoptilum carpenteri*, E) *Kophobelemnion stelliferum*, and their whole colonies (F-J), and their cross sections under SEM (K-O), respectively. Tape measurements are in cm.

2.2.3 Growth ring microanalysis via SEM-EDX

The estimated detection limit of each element in SEM-EDX spot analysis is shown in Table 2-3. Five spots were taken in the dark rings and five spots were taken in the light rings in each colony for each species. The ability to obtain high-resolution images and elemental compositions within sea pen skeletons has the potential for determination of cyclicity among the elements, detection of elemental concentrations that can be used as proxies that might be correlated to growth (i.e., porosity via calcium concentrations), and elucidation of anatomical detail. The elements monitored during these analyses were Na, Mg, Al, Si, P, S, Cl, Ca, and Ba due to their detectability using SEM-EDX analyses and their presence in seawater. Lighter elements such as carbon, nitrogen, and oxygen are not detectable in the SEM-EDX and thus were not measured. These analyses were performed using a FEI MLA 650F equipped with dual Bruker 5th generation Xflash SDD X-ray detectors (CREAIT MAF-Facility, Memorial University of Newfoundland). Elemental spot analysis made it possible to view the composition of the skeleton in general, while highlighting sulfur and chlorine-rich inclusions such as silt and grains that most likely come from evaporated seawater or organics. For the collection of spectra, dwell time was set to 20 μ s with an electron beam diameter of 1-2 microns. The overall detection area of the SEM-EDX beam spot size was \sim 5 μ m, and the effective spatial resolution was \sim 10 μ m.

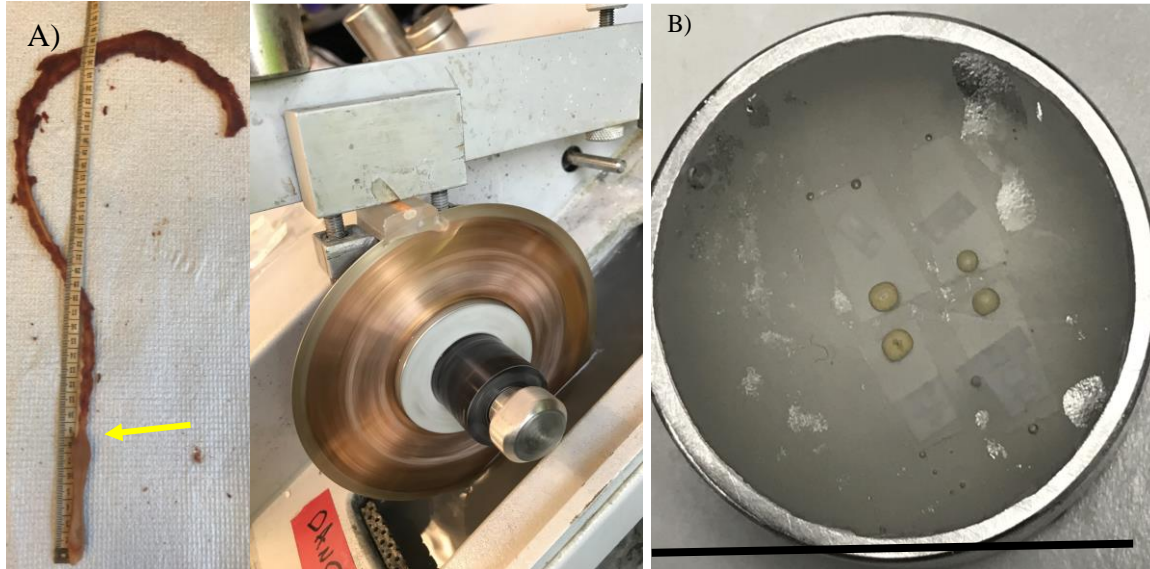


Figure 2-6. (A) Thickest point in *Anthoptilum* sp. (indicated by a yellow arrow) and an Isomet saw, (B) cut thin sections placed in metal rings for SEM-BSE imaging. Scale bar: 1.5 cm.

2.2.4 Skeletal composition via XRD

X-ray diffraction (XRD) analysis was used to characterize the bulk mineralogy of the axis in one colony from each species of sea pen (*Anthoptilum grandiflorum*, *Pennatula aculeata*, *Funiculina quadrangularis*, *Protoptilum carpenteri*, *Kophobelemnon stelliferum*). One complete axis from each species was crushed into a fine powder weighing 0.5-1 g using a ceramic mortar and pestle. The XRD analysis was conducted at the Earth Resources Research and Analysis (CREAIT TERRA) Facility, Memorial University of Newfoundland, using a Rigaku Ultima-IV with a Cu source used in Bragg-Brentano configuration (Neves et al., 2015; Neves et al., 2018b). Due to their small axes, ages, and porous skeletons, the application of bomb- ^{14}C analysis or other isotope analyses to verify the growth rates and ages for these samples was not possible.

2.3 Results

2.3.1 Growth ring characteristics

Based on the XRD analyses, the sea pens discussed in this thesis are all composed of high magnesium calcite (Fig. 2-7A-E). Each species presented distinct dark and light growth rings within their axes. High concentrations of pores approximately 1-3 μm in size made up the dark growth rings, while fewer, smaller pores made up the light growth rings (Fig. 2-8, 2-9). High resolution images of each species' growth rings are shown to highlight the slight differences in growth ring formation between species (i.e., growth ring ambiguity). Growth rings were not uniformly distributed due in part to the changing axis shape as each species grew. *Anthoptilum* spp. began with an elongated shape in the peduncle that transitioned into a circular shape with distance from the base (Fig. 2-10). *P. aculeata* began with a squared shape in the peduncle and evolved into a circular shape with distance from the base (Fig. 2-11). *F. quadrangularis* maintained its four-lobed structure throughout its axis, becoming thinner with distance from the base (Fig. 2-12). *P. carpenteri* and *K. stelliferum* both maintained a rounded structure throughout their axes, becoming thinner with distance from the base (Fig. 2-13, 2-14). Based on the distances between each growth ring couplet, rings were observed to be thickest around the center of the axis, thinnest in the middle, becoming thicker again in the outermost region (Fig. 2-15). Observed in all species in between these thicker growth ring couplets were several thinner, less prominent light and dark growth rings that were difficult to enumerate (Fig. 2-15). Found dispersed within the growth rings of each species in all colonies were a variety of additional anatomical features that occurred throughout the axes (Fig. 2-16). Within *Anthoptilum* spp., tadpole-like anatomical features were present that were both black and light in color and were up to 100 μm in size (Fig. 2-16A). These tadpole-like

features were not found in the other species. The features within *P. aculeata* (Fig. 2-16B), *F. quadrangularis* (Fig. 2-16C), *P. carpenteri* (Fig. 2-16D) and *K. stelliferum* (Fig. 2-16E) varied in their shapes, were light in color, and were up to 10 μm in size.

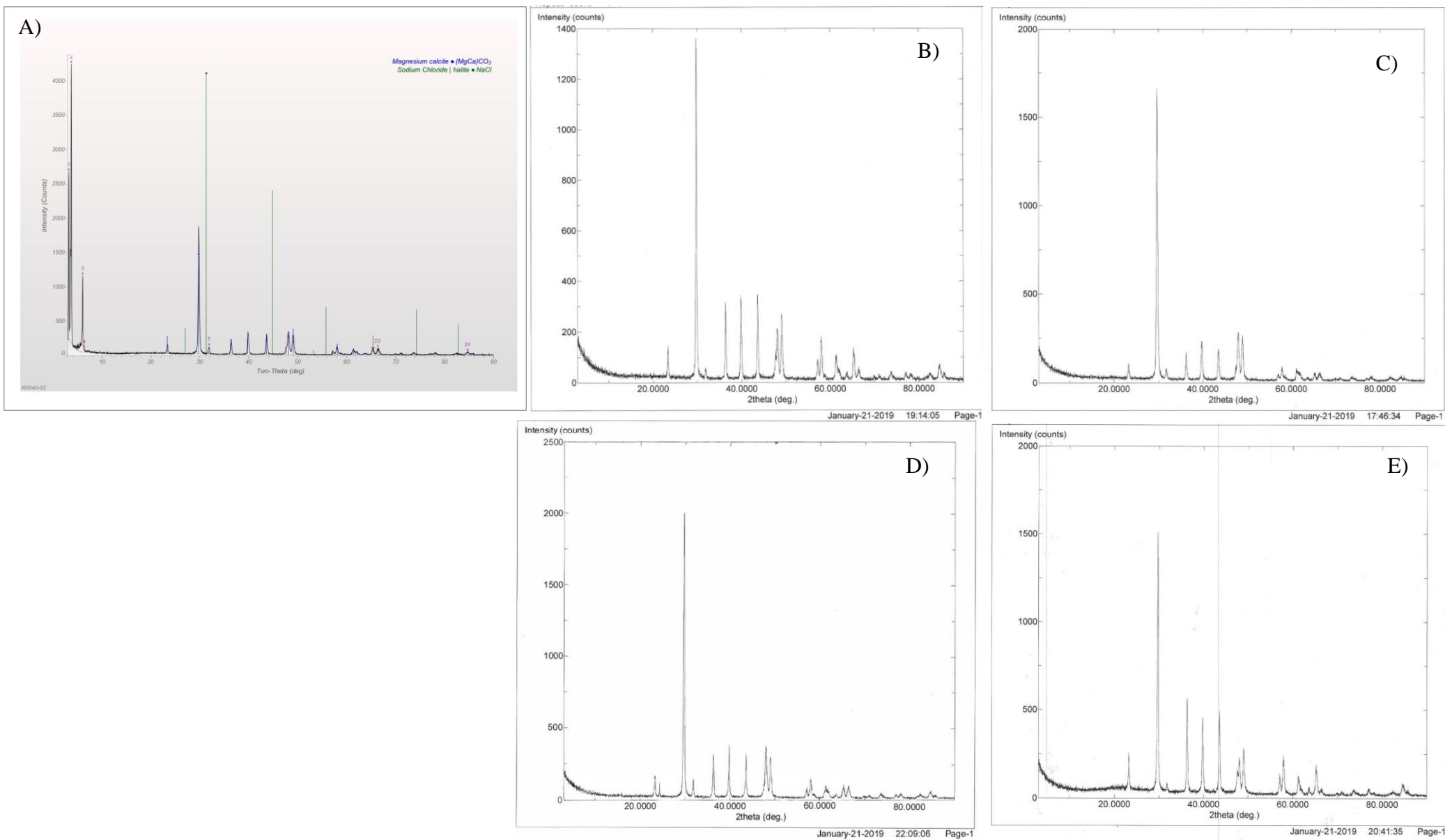


Figure 2-7. X-ray diffraction analysis for the carbonate portion of the skeleton in (A) *Anthoptilum grandiflorum*, (B) *Pennatula aculeata*, (C) *Funiculina quadrangularis*, (D) *Kophobelemnon stelliferum*, and (E) *Protophilum carpenteri*.

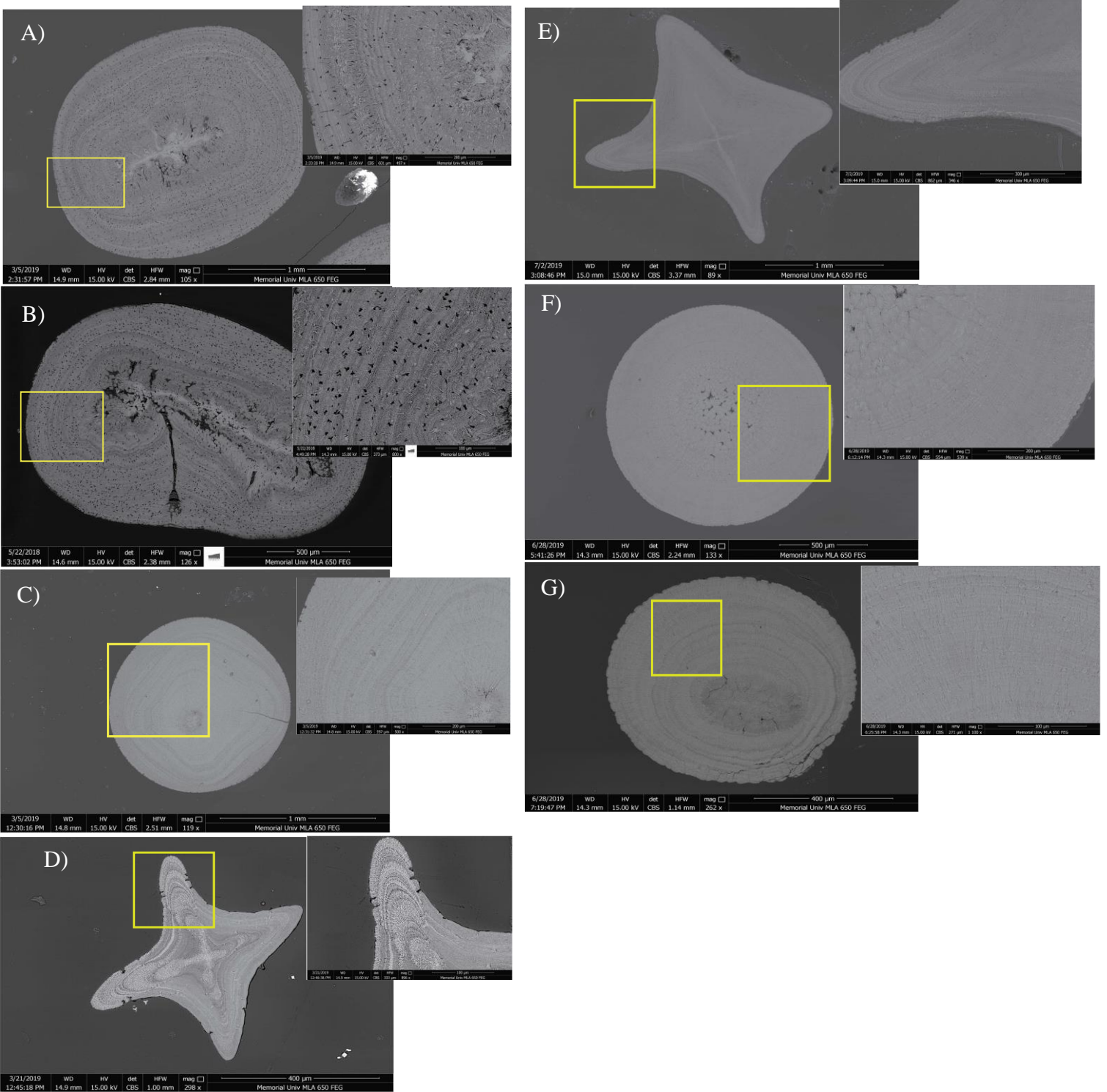


Figure 2-8. A-G) SEM-BSE images of cross-sections taken from the axis of several sea pen species with high magnification images of their growth rings: (A) *Anthoptilum grandiflorum*, (B) *Anthoptilum murrayi*, (C) *Pennatula aculeata*, (D) juvenile *Funiculina quadrangularis*, (E) adult *Funiculina quadrangularis*, (F) *Protoptilum carpenteri*, (G) *Kophobelemnion stelliferum*.

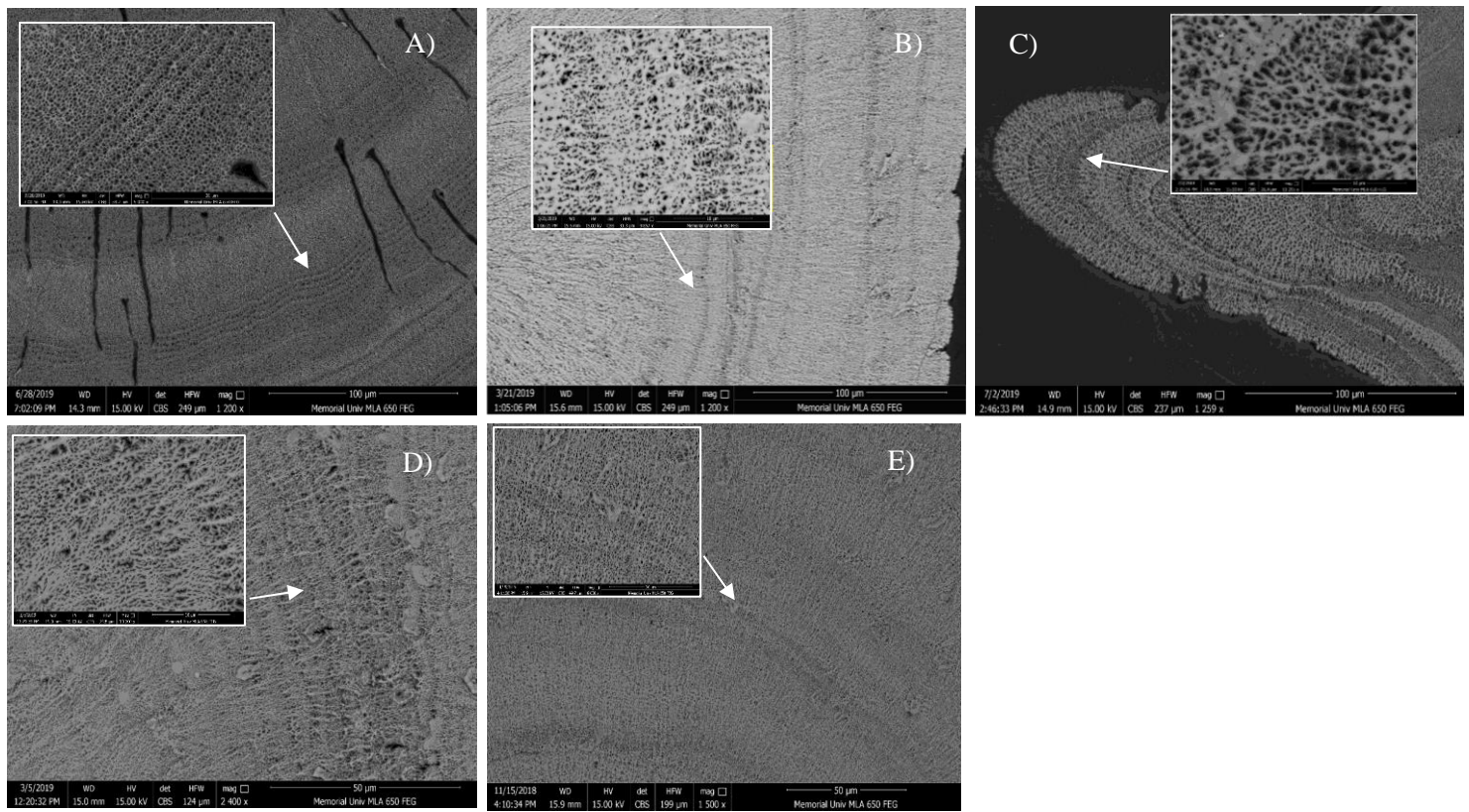


Figure 2-9. SEM-BSE images of the light and dark growth rings found in: (A) *Anthoptilum grandiflorum*, (B) *Pennatula aculeata*, (C) *Funiculina quadrangularis*, (D) *Protoptilum carpenteri*, (E) *Kophobelemnon stelliferum*.



Figure 2-10. Image of a colony of *Anthoptilum* sp. (sample # R2038-8) (right), (A) its cross-sections taken at 30 cm in the rachis, (B) at 12 cm in the rachis above the peduncle, (C) and at the transition point between the end of the peduncle and the beginning of the rachis (location of cross sections indicated by yellow arrows). Cross-sections were imaged under SEM-BSE.

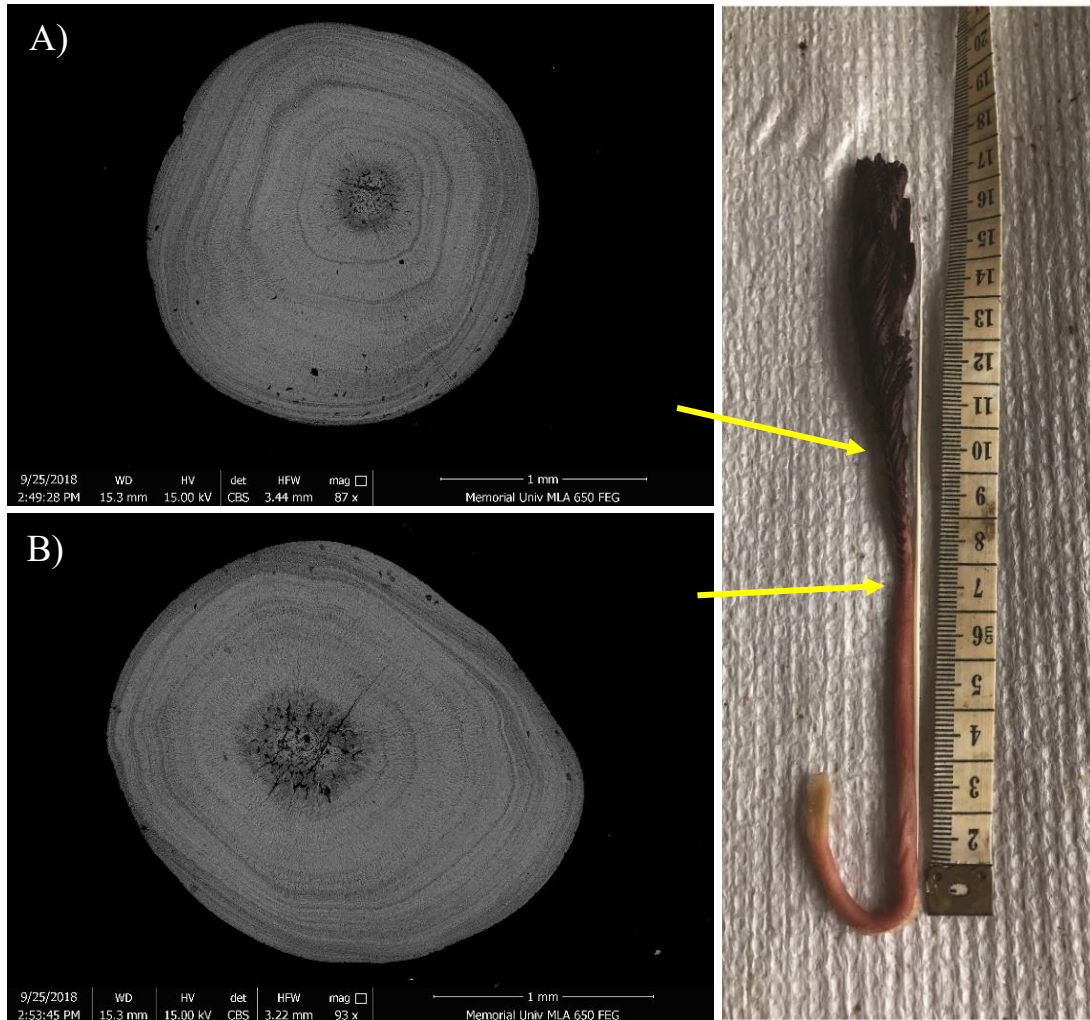


Figure 2-11. Image of a colony of *Pennatula aculeata* (sample # R2038-18) (right), (A) its cross-sections taken at 10 cm in the rachis, (B) and at the transition point between the end of the peduncle and the beginning of the rachis (location of cross-sections indicated by yellow arrows). Cross-sections were imaged under SEM-BSE.

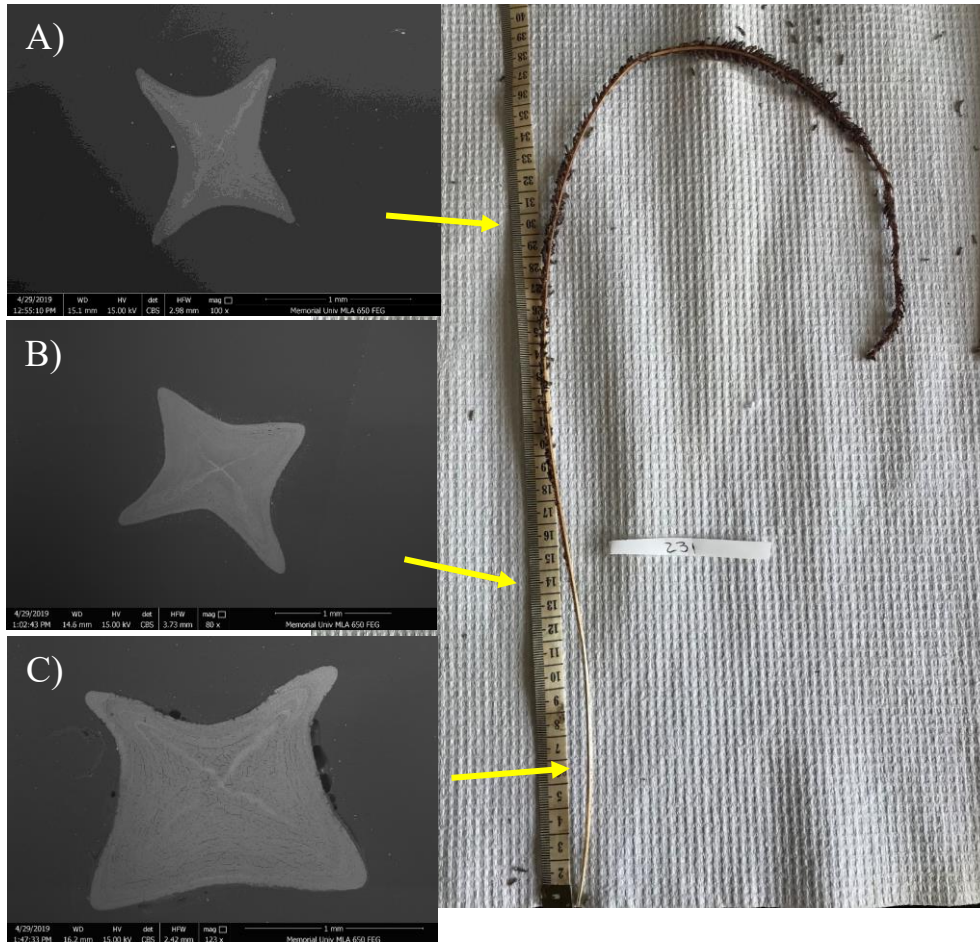


Figure 2-12. Image of a colony of *Funiculina quadrangularis* from within the Laurentian Channel MPA (sample # 231) (right), (A) its cross-sections taken at 30 cm in the rachis, (B) at the transition point between the peduncle and the rachis, (C) and below this point in the peduncle (location of cross-sections indicated by yellow arrows). Cross-sections were imaged under SEM-BSE.

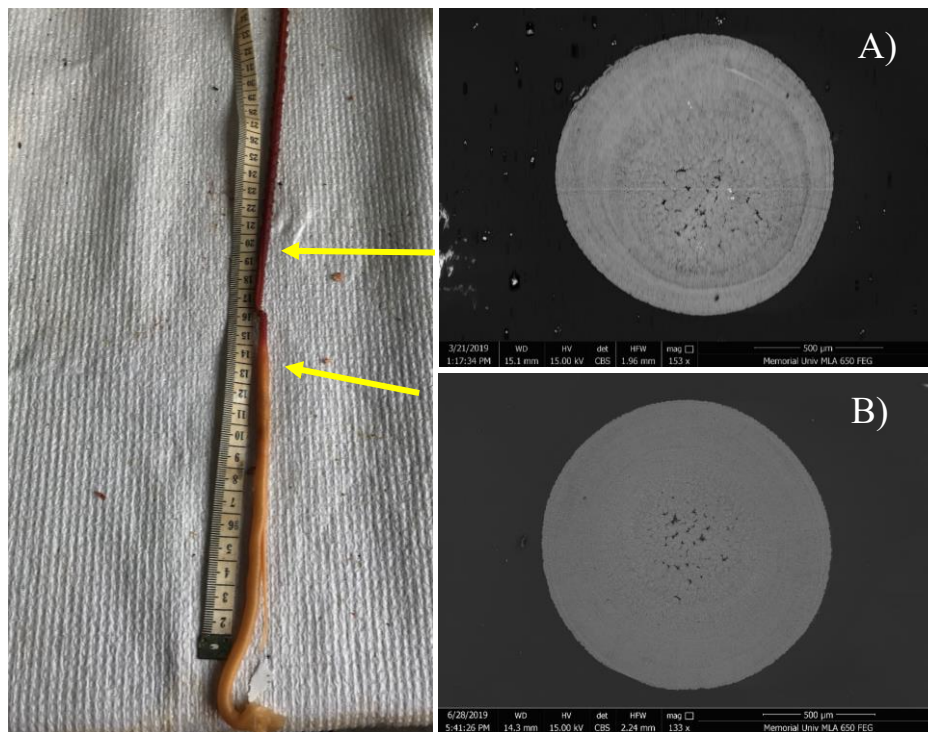


Figure 2-13. Image of *Protopitulum carpenteri* colony (left), (A) its cross-sections taken at 20 cm in the rachis, (B) and at the transition point between the end of the peduncle and the beginning of the rachis (location of cross-sections indicated by yellow arrows). Images on right were taken with SEM-BSE for the cross sections indicated by yellow arrows.



Figure 2-14. Image of a *Kophobelemnion stelliferum* colony (right), (A) its cross-sections taken at 8 cm in the rachis, (B) and at the transition point between the end of the peduncle and beginning of the rachis (location of cross-sections indicated by yellow arrows).

Cross-sections were taken under SEM-BSE.

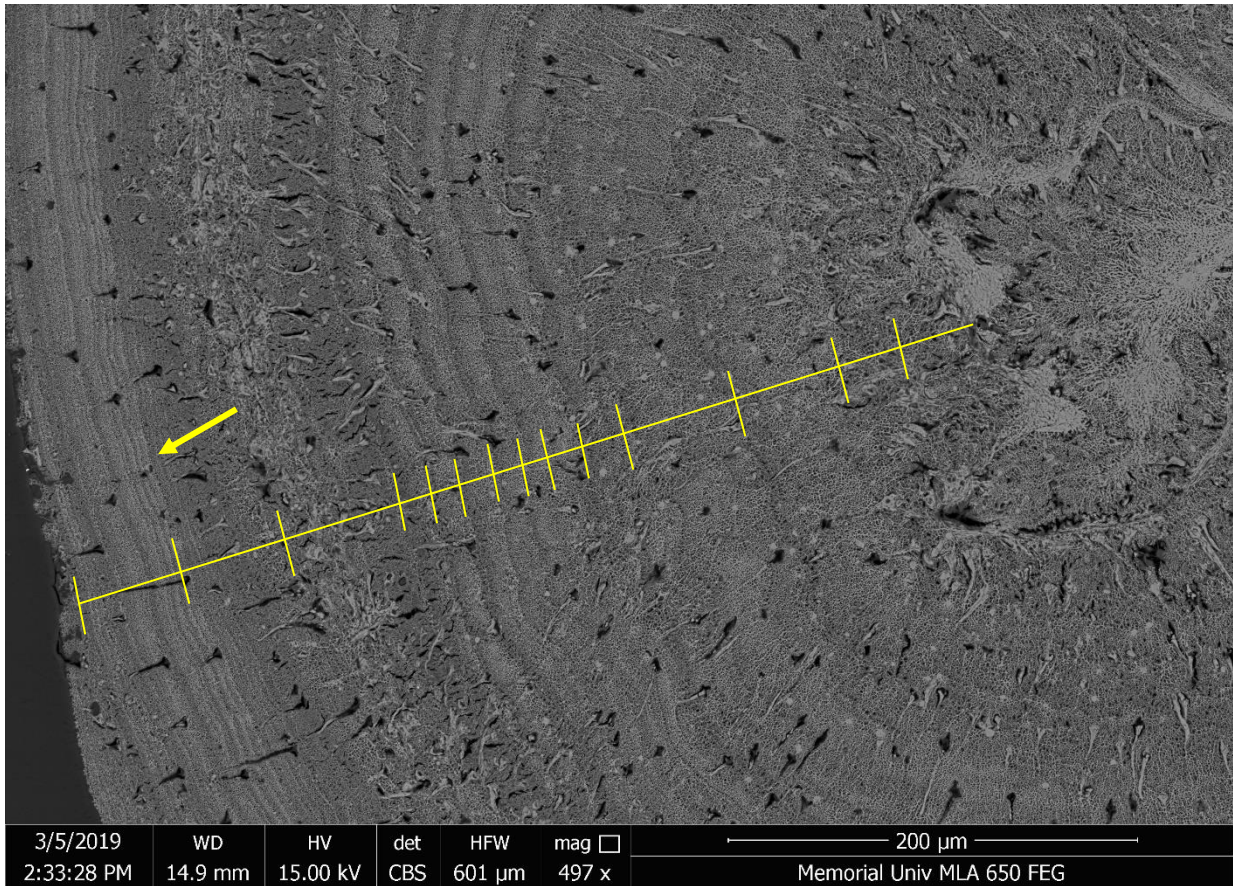


Figure 2-15. 200 μm SEM-BSE image of the growth ring increments in a cross-section of *Anthoptilum* sp. showing the thicker banding in the beginning of growth, thinner banding in the middle of growth, and thicker banding towards the end of growth (indicated by the yellow markings). Also shown are the thinner growth rings observed in between the thicker growth rings (indicated by the yellow arrow) (sample R2041-22).

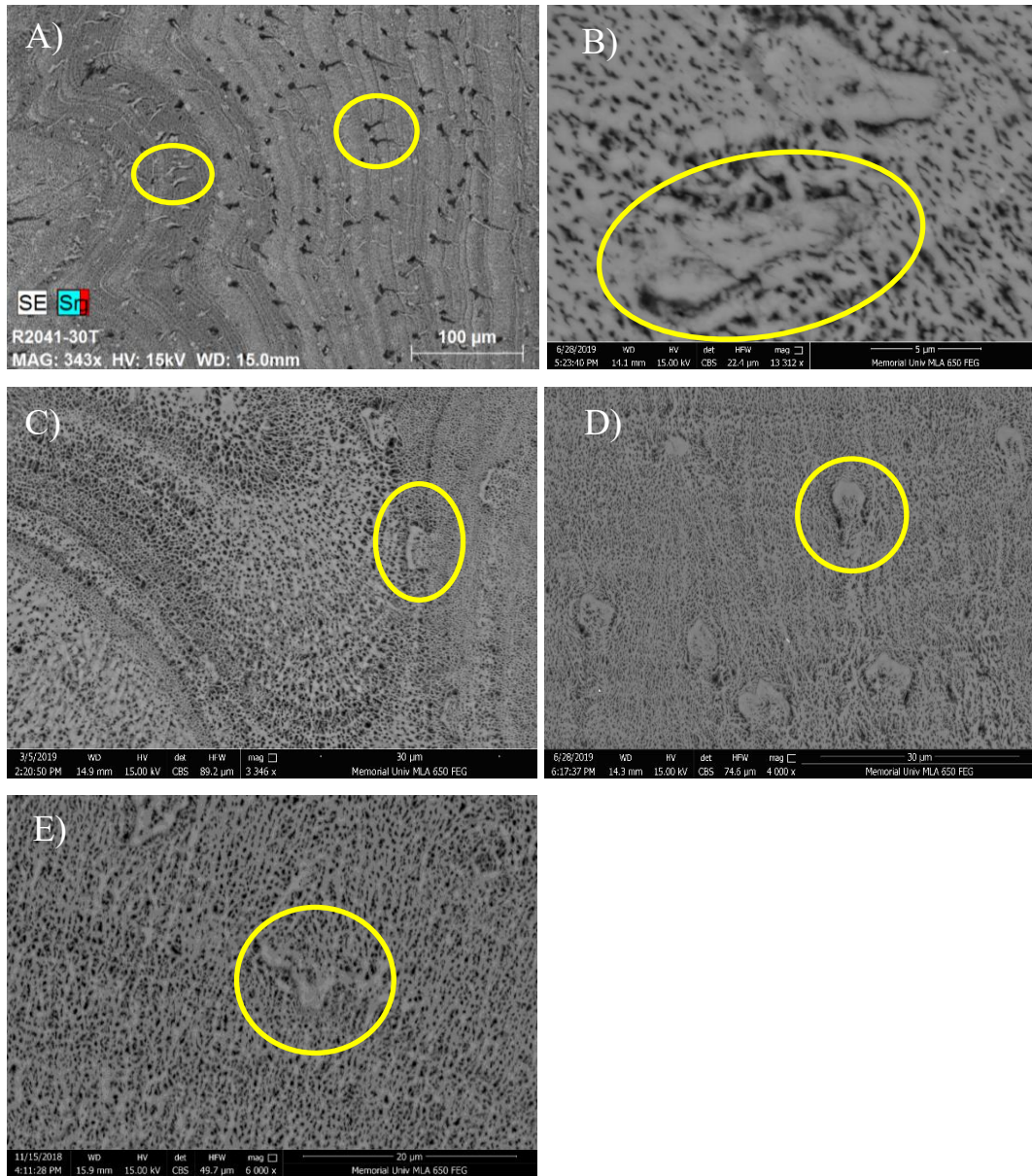


Figure 2-16. SEM-BSE images of the additional anatomical features within the growth rings of each species (indicated by yellow circles): (A) *Anthoptilum grandiflorum*, (B) *Pennatula aculeata*, (C) *Funiculina quadrangularis*, (D) *Protoptilum carpenteri*, (E) and *Kophobelemnon stelliferum*.

2.3.2 Characteristics in the center of the axis

The center region of the axis in each species presented unique structures and patterns with various cracks, holes and black spots that are different than what is found in the surrounding growth rings. *Anthoptilum grandiflorum* and *Anthoptilum murrayi* both had long, thin centers that were lighter in color than the surrounding skeleton (Fig. 2-17, 2-18A). Large and small cracks were observed in almost all colonies except for those with round centers. *P. aculeata* colonies presented centers circular in shape with several large holes, cracks, and an abundance of tiny black spots (Fig 2-18B). *Funiculina quadrangularis* presented a four-lobed center that was thicker in juveniles compared to the adult colonies (Fig. 2-18C,D). Black pores and circular features were common and dispersed throughout this region in all colonies. Cracks were most present within the center region of adult colonies and were not found within the juvenile colonies. *Protoptilum carpenteri* presented a circular center made up of pentagon-shaped features and large holes in all colonies (Fig. 2-18E, 2-19). In one colony a tiny hole around 1 μm in size was found (Fig. 2-19D). *Kophobelemnon stelliferum*'s center was oval-shaped in all colonies with a high concentration of tiny black pores, some cracks, and several rounded features (Fig. 2-18F, 2-20, 2-21).

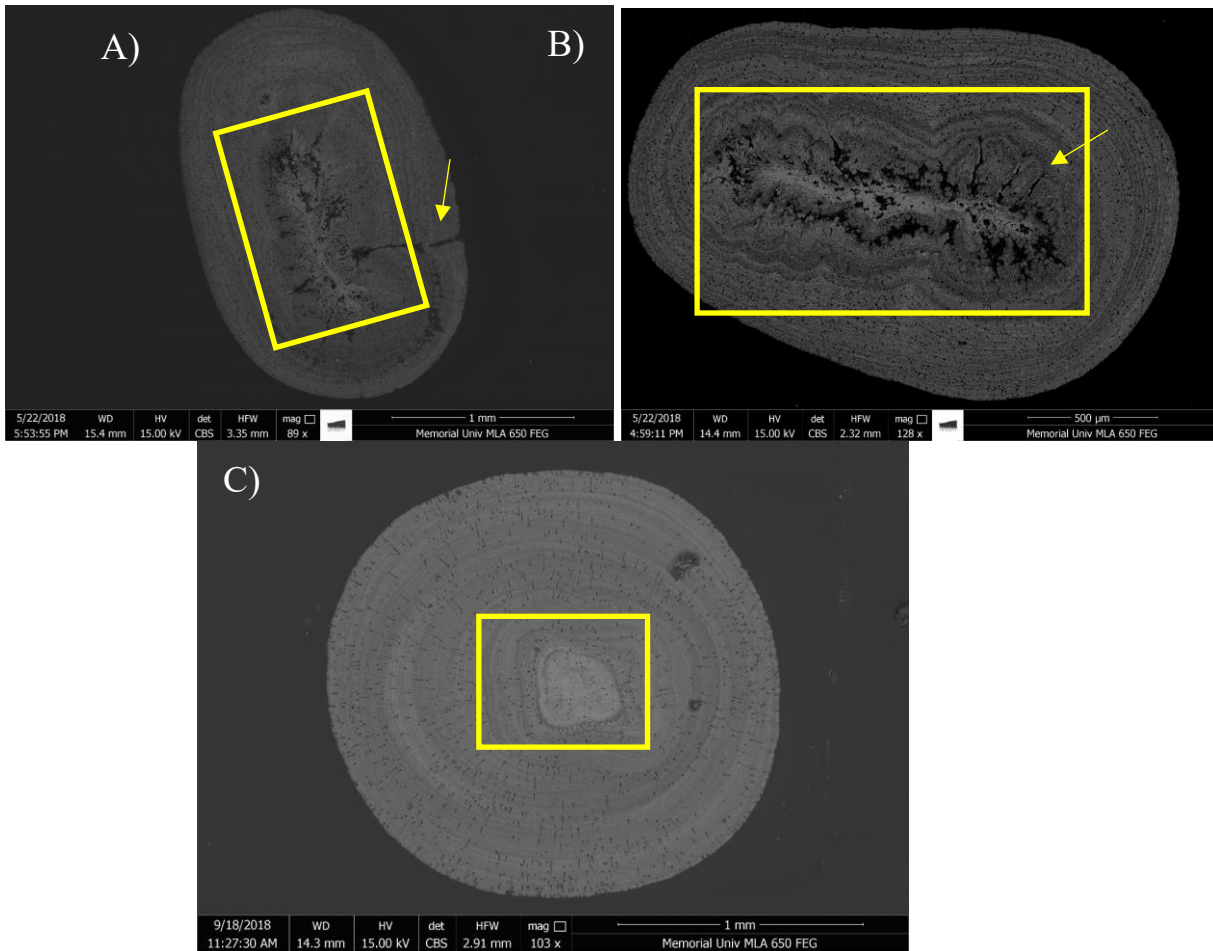


Figure 2-17. SEM-BSE images of cross sections taken in the rachis of (A) *Anthoptilum grandiflorum* (sample # R2041-23), (B) *Anthoptilum murrayi* (sample # R2041-30), and (C) *Anthoptilum* sp. (sample # R2038-6). Highlighted are the elongated, light-colored centers and the rounded center (yellow rectangle), and the cracks present (yellow arrows).

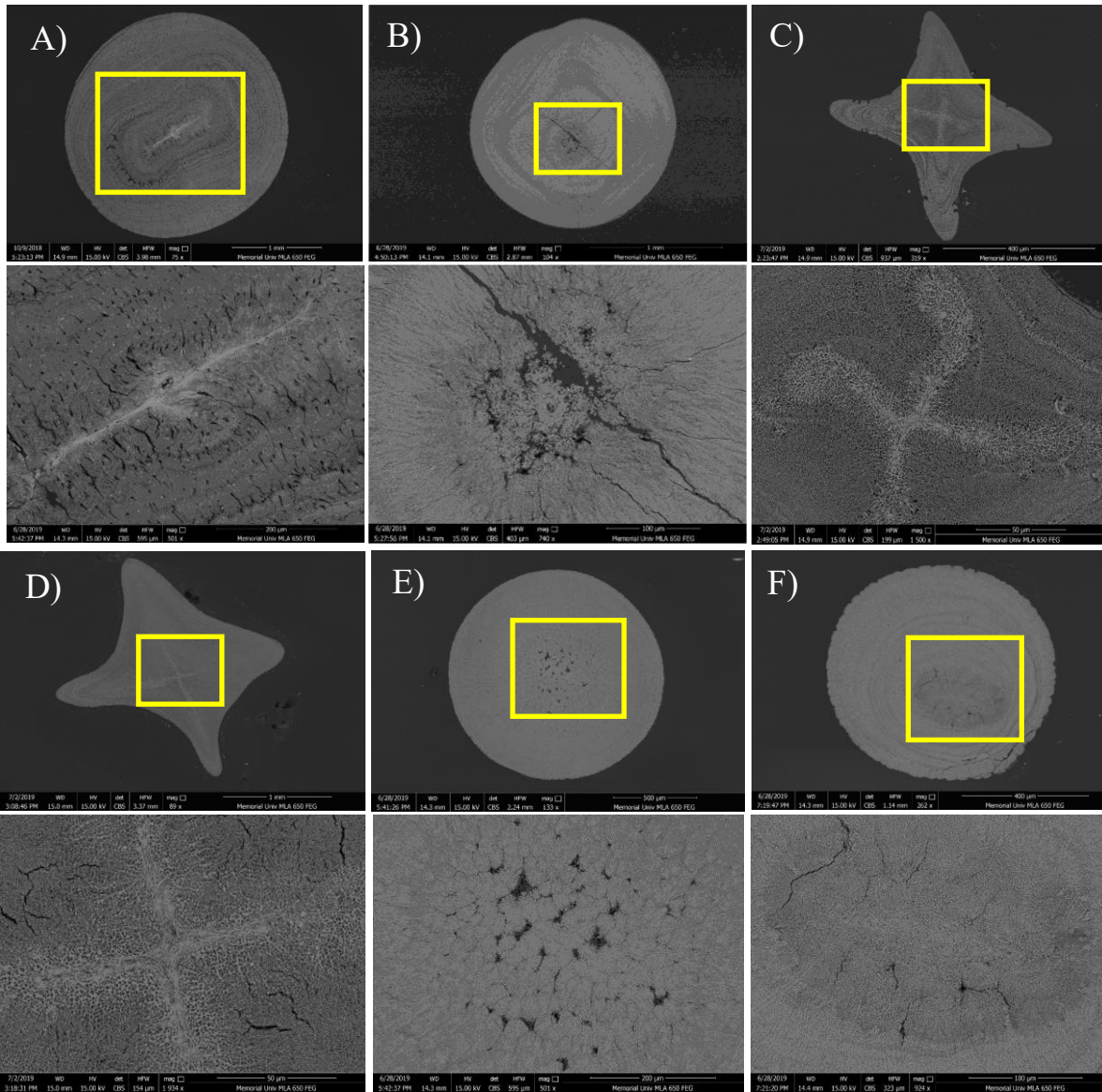


Figure 2-18. SEM-BSE images of the centers observed in: (A) *Anthoptilum grandiflorum*, (B) *Pennatula aculeata*, (C) juvenile *Funiculina quadrangularis*, (D) adult *Funiculina quadrangularis*, (E) *Protoptilum carpenteri*, and (F) *Kophobelemnon stelliferum*.

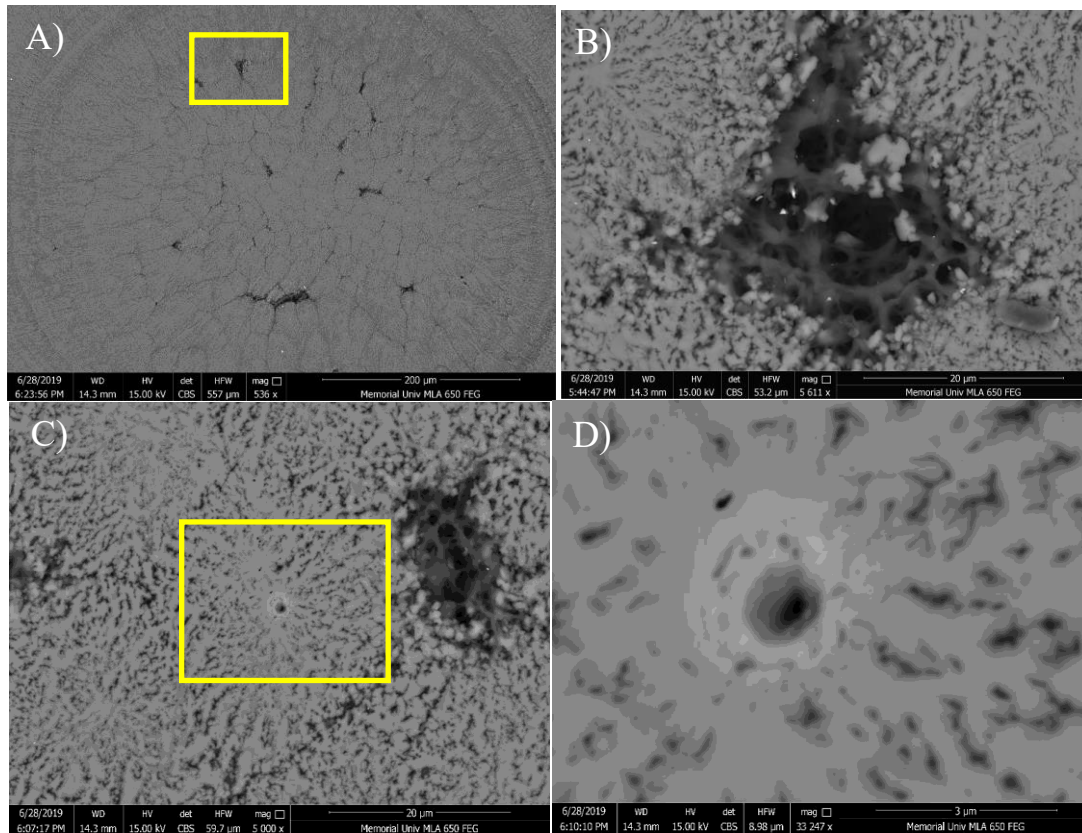


Figure 2-19. (A) 200 μm SEM-BSE image of the center in a colony of *Protoptilum carpenteri*, (B) 20 μm SEM-BSE image of a large void in the center (sample # R2039-3), (C) 20 μm SEM-BSE image of the tiny burrow-like hole in the center, (D) 3 μm close-up SEM-BSE of this same feature.

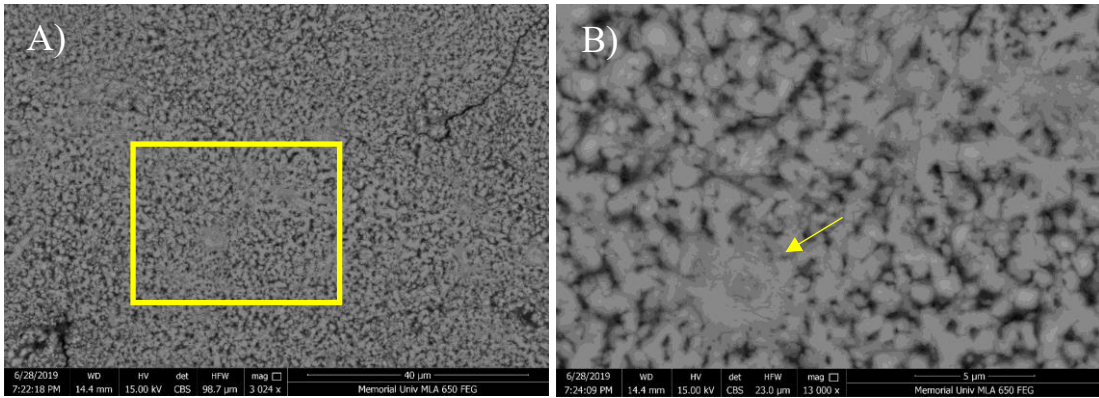


Figure 2-20. (A) 40 μm SEM-BSE image of the center in a colony of *Kophobelemnon stelliferum* showing the tiny black spots, rounded features, and cracks, (B) 5 μm SEM-BSE image of the rounded features found in the center (indicated by yellow arrow).

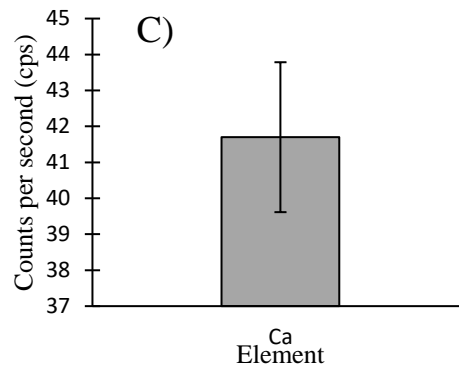
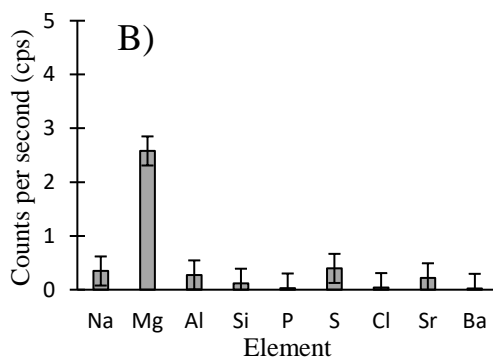
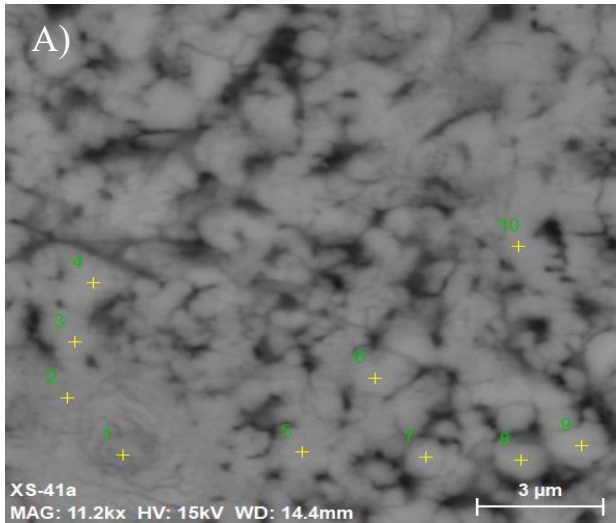


Figure 2-21. (A) SEM image showing the EDX spots taken in the center of a colony of *Kophobelemnon stelliferum*, (B) graph showing elemental X-ray intensities in counts per second (cps) in the light spots, (C) graph showing the calcium present in counts per second (cps) in the light spots. Element composition in the center of the axis was similar across all species. Error bars represent standard error.

2.3.3 Growth ring microanalysis via SEM-EDX

Primary elements that are found in seawater and coral skeletons and that are detectable in SEM-EDX were observed as counts per second (intensity X-rays) (Table 2-3). These values are reported as individual element counts (Me) and as Me/Ca ratio with little variation found between light and dark growth rings (Table 2-4, 2-5). Overall, EDX counts were indiscernible between light and dark rings implying a similar composition (Table 2-4, 2-5). Light rings did not vary from the center to the outer region, generally containing high amounts of Ca averaging between 39-57 counts, low amounts of Mg averaging between 1.9-3.3 counts, and trace amounts of Na, Al, Si, P, S, Cl, Sr, Ba averaging between 0.02-0.64 counts (Fig. 2-22). Dark rings averaged 39-60 counts for Ca, 1.8-3.1 for Mg, and 0.01-0.8 counts for Na, Al, Si, P, S, Cl, Sr, and Ba. Me/Ca ratios in the light and dark rings were both very low (<0.06) (Fig. 2-22). *K. stelliferum* presented the highest counts of Ca in its light rings (57 counts), and *F. quadrangularis* presented the highest counts of Ca in its dark rings (60 counts). Conversely, Mg counts were highest in the light rings of *F. quadrangularis* (3.3 counts), while *K. stelliferum* presented the highest counts of Mg in its dark rings (2.9 counts). Mg/Ca was highest in the light rings in *Anthoptilum* spp. (0.06 counts), and highest in the dark rings in *K. stelliferum* (0.051 counts). The additional anatomical features within the growth rings of each species presented very similar compositions to the bulk growth ring material (Fig. 2-23). The black features within *Anthoptilum* spp. displayed high counts of Ca, and little to no counts of Na, Mg, Al, Si, P, S, Cl, Sr, or Ba. However, the lighter additional features within *Anthoptilum* spp. displayed element counts like that observed in the lighter growth rings.

Table 2-3. Detection limit of each element measured in SEM-EDX spot analyses.

Element	EDX Detection Limit
Na	100 ppm
Mg	100 ppm
Al	10 ppm
Si	10 ppm
P	10 ppm
S	10 ppm
Cl	10 ppm
Ca	1 ppm
Sr	0.1 ppm
Ba	1 ppm

Table 2-4. SEM-EDX spot analysis taken in the light and dark rings in all colonies for each species (*Anthoptilum* spp., *Pennatula aculeata*, *Funiculina quadrangularis*, *Protoptilum carpenteri*, and *Kophobelemnion stelliferum*) showing major elements present in average counts per second (cps). Error is in standard deviation.

Species	Ring	Na	Mg	Al	Si	P	S
<i>Anthoptilum</i> spp.	Light	0.32±0.18	2.4±0.79	0.32±0.17	0.07±0.07	0.04±0.03	0.51±0.0
<i>Anthoptilum</i> spp.	Dark	0.22±0.11	1.8±0.83	0.81±0.39	0.13±0.07	0.15±0.13	0.86±0.1
<i>P. aculeata</i>	Light	0.24±0.14	2.2±0.67	0.11±0.06	0.06±0.05	0.03±0.04	0.43±0.1
<i>P. aculeata</i>	Dark	0.23±0.21	2.2±0.84	0.18±0.13	0.09±0.08	0.07±0.06	0.55±0.1
<i>F. quadrangularis</i>	Light	0.49±0.28	3.3±0.84	0.31±0.23	0.20±0.12	0.08±0.00	0.64±0.1
<i>F. quadrangularis</i>	Dark	0.28±0.21	2.2±0.45	0.22±0.20	0.16±0.05	0.16±0.00	0.86±0.1
<i>P. carpenteri</i>	Light	0.24±0.15	1.9±0.30	0.12±0.04	0.04±0.01	0.01±0.00	0.38±0.0
<i>P. carpenteri</i>	Dark	0.12±0.01	1.8±0.24	0.04±0.02	0.05±0.01	0.03±0.01	0.50±0.0
<i>K. stelliferum</i>	Light	0.21±0.11	3.1±0.94	0.39±0.29	0.16±0.06	0.17±0.00	0.61±0.1
<i>K. stelliferum</i>	Dark	0.28±0.10	2.9±0.82	0.29±0.20	0.13±0.08	0.003±0.00	0.58±0.2

Table 2-5. SEM-EDX spot analysis taken in the light and dark rings of all colonies of *Anthoptilum* spp., *Pennatula aculeata*, *Funiculina quadrangularis*, *Protoptilum carpenteri*, and *Kophobelemnon stelliferum* showing the average major elements to calcium ratios.

Numbers highlighted indicate which ring (light or dark) has a higher ratio for each element per species.

Species	Ring	Na/Ca	Mg/Ca	Al/Ca	Si/Ca	P/Ca	S/Ca	Cl/Ca	Sr/Ca	Ba/Ca
<i>Anthoptilum</i> <i>spp.</i>	Light	0.008	0.06	0.008	1×10^{-3}	1×10^{-3}	0.012	0.008	0.003	0.000
<i>Anthoptilum</i> <i>spp.</i>	Dark	0.005	0.041	0.018	2×10^{-3}	3×10^{-3}	0.019	0.017	0.004	0.000
<i>P. aculeata</i>	Light	0.005	0.05	0.002	1×10^{-3}	0.000	0.009	0.002	0.003	0.000
<i>P. aculeata</i>	Dark	0.005	0.046	0.003	1×10^{-3}	1×10^{-3}	0.011	0.003	0.004	0.000
<i>F.</i>	Light	0.008	0.05	0.005	3×10^{-3}	1×10^{-3}	0.011	0.000	0.008	0.000
<i>quadrangularis</i>										
<i>F.</i>	Dark	0.004	0.037	0.003	2×10^{-3}	2×10^{-3}	0.014	0.001	0.005	0.000
<i>quadrangularis</i>										
<i>P. carpenteri</i>	Light	0.006	0.05	0.003	1×10^{-3}	0.000	0.009	0.003	0.002	0.000
<i>P. carpenteri</i>	Dark	0.002	0.042	1×10^{-3}	1×10^{-3}	0.000	0.011	0.006	0.002	1×10^{-3}
<i>K. stelliferum</i>	Light	0.003	0.05	0.006	2×10^{-3}	0.003	0.010	1×10^{-3}	0.006	0.000
<i>K. stelliferum</i>	Dark	0.004	0.051	0.005	2×10^{-3}	0.000	0.010	1×10^{-3}	0.005	0.000

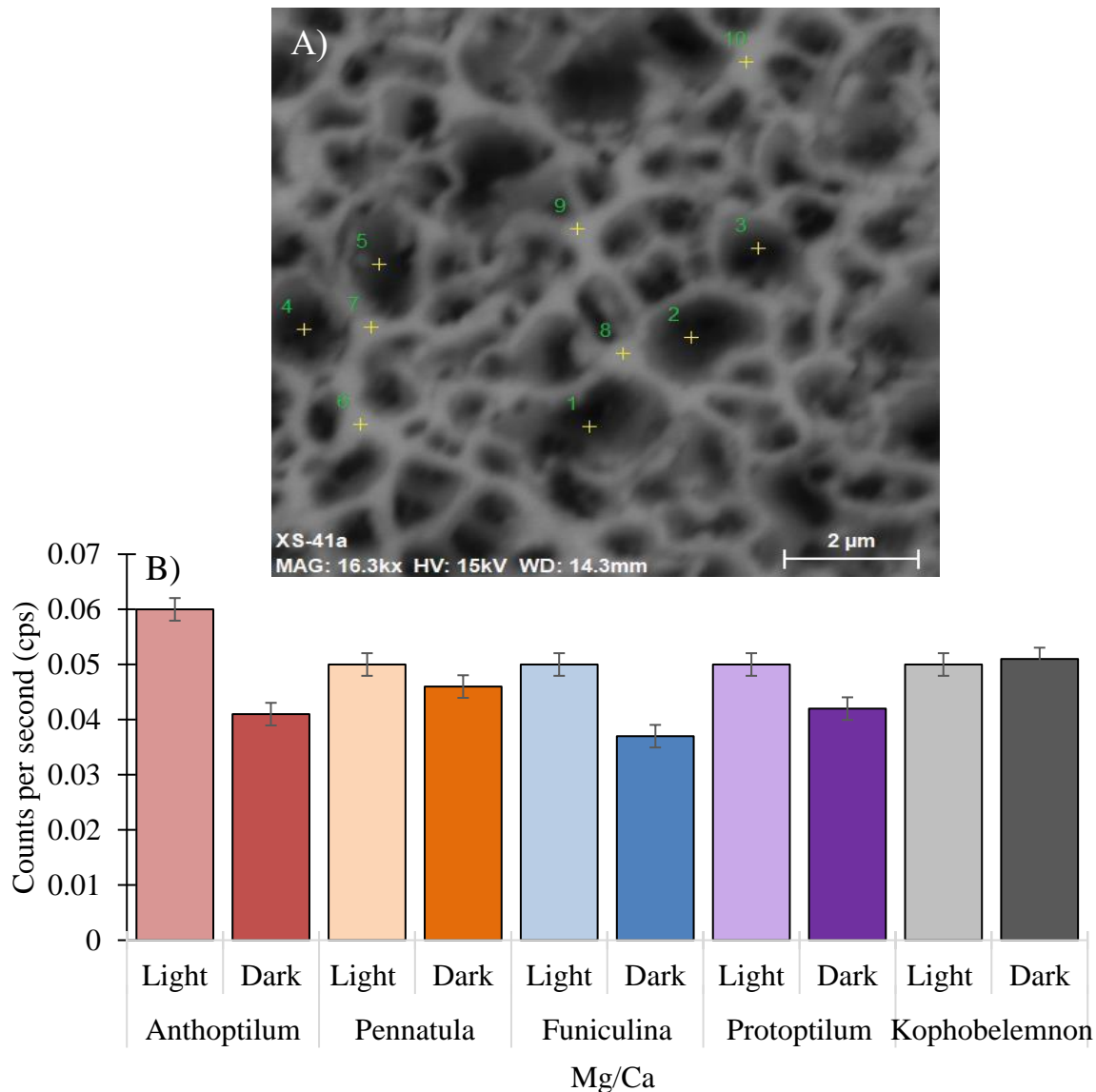


Figure 2-22. (A) Example of the 10 EDX spots chosen in the dark and light growth rings within a colony of *Anthoptilum grandiflorum*, (B) bar graph showing the average ratio for Mg/Ca detected in light and dark growth rings in all colonies collected for each species with a total of 10 spot analyses. Spot numbers (represented by the “+”) 6, 7, 9, and 10 are taken in the light rings while spot numbers 1, 2, 3, 4, and 5 are taken in the dark rings. Dark rings contained a higher proportion of pores. Error bars show standard error.

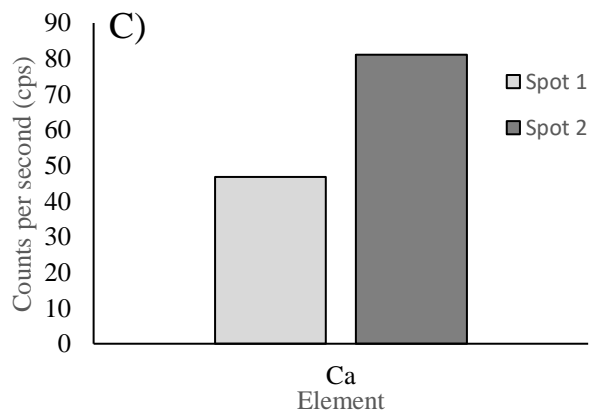
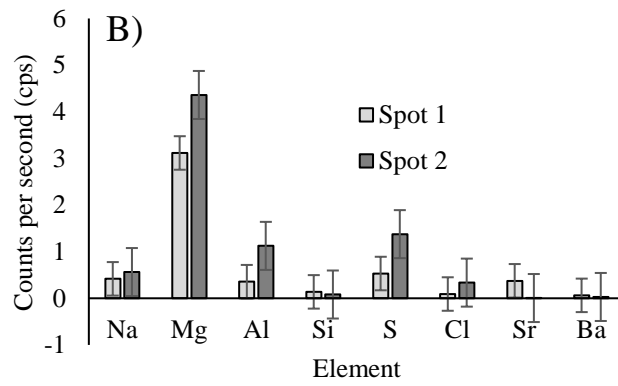
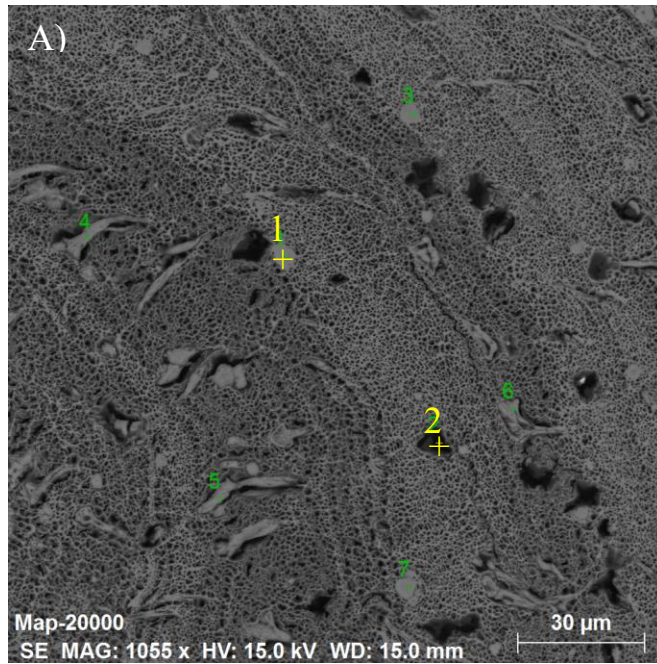


Figure 2-23. (A) SEM-EDX spot analysis (spot locations are represented by the “+”) taken in a colony of *Anthoptilum murrayi* (sample # R2041-30), (B) a bar graph showing the differences in counts per second of each element between the light feature (spot 1) and the dark feature (spot 2), (C) bar graph showing the differences in calcium counts per second between spot 1 and 2. Error bars shown as standard error.

2.4 Discussion

2.4.1 Growth ring characteristics

Six sea pen species were collected from the Laurentian Channel MPA for this study. Growth in each species was indicated by clear, thick couplets of dark and light growth rings that were generally concentric depending on the shape of the cross-section and its center. Each species was very similar in the composition of their light and dark growth rings but presented varying ring shapes and sizes that weren't consistent throughout the cross-section. A Scanning Electron Microscope (SEM) (CREAIT, Memorial University of Newfoundland and Labrador) was used with Back Scattered Electron imaging (BSE), and Energy Dispersive X-ray Spectroscopy (EDX) analysis to characterize growth rings at high resolution. Each species' cross-section became thinner with distance from the base. Cross-sectional shape varied by species: *Anthoptilum* spp. was oval-shaped in its peduncle but became circular in the rachis; *P. aculeata* was squared-shape in its peduncle but became circular in the rachis; *F. quadrangularis* was four-lobed throughout its axis; *P. aculeata* and *K. stelliferum* were circular throughout their axes.

While the overall shape of the growth rings was similar within a single species, no two colonies were identical. Ring widths were quantitatively analyzed in chapter 3 to determine if an event (i.e. high food availability) might have occurred in which all colonies generated thicker growth rings at the same time. While no major event was observed, a common growth pattern was shown amongst all species in which rings were thickest closer to the center of the axis, thinnest in the middle section, and became thick again towards the outer section. This data is shown in chapter 3 and suggests that growth

for these species was slow initially, fast during intermediate stages of growth, and slowed down again as they aged. This change in growth rates might have had an influence on how growth rings were laid down as ring width narrowed in some regions of the cross-section. Marschal et al., (2004) also documented this change in ring width in *Corallium rubrum*, suggesting separate regions of the cross-section could have grown at different growth rates.

Shown in all species within the thicker light and dark couplets were several thin, faint growth rings. These finer growth rings were most discernable within *Anthoptilum* spp. and within the lobes of *F. quadrangularis*, however they were still difficult to enumerate due to their ambiguity. Fine growth rings have been observed in shallow-water corals such as *Porites lobata* and *Porites solida* (Barnes and Lough 1989) and in *Porites australiensis* (Mitsuguchi et al., 2003). These fine rings have been attributed to seasonal flux (i.e., phytoplankton blooms), but have also been documented in certain deep-sea coral species including *Primnoa resedaeformis* (Risk et al., 2002), bamboo corals (Roark et al., 2005), and *Halipterus willemoesi* (Wilson 2002) in which they were found in between thicker, annual bands. Faint, thin bands have also been documented in sea pens *A. grandiflorum* and *P. aculeata* by Murillo et al., (2018), however their periodicity was not proven. Overall, the relationship between food availability and skeletal growth might be relevant to the growth band characteristics observed in these sea pens species and thus more research is necessary to identify the environmental factors responsible for these specific growth patterns at depth.

2.4.2 Growth ring elemental analysis

SEM-EDX spot analyses provided elemental data in counts per second (X-ray intensity of characteristic peaks) for Na, Mg, Al, Si, P, S, Ca, Cl, Sr, and Ba found in light and dark growth rings. These elements were chosen due to their presence in seawater and in coral skeletons (Amiel et al., 1973). In all specimens analyzed, the Mg and Ca counts were effectively the same between the light and dark growth rings as the material detected in the pores of the dark rings was the same as the material detected in the light rings. In the light rings, Mg ranged from 1.9-3.3 cps and 1.8-3.1 cps in the dark rings. Ca ranged from 39-57 cps in the light rings and 39-60 cps in the dark rings. Na, Al, Si, P, S, Cl, and Ba varied depending on the species, however their cps within light rings (0.02-0.64 cps) and dark rings were very similar (0.01-0.8 cps). Element ratios (Me/Ca) for Mg/Ca were slightly higher in light rings for all species (0.05-0.06), while Na/Ca, Al/Ca, Si/Ca, P/Ca, S/Ca, Cl/Ca, Sr/Ca and Ba/Ca varied slightly depending on the species (0.00-0.019). Mg counts were highest in the light rings of *F. quadrangularis* (3.3 cps), while *K. stelliferum* presented the highest counts of Mg in its dark rings (2.9 cps). Mg/Ca was highest in the light rings in *Anthoptilum* spp. (0.06 cps), and highest in the dark rings in *K. stelliferum* (0.051 cps). The additional anatomical features within the growth rings of each species presented very similar compositions to the bulk material of the growth rings (Fig. 2-21). The anatomical black tadpole-like features within *Anthoptilum* spp. displayed high cps of Ca, and little to no cps of Na, Mg, Al, Si, P, S, Cl, Sr, or Ba, and the lighter tadpole-like features within *Anthoptilum* spp. were composed of the same material that was found in the lighter growth rings (Fig. 2-21). These tadpole-like anatomical features might have been where siphonophores occurred prior to collection, however this is yet to be determined. While the element composition in dark rings was

very similar to light rings, dark ring formation could be advantageous for a colony's growth if the darker rings have less dense material than the lighter rings and thus require less energy to produce. We believe it is possible that darker rings take less energy to construct compared to the lighter rings, thus allowing the sea pen colony to continue growing during periods of low energy availability (i.e., food availability). This implies that the dark rings have a lower density than the lighter rings and are primarily composed of pores. Seasonal phytoplankton blooms are known to result in productivity for deep-sea organisms during specific times (Maier et al., 2019a). In cold water coral *Lophelia pertusa*, a long-term reduction in food availability did not reduce skeletal growth, thus suggesting that deep-sea corals quickly adapt to this environment and find other ways to continue growing (i.e., stored energy) (Maier et al., 2019b).

2.5 Conclusions

Light and dark growth rings were present in all species as thick and thin couplets. Dark rings contained a high concentration of pores. Growth ring shapes were rounded in all species except for *Funiculina quadrangularis* which had a four-lobed axis. Based on growth ring thicknesses, growth in each species was observed to be slow in the beginning stages of growth, fast during the intermediate stages of growth, and slow again during the later stages of growth. Element compositions were indistinguishable between these two types of rings with both having very high counts of Ca, high counts of Mg, and very low counts of Na, Al, Si, P, S, Cl, Sr, and Ba. Average counts of Ca were slightly higher in dark rings compared to light rings, and average Mg counts were slightly higher in light rings compared to dark rings. Element composition did not vary much from the center of the axis to the outer regions. Additional anatomical features also presented similar

compositions to the surrounding growth rings. Overall, the darker rings in each species have higher concentrations of black pores compared to the lighter rings, and both rings differ minimally in their elemental counts within each species. While it is unknown what the function of these black pores is and why they have only been observed in the sea pen species discussed in this paper, these findings are imperative in our understanding of growth ring formation in deep-sea corals.

2.6 References

- Adkins J.F., Henderson G.M., Wang S.-L., O'Shea S, Mokadem F., 2004. Growth rates of deep-sea Scleractinia *Desmophyllum cristagalli* and *Enallopsammia rostrata*. *Earth and Planetary Science Letters* 227: 481-490.
- Amiel A.J., Friedman G.M., Miller D.S., 1973. Distribution and nature of incorporation of trace elements in modern aragonitic corals. *Sedimentology* vol 20.
- Andrews A.H., Cordes E.E., Mahoney M.M., Munk K., Coale K.H., Cailliet G.M., Heifetz J., 2002. Age, growth, and radiometric age validation of a deep-sea, habitat-forming gorgonian (*Primnoa resedaeformis*) from the Gulf of Alaska. *Hydrobiologia* 471: 101-110.
- Aranha, R., E. Edinger, G. Layne & G. Piercey, 2014. Growth rate variation and potential paleoceanographic proxies in *Primnoa pacifica*: Insights from high-resolution trace element microanalysis. *Deep Sea Research Part II: Topical Studies in Oceanography* 99: 213-226.
- Atkinson M.J., Carlson B, Crow G.L., 1995. Coral growth in high-nutrient, low-pH seawater: a case study of corals cultured at the Waikiki Aquarium, Honolulu, Hawaii. *Coral Reefs* 14:215–223.
- Baker P.A., Weber J.N., 1975. Coral growth rate: variation with depth. *Earth Planet Sci Lett* 27:57–61.
- Baillon S., English M., Hamel J.F., Mercier A., 2015. Comparative biometry and isotopy of three dominant pennatulacean corals in the Northwest Atlantic. *Acta Zoologica (Stockholm)* 00: 000-000.

- Birkeland C., 1974. Interactions between a sea pen and seven of its predators. *Ecological Monographs* 44:211–232. doi:10.2307/1942312
- Brahmi C., Kopp C., Domart-Coulon I., Stolarski J., Meibom A., 2012. Skeletal growth dynamics linked to trace-element composition in the scleractinian coral *Pocillopora damicornis*. *Geochimica et Cosmochimica Acta* 99: 146-158.
- Cohen A., Gaetani G., 2010. Ion partitioning and the geochemistry of coral skeletons: solving the mystery of the vital effect. *EMU Notes in Mineralogy*, Vol. 11:377-397.
- Coppari M., Mestice F., Betti F., Bavestrello G., Catellano L., Bo M., 2019. Fragmentation, re-attachment ability and growth rate of the Mediterranean black coral *Antipathella subpinnata*. *Coral Reefs* 38:1-14.
- Fisheries and Oceans Canada, 2020. Atlantic Zone Monitoring Program Website. Retrieved 10 February 2020 from Fisheries and Oceans Canada.
- Gage, J. D. and Tyler, P. A. 1992. Deep-Sea Biology: A Natural History of Organisms at the Deep-Sea Floor. *Cambridge University Press*, Cambridge.
- Gagnon A., Adkins J., Fernandez D., Robinson L., 2007. Sr/Ca and Mg/Ca vital effects correlated with skeletal architecture in a Scleractinian deep-sea coral and the role of Rayleigh fractionation. *Earth and Planetary Science Letters*: Vol. 261(1-2), pp. 280-295.
- Goody A.J., Pond D.W., Bowser S.S., 2002. Ecology and nutrition of the large agglutinated foraminiferan *Bathysiphon capillare* in the bathyal NE Atlantic: distribution within the sediment profile and lipid biomarker composition. *MEPS* 245: 69-82.

Heikoop J.M., Hickmott D.D., Risk M.J., Shearer C.K., Atudorei V., 2002. Potential climate signals from the deep-sea gorgonian coral *Primnoa resedaeformis*. *Hydrobiologia* 471:117-124.

Kulka D.W., Templeman N., 2013. Distribution and habitat associations of selected demersal fish species in the Laurentian Channel and Laurentian Area of Interest (AOI). *DFO Can. Sci. Advis. Sec. Res. Doc. 2013/099*. v + 44 p.

Lough J.M., Barnes D.J., 1989. Possible relationships between environmental variables and skeletal density in a coral colony from the central Great Barrier Reef. *J Exp Mar Bio Eco* 134:221-241.

Lough J.M., Barnes D.J., 2000. Environmental controls on growth of the massive coral *Porites*. *J Exp Mar Biol Ecol* 245:225–243.

Maier S.R., Bannister R.J., Oevelen D., Kutti T., 2019a. Seasonal controls on the diet, metabolic activity, tissue reserves and growth of the cold-water coral *Lophelia pertusa*. *Coral Reefs* 39:173-187.

Maier S.R., Kutti T., Bannister R.J., Breugel P.V., Rijswijk P.V., Oevelen D.V., 2019b. Survival under conditions of variable food variability: Resource utilization and storage in the cold-water coral *Lophelia pertusa*. *Limnology and Oceanography* 64:4.

Marschal C., Garrabou J., Harmelin J.G., Pichon M., 2004. A new method for measuring growth and age in the precious red coral *Corallium rubrum* (L.). *Coral Reefs* 23:423-432.

Meibom A., Cuif J.P., Hillion F., Constantz B.R., Juillet-Leclerc A., Dauphin Y., Watanabe T., Dunbar R.B., 2004. Distribution of magnesium in coral skeleton. *Geophysical Research Letters* Vol. 31, L23306.

Memorial University of Newfoundland, 2019. The Earth Resources Research and Analysis

Facility: Powder X-Ray Diffractor (XRD).

https://www.mun.ca/creait/TERRA/XRD_Main_cs.php

- Mitsuguchi T., Matsumoto E., Uchida T., 2003. Mg/Ca and Sr/Ca ratios of *Porites* coral skeleton: Evaluation of the effect of skeletal growth rate. *Coral Reefs* 22:381-388.
- Mortensen P.B, Buhl-Mortensen L., 2005. Morphology and growth of the deep-water gorgonians *Primnoa resedaeformis* and *Paragorgia arborea*. *Mar Bio* 147:775-788.
- Murillo F.J, MacDonald B.W., Kenchington E., Campana S.E., Sainte-Marie B. & Sacau M., 2018. Morphometry and growth of sea pen species from dense habitats in the Gulf of St. Lawrence, eastern Canada. *Marine Biology Research*, 14:4, 366-382.
- Neves B., Edinger E., Wareham V., Layne G., 2018a. Size metrics, longevity, and growth rates in *Umbellula encrinus* (Cnidaria: Pennatulacea) from the Eastern Canadian Arctic. *Arctic Science* 00: 1-28.
- Neves B., Edinger E., Wareham V., 2018b. Morphology and composition of the internal axis in two morphologically contrasting deep-water sea pens (Cnidaria: Octocorallia). *J Nat Hist*, 52:11-12, 659-685.
- Neves B., Edinger E., Layne G., Hayes V., 2015. Decadal longevity and slow growth rates in the deep-water sea pen *Halipteris finmarchica* (Sars, 1851) (Octocorallia: Pennatulacea): Implications for vulnerability and recovery from anthropogenic disturbance. *The International Journal of Aquatic Sciences, Hydrobiologia* 759: 147-170.
- Risk M.J., Heikoop J.M., Snow M.G., Beukens R., 2002. Lifespans and growth patterns of two deep-sea corals: *Primnoa resedaeformis* and *Desmophyllum cristagalli*. *Biology of Cold Water Corals. Hydrobiologia* 471: 125-131.

- Roark E.B., Guilderson T.P., Flood-Page S.R., Dunbar R.B., Ingram B.L., Fallon S.J., McCulloch M.T., (2005) Radiocarbon-based ages and growth rates for bamboo corals from the Gulf of Alaska. *Geophys Res Lett* 32:L04606.
- Roark E.B., Guilderson T.P., Dunbar R.B., Lynn Ingram B., 2006. Radiocarbon-based ages and growth rates of Hawaiian deep-sea corals. *Mar Ecol Prog Ser* Vol. 327: 1-14.
- Roark E.B., Guilderson T.P., Dunbar R.B., Fallon S.J., Mucciarone D.A., 2009. Extreme longevity in proteinaceous deep-sea corals. *PNAS* 106: 5204-5208.
- Robinson L., Adkins J., Frank N., Gagnon A., Prouty N., Roark B., Flierdt T., 2014. The geochemistry of deep-sea coral skeleton: A review of vital effects and applications for palaeoceanography. *Deep-Sea Research II* 99: 184-198.
- Rollion-Bard C., Blamart D., Cuif J.-P., Juillet-Leclerc A., 2003. Microanalysis of C and O isotopes of azooxanthellate and zooxanthellate corals by ion microprobe. *Coral Reefs* 22:405-415.
- Sherwood, O., Heikoop, A., Sinclair, J.M., Scott, D.J., Shearer C., and Azetsu-Scott, K., 2005a. Skeletal Mg/Ca in *Primnoa resedaeformis*: relationship to temperature. Friewald A, Murray JM (eds) Cold-water corals and ecosystems. *Springer*, Berlin, p. 1061-1079.
- Sherwood O., and Edinger E., 2009. Ages and growth rates of some deep-sea gorgonian and anthipatharian corals of Newfoundland and Labrador. *Can. J Fish. Aquat. Sci.* 66: 142-152.
- Sinclair AF, Conway KW, Crawford WR (2005) Associations between bathymetric, geologic and oceanographic features and the distribution of the British Columbia bottom trawl fishery. ICES CM 2005/L:25.

Wilson M., Andrews A., Brown, A., Cordes E., 2002. Axial rod growth and age estimation of the sea pen, *Halipteris willemoesi* Kolliker. *Hydrobiologia* 471:133-142.

Williams B., Risk M.J., Ross S.W., Sulak K.J., 2006. Deep-water antipatharians: Proxies of environmental change. *USGS Staff Published Research* 1057.

Appendix 2-1. Image of a *Funiculina quadrangularis* colony showing its flexible axis (sample #231).



3. Colony metrics, ages, and growth rates of six sea pen species from the Laurentian Channel Marine Protected Area, Atlantic Canada

Abstract

Six sea pen species were examined from the Laurentian Channel, MPA in the Northwest Atlantic: *Anthoptilum grandiflorum*, *Anthoptilum murrayi*, *Pennatula aculeata*, *Funiculina quadrangularis*, *Protoptilum carpenteri*, and *Kophobelemnon stelliferum*. Major growth rings best represented annual periodicity while minor growth rings best represented seasonal periodicity in all species. A logistic relationship best fit the data between colony metrics and colony length, while a Gompertz relationship best fit the data between number of growth rings and colony length. Number of major growth rings ranged from 3-23 with average in thicknesses between 18 μm and 88 μm wide. Radial growth rates were 0.12 $\text{mm}\cdot\text{year}^{-1}$ for *Anthoptilum* spp., 0.10 $\text{mm}\cdot\text{year}^{-1}$ for *P. aculeata*, 0.08 $\text{mm}\cdot\text{year}^{-1}$ for *F. quadrangularis*, 0.23 $\text{mm}\cdot\text{year}^{-1}$ for *P. carpenteri*, and 0.06 $\text{mm}\cdot\text{year}^{-1}$ for *K. stelliferum*. This is the first study to measure colony metrics and number of growth rings in sea pen *Funiculina quadrangularis*, *Protoptilum carpenteri*, and *Kophobelemnon stelliferum*.

3.1 Introduction

With the knowledge of sea pen growth and longevity, research has now characterized these organisms as VME indicator species based on their sensitivity to anthropogenic disturbances, their slow growth rates, and their slow recovery time (Kenchington et al.,

2014; Murillo et al., 2011, Fuller et al., 2008). The largest marine protected area (MPA) in Atlantic Canada, the Laurentian Channel, is home to large sea pen fields that provide biodiversity and nurseries on the seafloor for a variety of essential species (Fisheries and Oceans Canada 2010). Advancements in age-dating techniques to determine growth rates and longevity in sea pen species is critical for assessing their population structure to establish effective marine conservation (Murillo et al., 2018; Neves et al., 2018a,b, 2015; Wilson et al., 2002).

Growth rings have been recorded within the axis (i.e. skeleton) of several sea pen species that are believed to be indicative of their age (Neves et al., 2018a,b, 2015; Murillo et al., 2018; Sherwood & Edinger 2009; Wilson et al., 2002; Birkeland 1974). Thus far, bomb-radiocarbon dating (bomb-¹⁴C), lead-210 (²¹⁰Pb), and SIMS trace element analysis paired with growth ring counting have been the primary methods used to estimate growth rates and longevity in sea pen species (Neves et al., 2018a; Murillo et al., 2018; Wilson et al., 2002). These applications can be limiting as growth ring counting even when paired with SIMS analyses does not prove periodicity, and bomb-¹⁴C measurements are difficult to take in samples with micrometer-scale growth rings (Murillo et al., 2018). Regardless, techniques such as bomb-¹⁴C, ²¹⁰Pb, U-Th, Accelerator Mass Spectrometry (¹⁴C-AMS), SIMS, trace element analyses, and growth ring counting have proven useful for estimating growth rate and longevity in other deep-sea coral species such as gorgonians, antipatharians, bamboo corals and scleractinians (Hitt et al., 2020; Aranha et al., 2014; Sherwood & Edinger 2009; Roark et al., 2009; Tracey et al., 2007; Roark et al., 2006; Sherwood et al., 2005; Andrews et al., 2005, 2002; Cheng et al., 2000; Grigg 1972).

Growth rings have been presumed annual and sub-annual in certain sea pen species based on their level of ambiguity in which prominent growth rings might represent annual periodicity and faint, less prominent growth rings might represent sub-annual periodicity (Murillo et al., 2018; Neves et al., 2018a, 2015). Neves et al., (2018a) compared the observed number of rings to the estimated number of rings based on size in *Umbellula encrinus*, finding that the observed number of rings and the estimated number of rings were comparable. This suggests that it might be possible to estimate the age from colony size in certain sea pen species assuming that growth rings are annual. Murillo et al., (2018) carried out a similar comparison in *Anthoptilum grandiflorum*, estimating the age of a colony when assuming both faint and prominent rings are annual, and when only prominent rings are annual. Murillo et al., (2018) found that the resulting age estimation was significantly higher if assuming both faint and prominent rings are annual compared to only assuming if prominent rings are annual, however, this did not determine which rings were annual. When paired with logistic and Gompertz growth curves, Murillo et al., (2018) revealed that growth is slow initially, becoming faster during the intermediate stages of growth, and finally slowing down to a plateau once an optimal height is reached for the colony. Sub-annual banding has been documented in studies on cold-water hydrocorals, deep-water bamboo corals, and shallow-water corals, associating these occurrences with seasonal environmental changes (Aranha et al., 2011; Roark et al., 2005; Barnes and Lough 1993; Goldberg 1991; Grigg 1974). Such studies that have identified the relationship between environmental changes and skeletal growth is crucial when assessing the occurrence of sub-annual banding in deep-sea corals. Elucidating annual and sub-annual ring formation in sea pens is imperative to fully understand their growth and population structure as VMEs.

In this study we applied ring counting methods and growth curve analyses as tools for determining estimates of age, growth rates and longevity in sea pen species *Anthoptilum grandiflorum*, *Anthoptilum murrayi*, *Pennatula aculeata*, *Funiculina quadrangularis*, *Protoptilum carpenteri*, and *Kophobelemnion stelliferum* collected from the Laurentian Channel MPA. These are some of the most common sea pen species found in the Laurentian Channel, and this is the first study to document growth ring occurrences in *Funiculina quadrangularis*, *Protoptilum carpenteri*, and *Kophobelemnion stelliferum*.

3.2. Material and methods

3.2.1 Collection and measurements

In 2017, 56 sea pen samples (Table 3-1, Fig. 3-1) were collected from the Laurentian Channel during a joint CHONe DFO ROPOS cruise using ROV manipulator arms and video surveys. During a DFO multispecies trawl survey, 5 *Funiculina quadrangularis* colonies were collected within the Laurentian Channel in 2007, and 9 were collected just outside of the Laurentian Channel in 2009 (Table 3-1, Fig. 3-1). The depth range in which these samples were collected in the Laurentian Channel was between 400-600 m, and around 600 m outside of the Laurentian Channel. Within the Laurentian Channel, seawater temperatures were consistent at all sites at 6.2°C, pH was consistent at 7.9, and salinity was consistent at 35 PSU. Growth characteristics including colony length and peduncle length were measured post-collection using a measuring tape. The colony length was measured from the proximal tip (the base of the colony) to the distal tip (the uppermost point of the colony). The peduncle length for each colony was measured from the base of the colony to the very beginning of polyp appearance (Fig. 3-2). One sample of *Protoptilum carpenteri* was collected without a base or peduncle and

thus was not included in these measurements. Axis diameter, radial and linear growth rates, and growth ring increments were measured using SEM images. The wet weight for each sample was measured to the nearest 0.01 g, however samples with little to no flesh were not included in wet weight-length relationships. Cross-sections were taken within the axis of each specimen and imaged under SEM to count growth rings.

Table 3-1. Sample ID, latitude, longitude, and species collected from the Laurentian Channel MPA. Only 5 samples of *Funiculina quadrangularis* were collected from the MPA, and 14 were collected during the DFO multispecies trawl survey in 2007 and 2009 (Trawl).

Sample	Latitude	Longitude	Species
R2040-20	N45° 56.4349'	W57° 22.5652'	<i>Anthoptilum sp.</i>
R2037-6	N46° 12.6467'	W57° 31.6492'	<i>Anthoptilum sp.</i>
R2041-29	N46° 8.6816'	W57° 31.4488'	<i>Anthoptilum sp.</i>
R2038-6	N45° 43.7405'	W56° 51.1618'	<i>Anthoptilum sp.</i>
R2040-21	N45° 56.1789'	W57° 22.17'	<i>Anthoptilum sp.</i>
R2040-19	N45° 56.3497'	W57° 21.9456'	<i>Anthoptilum sp.</i>
R2040-18	N45° 56.3544'	W57° 21.9494'	<i>Anthoptilum sp.</i>
R2040-8	N45° 56.3544'	W57° 21.9494'	<i>Anthoptilum sp.</i>
R2038-19	N45° 43.743'	W56° 51.1671'	<i>Anthoptilum sp.</i>
R2041-12	N46° 8.7352'	W57° 31.5191'	<i>Anthoptilum sp.</i>
R2041-29	N46° 8.6816'	W57° 31.4488'	<i>Anthoptilum sp.</i>
R2036-14	N45° 52.0306'	W56° 12.1854'	<i>Anthoptilum sp.</i>
R2041-27	N46° 8.6846'	W57° 31.4447'	<i>Anthoptilum grandiflorum</i>
R2038-8	N45° 43.739'	W56° 51.1804'	<i>Anthoptilum grandiflorum</i>
R2041-22	N46° 8.7175'	W57° 31.4636'	<i>Anthoptilum grandiflorum</i>
R2041-23	N46° 8.6911'	W57° 31.4474'	<i>Anthoptilum grandiflorum</i>
R2041-25	N46° 8.6845'	W57° 31.4448'	<i>Anthoptilum grandiflorum</i>
R2041-24	N46° 8.691'	W57° 31.4476'	<i>Anthoptilum grandiflorum</i>
R2041-30	N46° 8.6813'	W57° 31.449'	<i>Anthoptilum murrayi</i>
R2041-32	N46° 8.6066'	W57° 31.4365'	<i>Anthoptilum murrayi</i>
R2041-21	N46° 8.7176'	W57° 31.4633'	<i>Anthoptilum sp.</i>
R2038-10	N45° 43.7391'	W56° 51.178'	<i>Pennatula aculeata</i>
R2035 #341	N45° 31.8903'	W56° 39.9928'	<i>Pennatula aculeata</i>
R2035 #378	N45° 31.8818'	W56° 39.9933'	<i>Pennatula aculeata</i>
R2035 #349	N45° 31.88'	W56° 39.9875'	<i>Pennatula aculeata</i>
R2035 #308	N45° 31.9009'	W56° 40.0436'	<i>Pennatula aculeata</i>
R2042-8	N46° 5.6136'	W57° 14.6986'	<i>Pennatula aculeata</i>
R2042-26	N46° 5.1909'	W57° 15.6002'	<i>Pennatula aculeata</i>

R2038-5	N45° 43.7456'	W56° 51.1678'	<i>Pennatula aculeata</i>
R2038-12	N45° 43.7412'	W56° 51.1613'	<i>Pennatula aculeata</i>
R2042-10	N46° 5.6095'	W57° 14.6969'	<i>Pennatula aculeata</i>
R2038-21	N45° 43.739'	W56° 51.1786'	<i>Pennatula aculeata</i>
R2042-9	N46° 5.6095'	W57° 14.697'	<i>Pennatula aculeata</i>
R2042-25	N46° 5.2121'	W57° 15.5825'	<i>Pennatula aculeata</i>
R2035-400	N45° 31.9268'	W56° 40.0923'	<i>Funiculina quadrangularis</i>
R2038-16	N45° 43.7268'	W56° 51.1813'	<i>Funiculina quadrangularis</i>
R2038-4	N45° 43.7462'	W56° 51.1689'	<i>Funiculina quadrangularis</i>
R2038-15	N45° 43.7294'	W56° 51.18'	<i>Funiculina quadrangularis</i>
R2038-17	N45° 43.7273'	W56° 51.1806'	<i>Funiculina quadrangularis</i>
5256-1	N43° 43.8233'	W52° 52.5667'	<i>Funiculina quadrangularis</i> (Trawl)
5256-2	N43° 43.8233'	W52° 52.5667'	<i>Funiculina quadrangularis</i> (Trawl)
5256-3	N43° 43.8233'	W52° 52.5667'	<i>Funiculina quadrangularis</i> (Trawl)
5256-4	N43° 43.8233'	W52° 52.5667'	<i>Funiculina quadrangularis</i> (Trawl)
5256-5	N43° 43.8233'	W52° 52.5667'	<i>Funiculina quadrangularis</i> (Trawl)
5256-6	N43° 43.8233'	W52° 52.5667'	<i>Funiculina quadrangularis</i> (Trawl)
5256-7	N43° 43.8233'	W52° 52.5667'	<i>Funiculina quadrangularis</i> (Trawl)
5256-8	N43° 43.8233'	W52° 52.5667'	<i>Funiculina quadrangularis</i> (Trawl)
5256-9	N43° 43.8233'	W52° 52.5667'	<i>Funiculina quadrangularis</i> (Trawl)
3491-230	N45° 45.7250'	W56° 56.8883'	<i>Funiculina quadrangularis</i> (Trawl)
3491-231	N45° 45.7250'	W56° 56.8883'	<i>Funiculina quadrangularis</i> (Trawl)
3491-232	N45° 45.7250'	W56° 56.8883'	<i>Funiculina quadrangularis</i> (Trawl)
3491-233	N45° 45.7250'	W56° 56.8883'	<i>Funiculina quadrangularis</i> (Trawl)
3491-234	N45° 45.7250'	W56° 56.8883'	<i>Funiculina quadrangularis</i> (Trawl)
R2035-20	N45° 31.9502'	W56° 40.1694'	<i>Protoptilum carpenteri</i>
R2042-14	N46° 5.7308'	W57° 14.6101'	<i>Protoptilum carpenteri</i>
R2039-3	N45° 44.0621'	W56° 50.9827'	<i>Protoptilum carpenteri</i>
R2041-31	N46° 8.6704'	W57° 31.4459'	<i>Kophobelemnion stelliferum</i>
R2041-28	N46° 8.6815'	W57° 31.4491'	<i>Kophobelemnion stelliferum</i>
R2040-22	N45° 56.4377'	W57° 22.56'	<i>Kophobelemnion stelliferum</i>
R2041-26	N46° 8.6848'	W57° 31.4447'	<i>Kophobelemnion stelliferum</i>
R2041-36	N46° 8.4914'	W57° 31.5157'	<i>Kophobelemnion stelliferum</i>

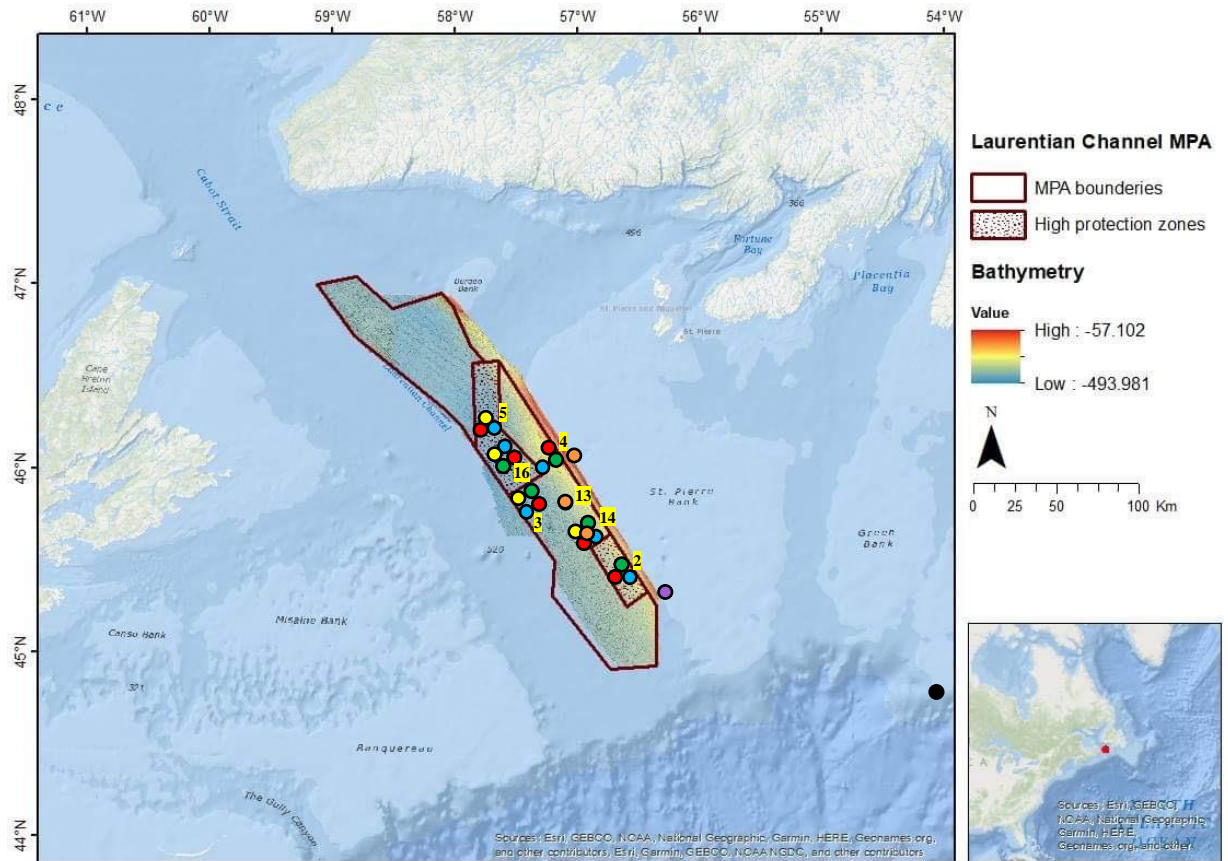


Figure 3-1. Bathymetric map of the boundaries within the Laurentian Channel MPA, the stations numbers from which sea pen samples were collected from for this study in 2017, and the locations of those samples collected for this study in 2017 (indicated by colored circles). *Anthoptilum* spp. samples collected are indicated by the blue circles, *P. aculeata* samples collected are indicated by the red circles, *F. quadrangularis* samples collected are indicated by the green circles, *P. carpenteri* samples collected are indicated by the orange circles, and *K. stelliferum* samples collected are indicated by the yellow circles. *F. quadrangularis* samples collected just outside of the MPA in 2007 during a DFO

multispecies trawl survey are indicated by a purple circle, and *F. quadrangularis* samples collected further outside of the MPA in 2009 during a DFO multispecies trawl survey are indicated by a black circle. The location of the MPA is shown on the bottom right.

3.2.2 Ring counting methods

The skeleton of each colony was cut into thick sections 3mm in size with an Isomet® Low Speed Saw at the thickest region of the axis, the transition point between the peduncle and the rachis. These sections were embedded in epoxy (Epofix™-Electron Microscopy Sciences) and placed in metal rings (2.5 cm diameter) where they were further embedded in epoxy. The rings were then polished using silicon grit and sulfite plates in a Struers TegraPol 31 lapping wheel and were then carbon coated. These sections were imaged under a Scanning Electron Microscope (SEM) to achieve high-resolution images of the growth bands. Dwell time was set to 20 μs with a beam diameter of 1-2 μm. Brightness was set to 96.50 with a contrast of 46.65.

Growth rings were present in each species, seen as wider dark and light couplets with occasional groups of finer rings within them (chapter 2). The wider couplets were labeled as “major” growth rings, while fine couplets found within the major rings were labeled as “minor” growth rings. The enumeration of growth rings consisted of two methods of ring counting: assuming “major” growth rings are representative of annual periodicity (referred to as “major rings” in growth models), and assuming both “major” and “minor” growth rings are representative of annual periodicity (referred to as “all rings” in growth models). I followed the ring counting method proposed by Marschal et al. (2004) and traced each ring around the entire section to ensure it presented itself as one growth ring. Growth ring counts were made by me individually. According to Marschal et al. (2004), the joining together of growth rings was due to differences in

growth rates in certain parts of the axis (i.e. as found in the red coral *Corallium rubrum*). If the growth ring combined with other rings, I interpreted that conglomerate of rings to be representative of one year (Fig. 3-3). Data examples for two methods of counting rings are provided: counting groups of rings that were clustered together as one year via SEM-BSE (Scanning Electron Microscopy-Backscattered Electron) images, and counting every prominent, visible ring as one year. Relationships between number of rings (assumed to represent age in years) and axis metrics were assessed using logistic models for *Anthoptilum* spp. *P. aculeata*, and *F. quadrangularis*. The sample size for species *K. stelliferum* and *P. carpenteri* was too low ($n < 5$) to be represented by these relationships.

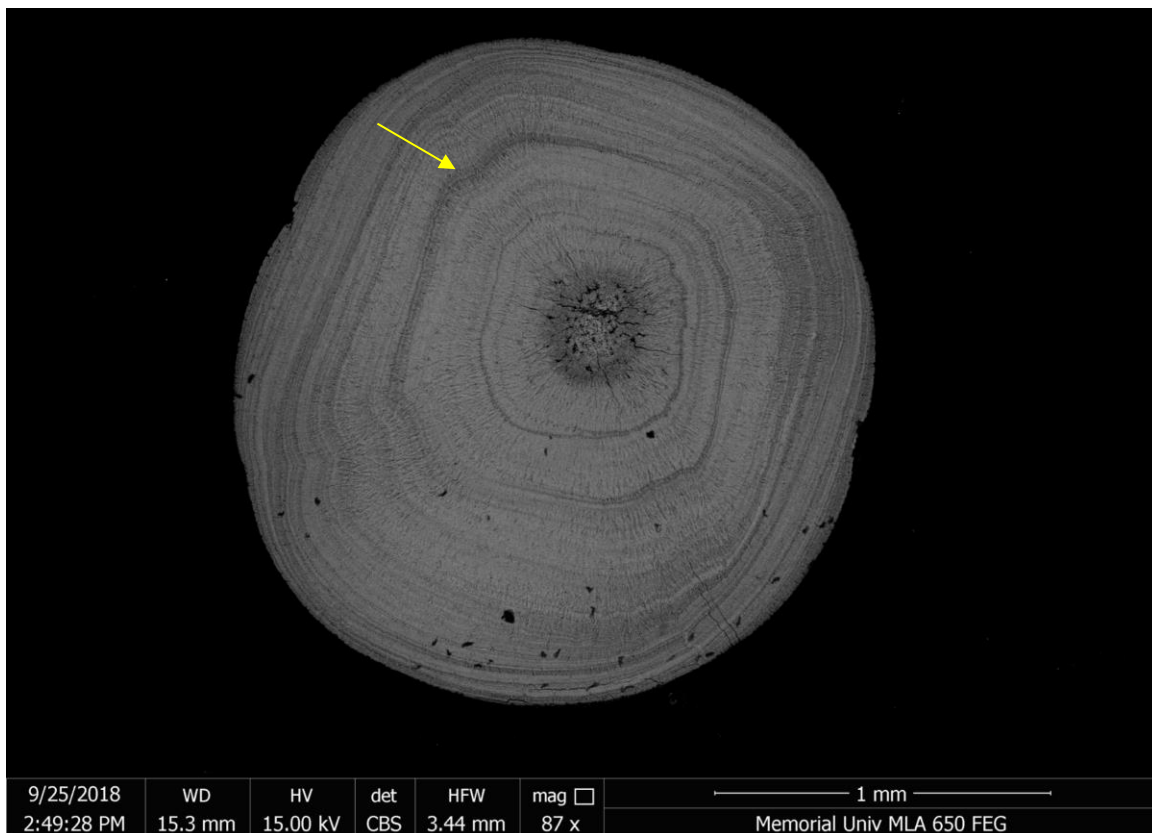


Figure 3-3. SEM-BSE image of the cross section in *Pennatula aculeata* (sample R2035-341) showing the thinner growth rings combining into a single, thicker growth ring that was used to represent one year (indicated by yellow arrow).

3.2.3. Growth curve analysis

Total colony length was plotted against colony metrics (peduncle length, axis diameter, and wet weight) as a logistic curve for each specimen, and the number of growth rings counted for each specimen was plotted against the total length of the colony as a Gompertz curve. These growth curves were used because they best represent biological growth in which an organisms' growth is slow at the beginning and at the end when an optimal height is reached. An example of this growth has been observed in bivalves (Urban 2002). Once this height is reached, the organism no longer needs to grow with age to survive and reproduce. Determining whether "major rings" or "all rings" were indicative of annual periodicity was shown using these curves to provide a better understanding of sea pen longevities, seeing which ring counts generated a better R^2 fit to this expected growth pattern. If we use the ring counting method ("major" vs. "all" rings) against colony length that produces the highest r^2 value as a determinant of which rings represent annual periodicity, then it may be possible to identify each species' longevities and compare them to the longevities previously published in other studies on sea pens.

3.3. Results

3.3.1 Colony metrics

The average total length differed among the six species. *F. quadrangularis* ranged from 19.5-87.5 cm, *A. grandiflorum* from 13-69.5 cm, *P. carpenteri* from 41.5-46.5 cm, *P. aculeata* from 3-23.5 cm, and *K. stelliferum* from 9-15 (Fig. 3-4). The axis composition for each species was determined to be primarily high magnesian calcite (Ca,Mg)CO₃ (chapter 2). Relationships between colony metrics and size were not considered for *P. carpenteri* and *K. stelliferum* due to their very small sample size (n<5).

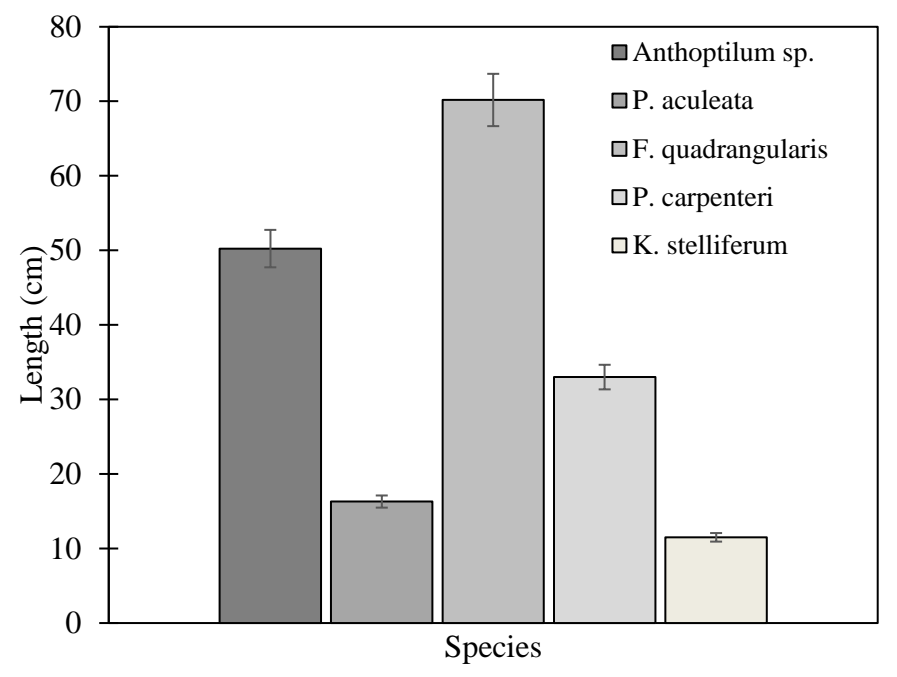


Figure 3-4. Bar graph showing the average length (cm) for 23 *Anthoptilum* spp., 20 *Pennatula aculeata*, 19 *Funiculina quadrangularis*, 3 *Protoptilum carpenteri*, and 5 *Kophobelemnon stelliferum*. Error bars are shown as standard error.

3.3.2 Colony and axis metrics in relation to colony length

A total of 70 specimens were analyzed to determine relationships between axis metrics and colony length. There was a positive trend between colony metrics and colony length for all species (Fig. 3-7). Among the three species, *P. aculeata* displayed the strongest relationship between colony length and peduncle length ($r^2=0.89$), colony length and axis diameter ($r^2=0.86$), and between colony length and wet weight ($r^2=0.87$). Comparatively, *Anthoptilum* spp. displayed the weakest relationships between colony length and peduncle length ($r^2=0.59$), colony length and axis diameter ($r^2=0.70$), and between colony length and wet weight ($r^2=0.31$). *F. quadrangularis* displayed stronger relationships than *Anthoptilum* spp. between colony length and peduncle length ($r^2=0.63$), colony length

and axis diameter ($r^2=0.87$), and colony length and wet weight ($r^2=0.58$). Logistic equations were used as they best fit the expected growth of a sea pen, having the highest r^2 in all relationships apart from the relationship between colony length and wet weight in *P. aculeata* in which a linear equation was used. Samples from *Anthoptilum* spp. and *F. quadrangularis* varied visually in their polyp thickness (Fig. 3-5, 3-6), while some specimens of *Anthoptilum* spp. and *F. quadrangularis* presented little to no flesh and resulted in a wet weight of zero. Examples of these specimens are shown in Fig. 3-5C and 3-6A and are believed to be juveniles. Differences in polyp thickness in certain *Anthoptilum* spp. and *F. quadrangularis* specimens might explain the variation in the relationship between colony length and wet weight (Fig. 3-7G,I).

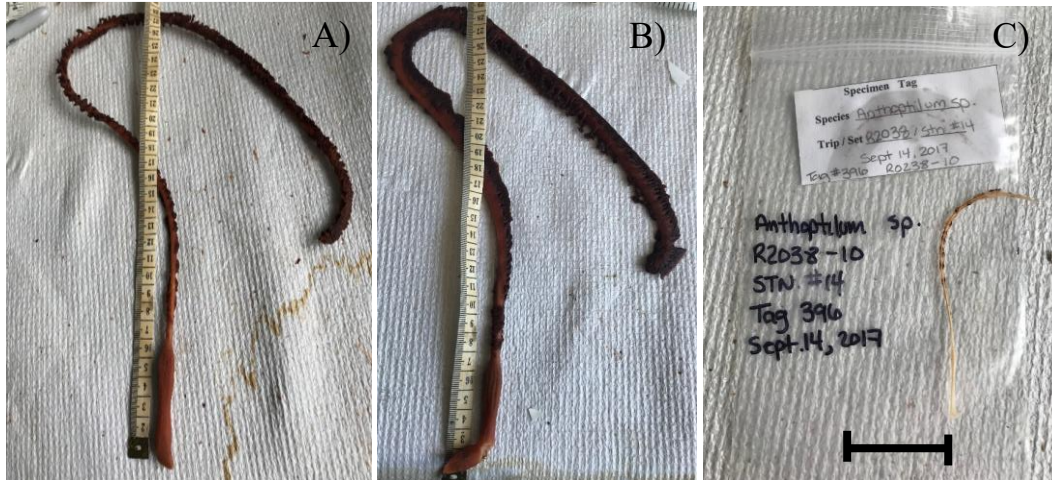


Figure 3-5. Images of *Anthoptilum* spp. showing differences in polyp densities in two colonies with the same height (28 cm) (A, B), and a juvenile colony with very few polyps and flesh (C). Scale bar 3.5 cm

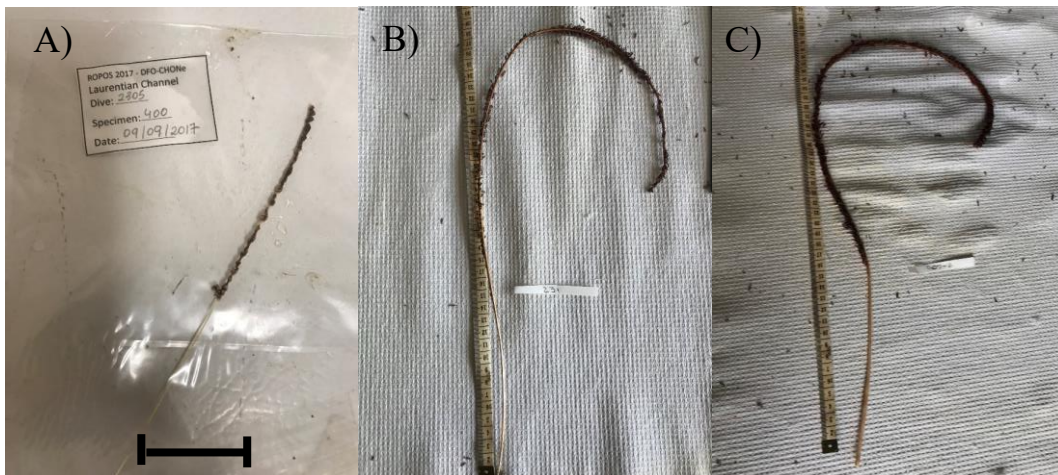


Figure 3-6. Image of the *Funiculina quadrangularis* collected from the Laurentian Channel MPA in 2017 (A), image of the *Funiculina quadrangularis* collected in 2007 in the Laurentian Channel MPA (B), image of the *Funiculina quadrangularis* collected in 2009 outside of the Laurentian Channel. Scale bar: 3.5 cm

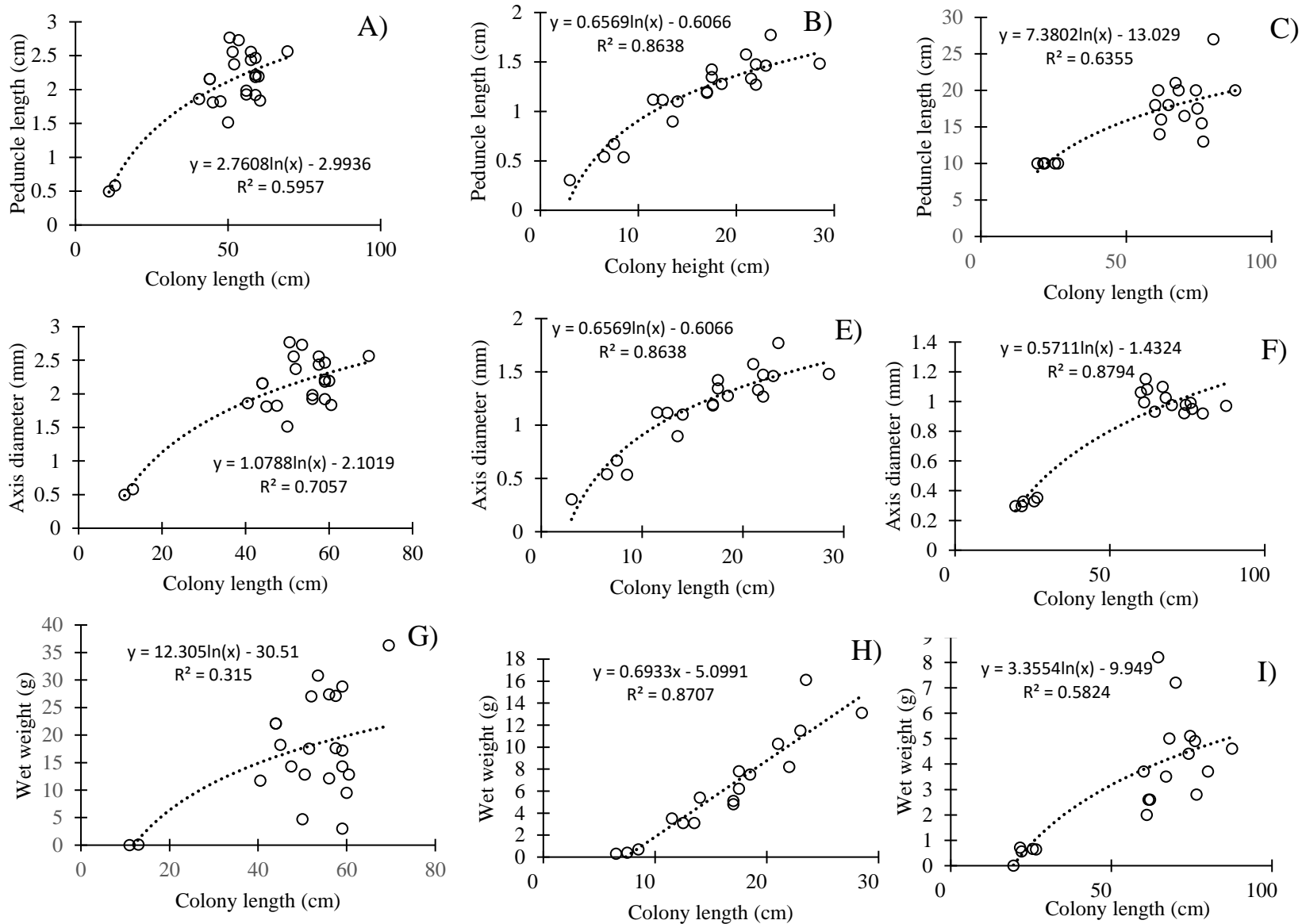


Figure 3-7. Peduncle length in relation to colony length in: *Anthoptilum* spp. (A), *Pennatula aculeata* (B), and *Funiculina quadrangularis* (C). Axis diameter in relation to colony length in: *Anthoptilum* spp. (D), *Pennatula aculeata* (E), and *Funiculina quadrangularis* (F). Wet weight in relation to colony length in: *Anthoptilum* spp., (G), *Pennatula aculeata* (H), and *Funiculina quadrangularis* (I).

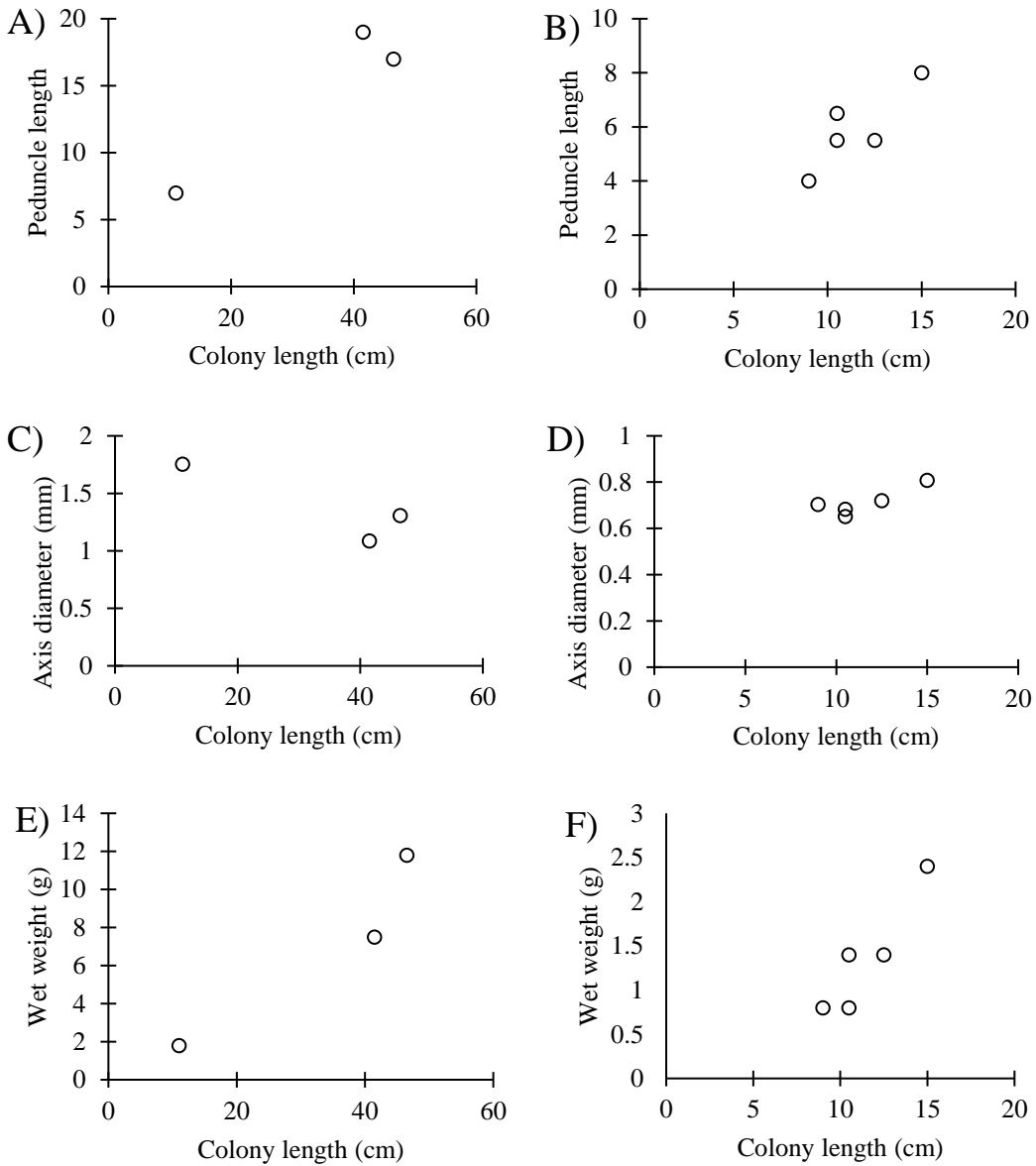
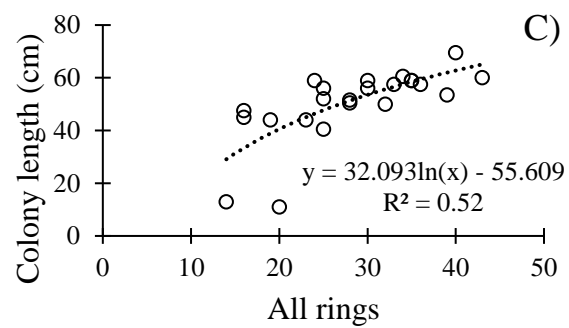
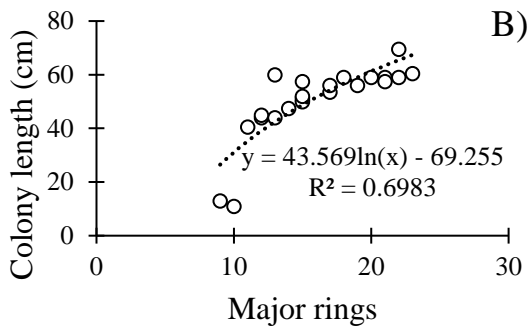
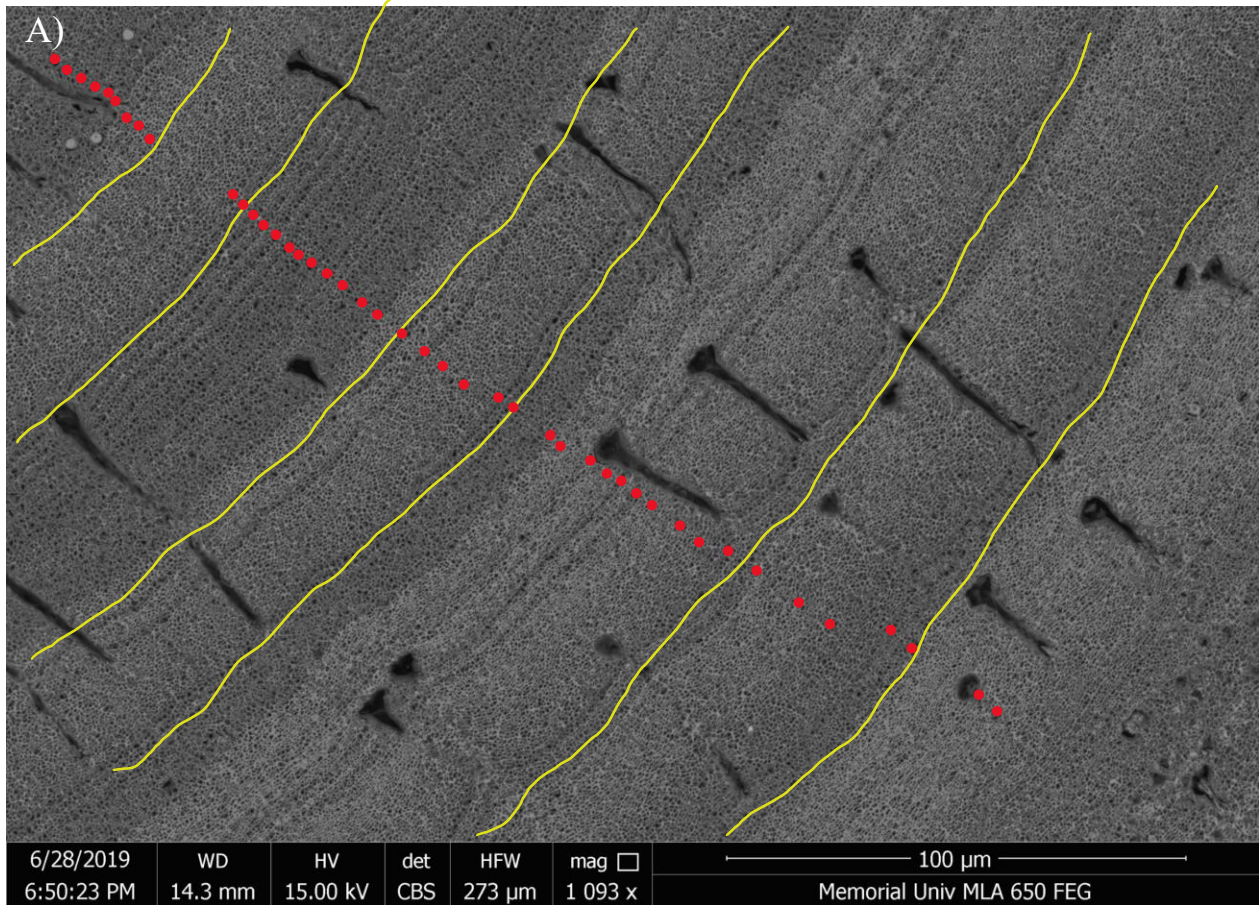


Figure 3-8. Peduncle length in relation to colony length in: *Protophilum carpenteri* (A), *Kophobelemnon stelliferum* (B). Axis diameter in relation to colony length in: *Protophilum carpenteri* (C), *Kophobelemnon stelliferum* (D). Wet weight in relation to colony length in: *Protophilum carpenteri* (E), *Kophobelemnon stelliferum* (F).

3.3.3 Estimated longevity and growth rates

Each species collected for this study exhibited very clear growth rings in the peduncle and within the rachis. Size differences between colonies did not affect growth ring visualization. Methods for counting growth rings involved counting major rings that were present as thick light and dark couplets as one year and counting all rings that were present as thin and thick light and dark couplets as one year (Fig. 3-9 through 3-13). Each graph displays points that represent a single colony from that species. Sample sizes varied between species, with there being 23 individuals of *Anthoptilum* spp., 20 individuals of *Pennatula aculeata*, 19 individuals of *Funiculina quadrangularis*, 3 individuals of *Protoptilum carpenteri*, and 5 individuals of *Kophobelemnon stelliferum*. Error bars found on each point are shown as standard error.

Logistic growth curves showed that when plotting major rings and all rings against total colony length, the relationship between major rings and colony length displayed a higher R^2 value (Fig. 3-9 through 3-13). Gompertz growth curves also showed a higher R^2 value for the relationship between major rings and colony length in all species compared to the relationship between all rings and colony length, estimating the maximum length in all species when the trend begins to plateau (Fig. 3-14).



B

Figure 3-9. 100 μm SEM-BSE image of the growth rings within a colony of *Anthoptilum* sp. showing the ring counting methods for “major rings” (indicated by yellow lines), and “all rings” (indicated by red dots) (A). Logistic graphs showing the relationship between: major rings and colony length (B), all rings and colony length (C). Each point represents a single colony.

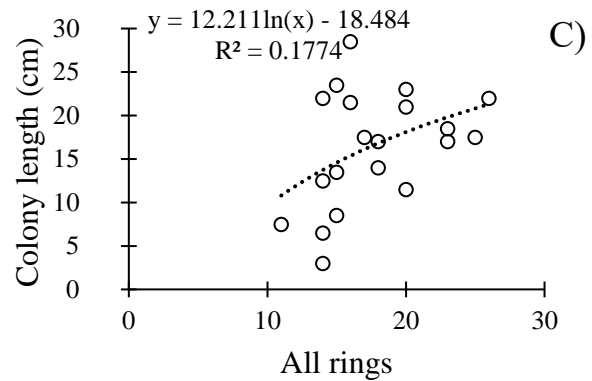
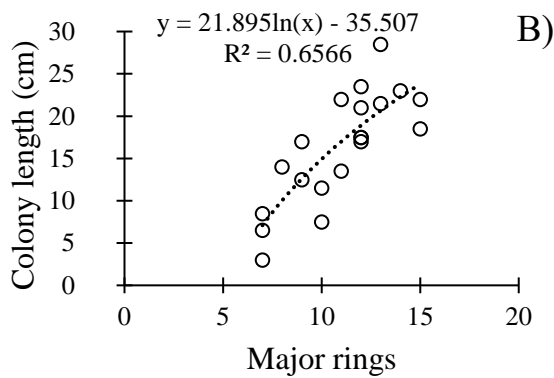
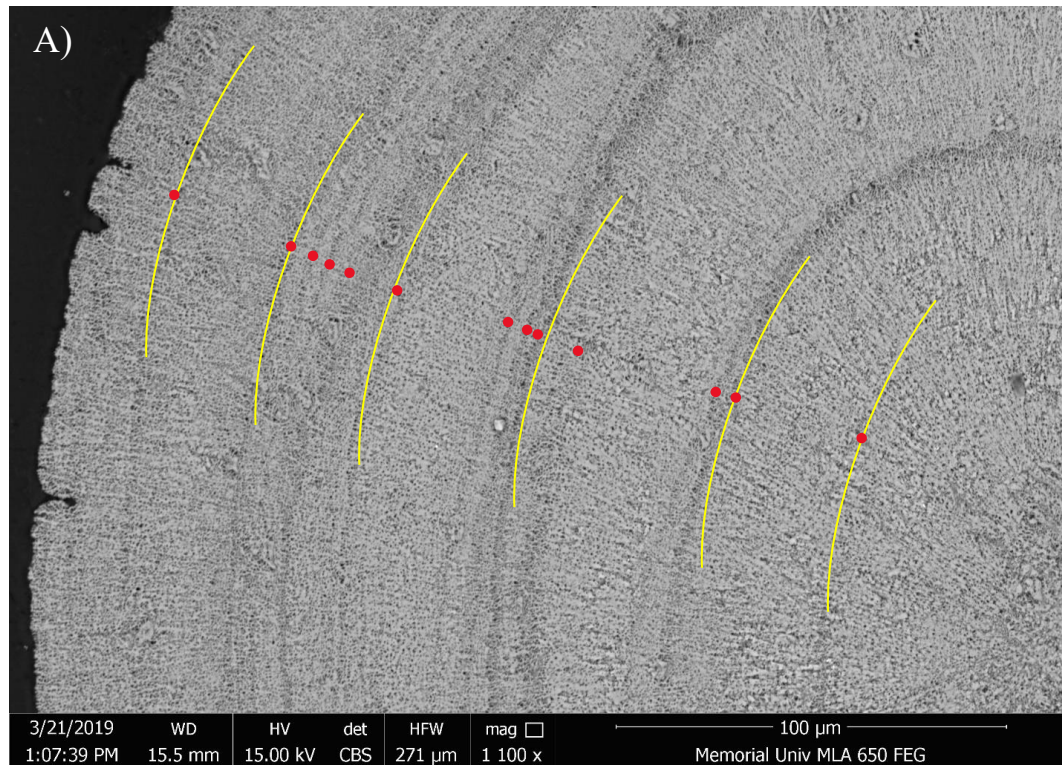


Figure 3-10. 100 μm SEM-BSE image of the growth rings within a colony of *Pennatula aculeata* showing the ring counting methods for “major rings” (indicated by yellow lines), and “all rings” (indicated by red dots) (A). Logistic graphs showing the relationship between: major rings and colony length (B), all rings and colony length (C). Each point represents a single colony.

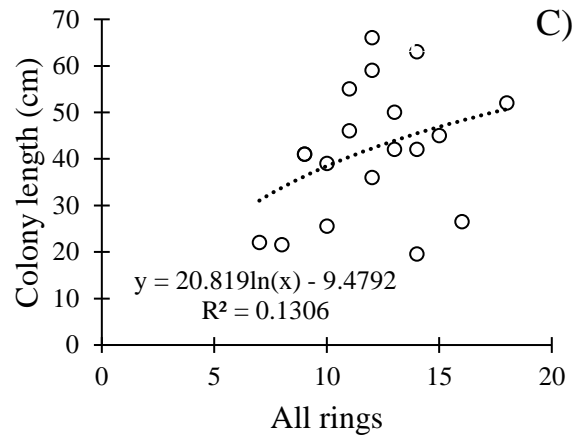
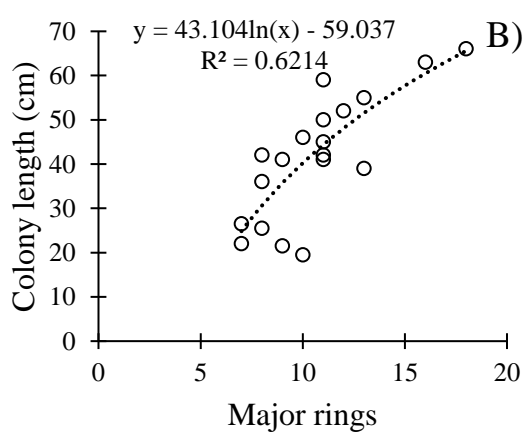
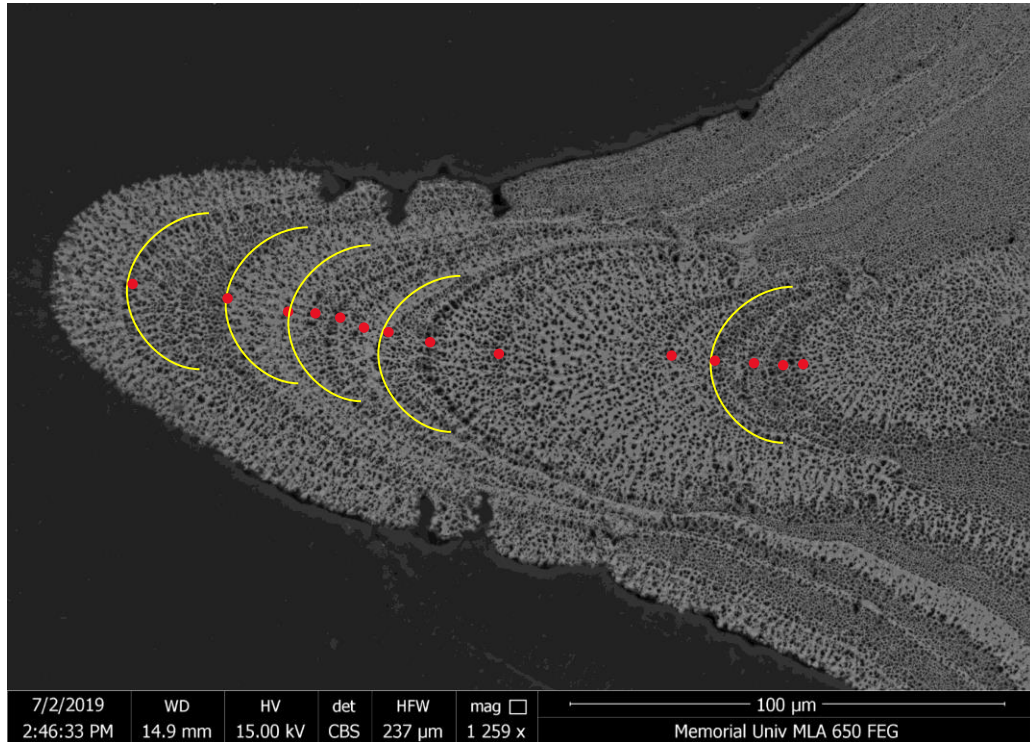


Figure 3-11. 100 µm SEM-BSE image of the growth rings within a colony of *Funiculina quadrangularis* showing the ring counting methods for “major rings” (indicated by yellow lines), and “all rings” (indicated by red dots) (A). Logistic graphs showing the relationship between: major rings and colony length (B), all rings and colony length (C). Each point represents a single colony.

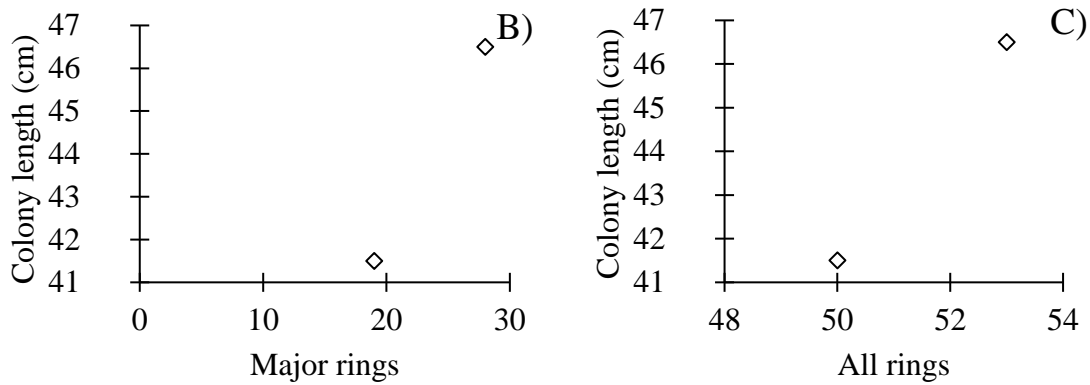
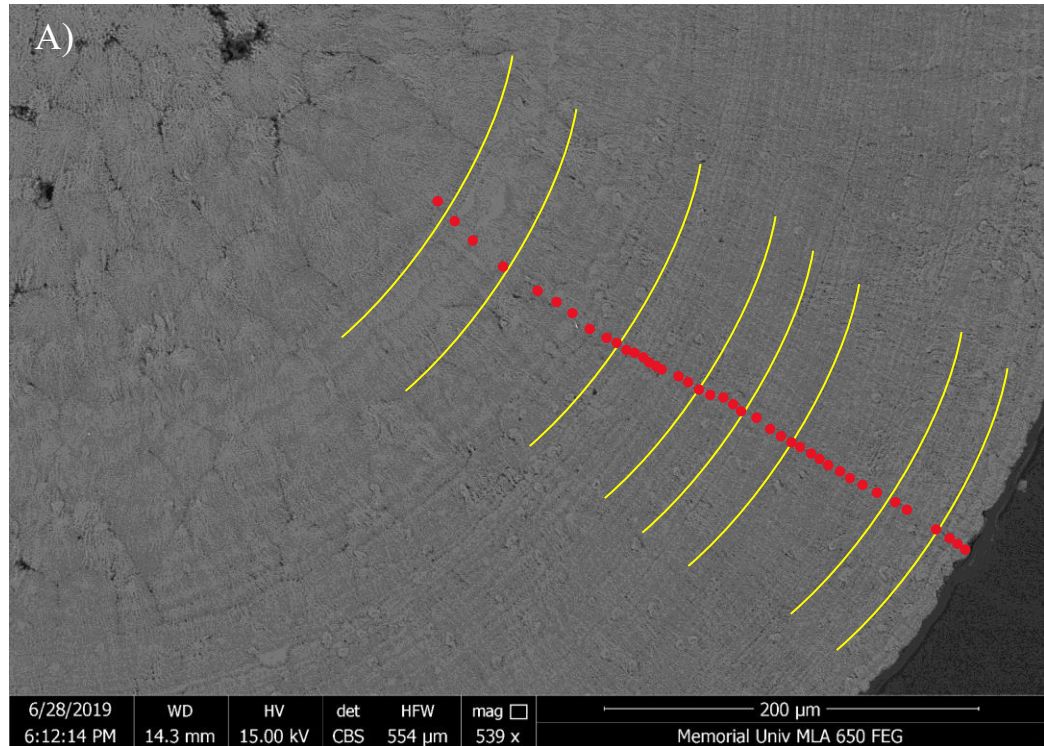


Figure 3-12. 200 μm SEM-BSE image of the growth rings within a colony of *Protophilum carpenteri* showing the ring counting methods for “major rings” (indicated by yellow lines), and “all rings” (indicated by red dots) (A). Graphs showing the relationship between: major rings and colony length (B), all rings and colony length (C). Each point represents a single colony.

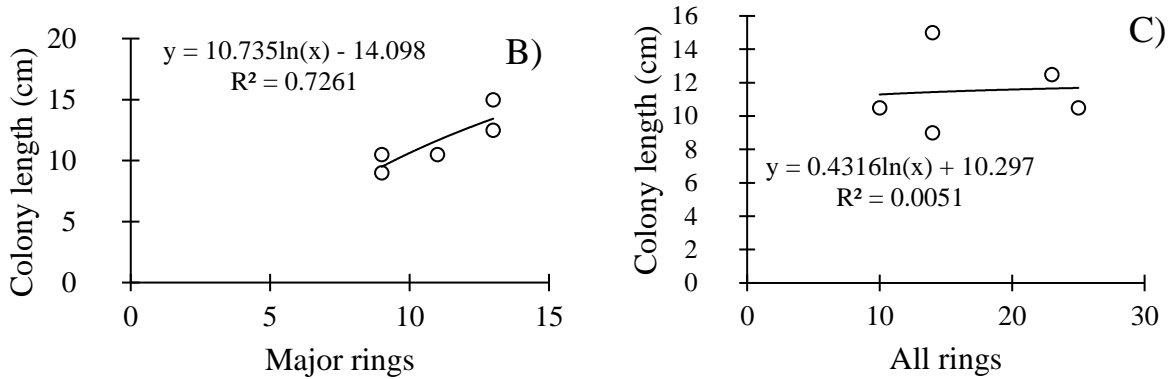
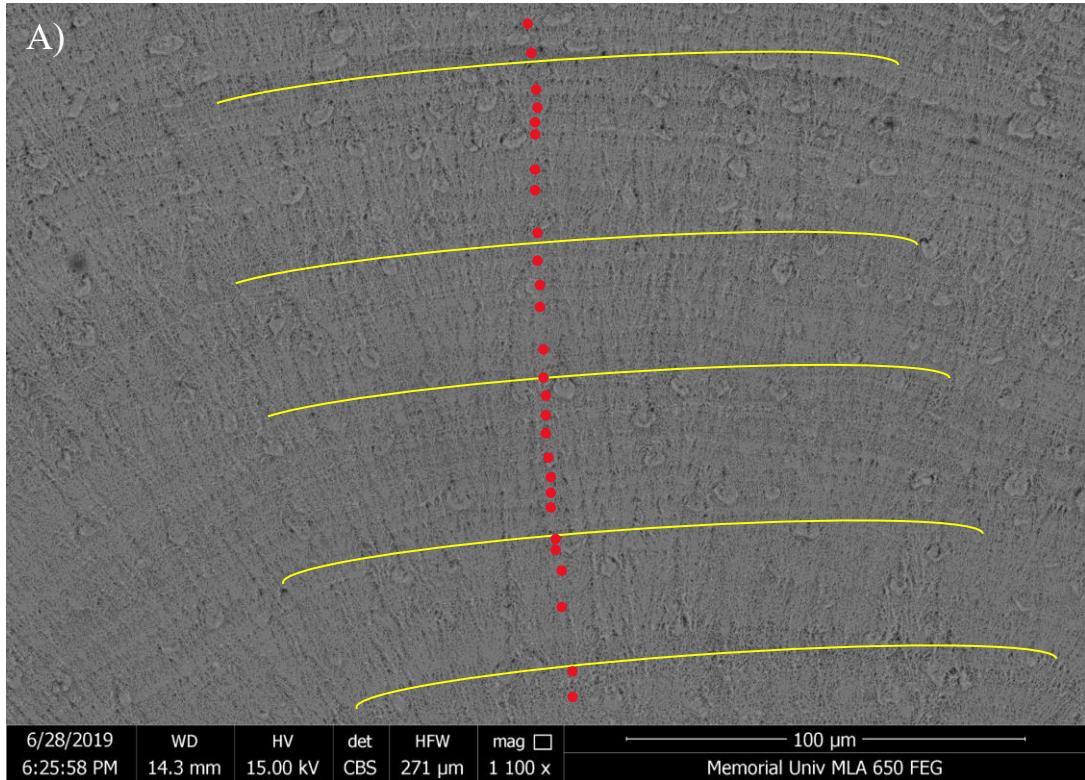


Figure 3-13. 100 μm SEM-BSE image of the growth rings within a colony of *Kophobelemnon stelliferum* showing the ring counting methods for “major rings” (indicated by yellow lines), and “all rings” (indicated by red dots) (A). Logistic graphs showing the relationship between: major rings and colony length (B), all rings and colony length (C). Each point represents a single colony.

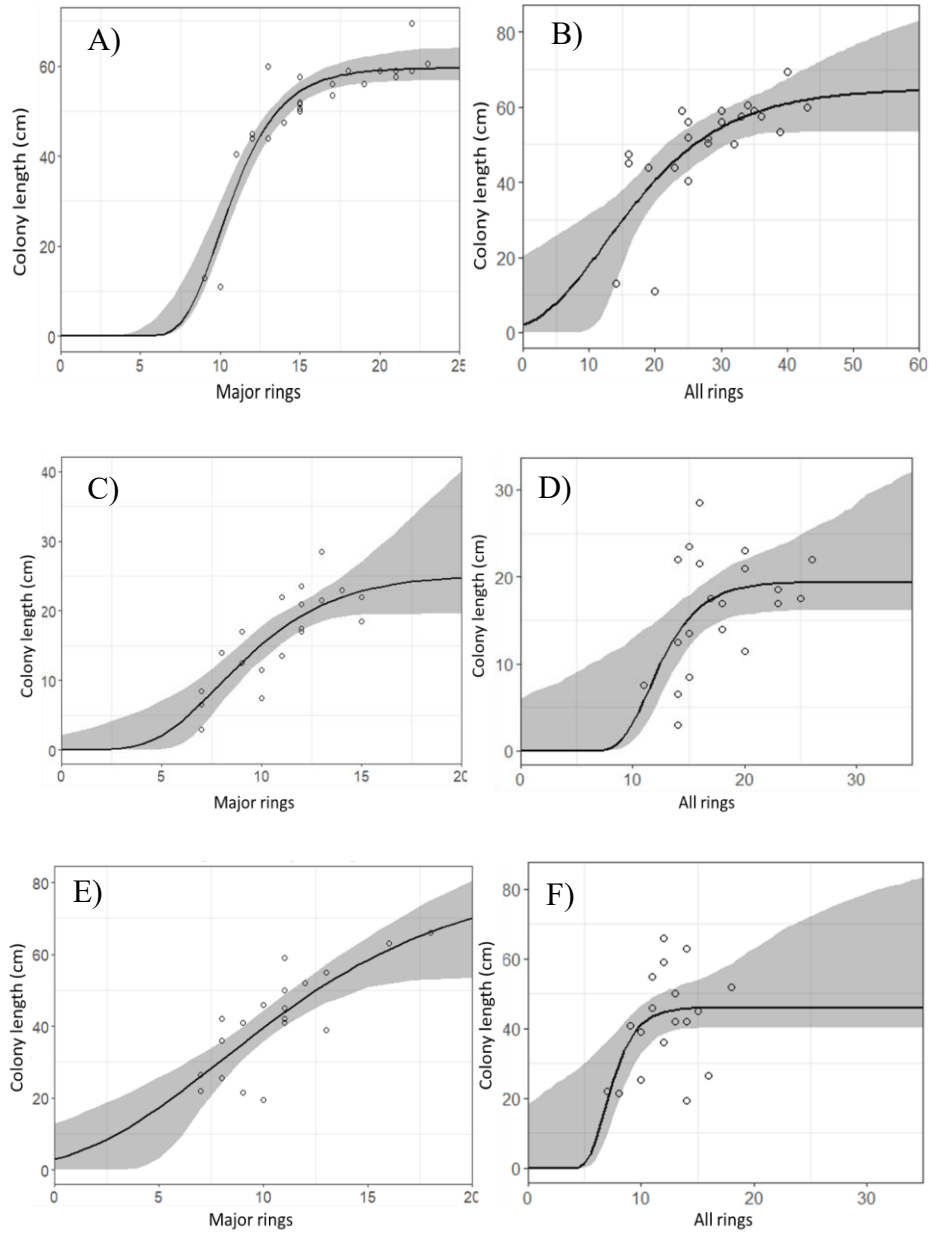


Figure 3-14. Gompertz relationships for *Anthoptilum* spp. between colony length and major rings (A), colony length and all rings (B), for *P. aculeata* between colony length and major rings (C), colony length and all rings (D), for *F. quadrangularis* between colony length and major rings (E), colony length and all rings (F). Relationships produced using the equation: $\text{Length} = \text{Lin}f \cdot \exp(\rho \cdot \exp(-k \cdot \text{Rings}))$ at a 95% confidence interval.

3.3.4 Age estimation from colony size

Thicknesses between major growth couplets showed slow initial growth, followed by fast intermediate growth, slowing down again during the later stages of growth (Fig. 3-15 through 3-19). This pattern showed that smaller colonies have slower growth rates, medium sized colonies have faster growth rates, and larger colonies reach an age where growth slows. Based on these growth models, *Anthoptilum* spp.'s growth begins to slow considerably after 60 cm in length, *P. aculeata* after 20 cm, and *F. quadrangularis* after 50-60 cm in length (Table 3-3). These lengths are referred to as the cut-off lengths for which age can be estimated based on colony size, a method that would enable visual estimates from size in video.

Radial growth rates differed slightly between *Anthoptilum* spp., *P. aculeata*, and *F. quadrangularis* (Table 3-3). The low sample size for *P. carpenteri* and *K. stelliferum* does not allow for the same comparisons to be made on their growth rates. When referring to major rings, *Anthoptilum* spp. presented the fastest radial growth rate (0.12 mm/year), while *F. quadrangularis* presented the slowest (0.08 mm/year). Meanwhile, *F. quadrangularis* presented the highest linear growth rate (3.8 cm/year), and *P. aculeata* presented the lowest (1.4 cm/year).

Table 3-2. List per species showing the range of major rings counted, the range of all rings counted, the radial growth rates determined from counting major rings, the radial growth rates determined from counting all rings, the linear growth rates determined from counting major rings, the linear growth rates determined from counting all rings, and the maximum cut-off from which age can be estimated based on size as shown from the Gompertz growth pattern. Sample sizes for each species included 23 *Anthoptilum* spp., 20 *Pennatula aculeata*, 19 *Funiculina quadrangularis*, 3 *Protoptilum carpenteri*, and 5 *Kophobelemnon stelliferum* individuals. Standard error was calculated from these values.

Species	Number of major rings (range)	Number of minor rings (range)	Radial growth rate from major rings (mm/year)	Radial growth rate from all rings (mm/year)	Linear growth rate from major rings (cm/year)	Linear growth rate from minor rings (cm/year)	Maximum length cut-off for age dating (cm)
<i>Anthoptilum</i> spp.	9-22	14-43	0.12±0.04	0.07±0.03	3.1±0.72	1.8±0.52	60
<i>P. aculeata</i>	7-15	11-26	0.10±0.04	0.06±0.02	1.4±0.42	0.92±0.38	20
<i>F. quadrangularis</i>	7-18	7-18	0.08±0.03	0.07±0.03	3.8±0.86	3.5±1.10	50-60
<i>P. carpenteri</i>	19-28	50-53	0.05±0.01	0.02±0.00	1.9±0.26	0.85±0.02	NA
<i>K. stelliferum</i>	9-13	10-25	0.06±0.01	0.04±0.01	1.0±0.09	0.74±0.27	NA

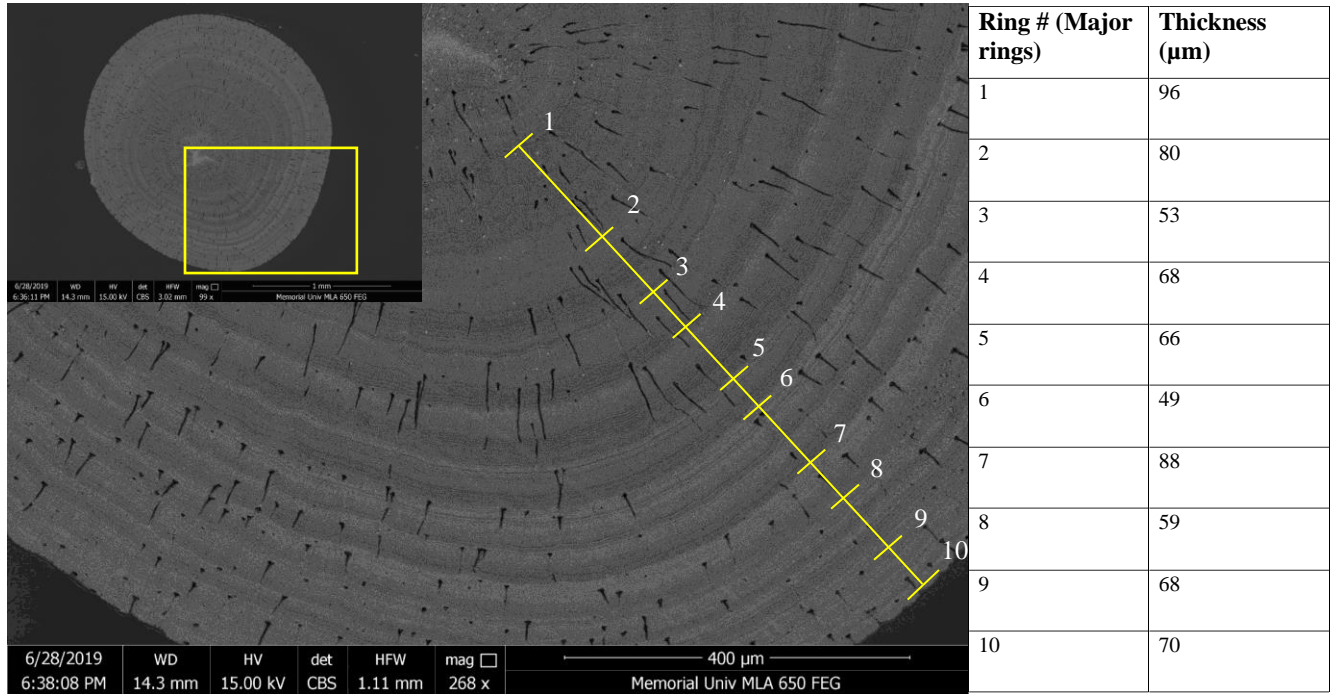


Figure 3-15. Thickness (μm) of each major couplet (indicated by the yellow line) in a colony of *Anthoptilum* spp. (sample # R2041-22). Number of rings and their thicknesses are shown in the adjacent table. Thickness measured with ImageJ software to the nearest μm .

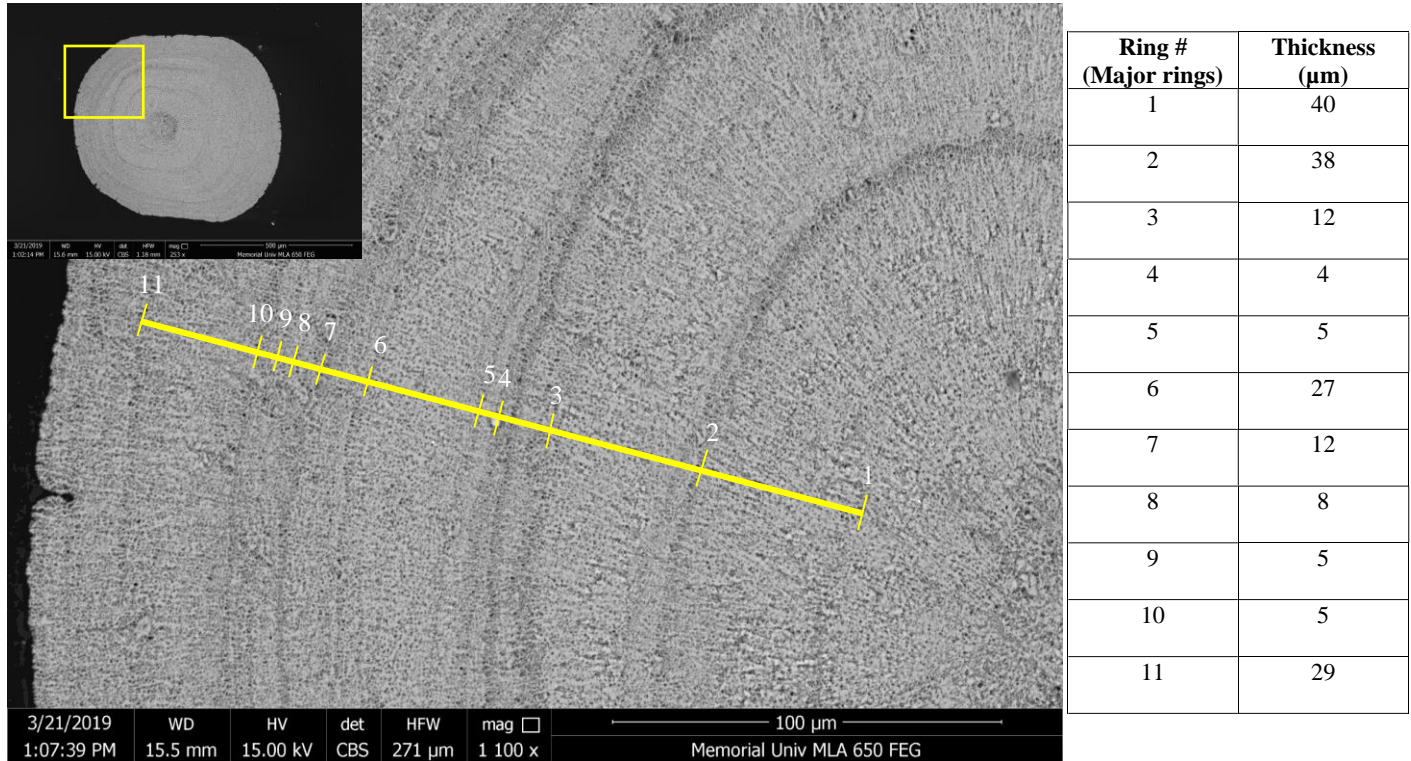


Figure 3-16. Thickness (μm) of each major couplet (indicated by the yellow line) in a colony of *Pennatulula aculeata* (sample # R2042-13). Number of rings and their thicknesses are shown in the adjacent table. Thickness measured with ImageJ software to the nearest μm .

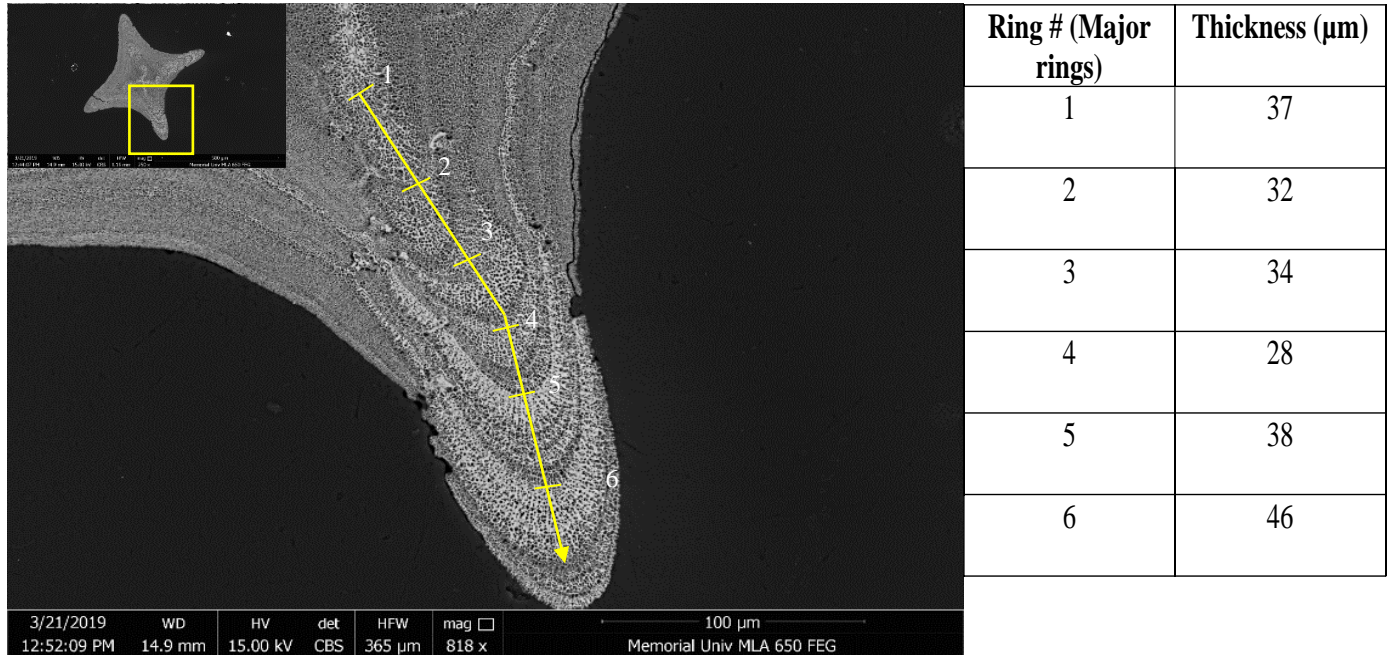


Figure 3-17. Thickness (μm) of each major couplet (indicated by the yellow line) in a colony of *Funiculina quadrangularis* (sample # R2038-4). Number of rings and their thicknesses are shown in the adjacent table. Thickness measured with ImageJ software to the nearest μm .

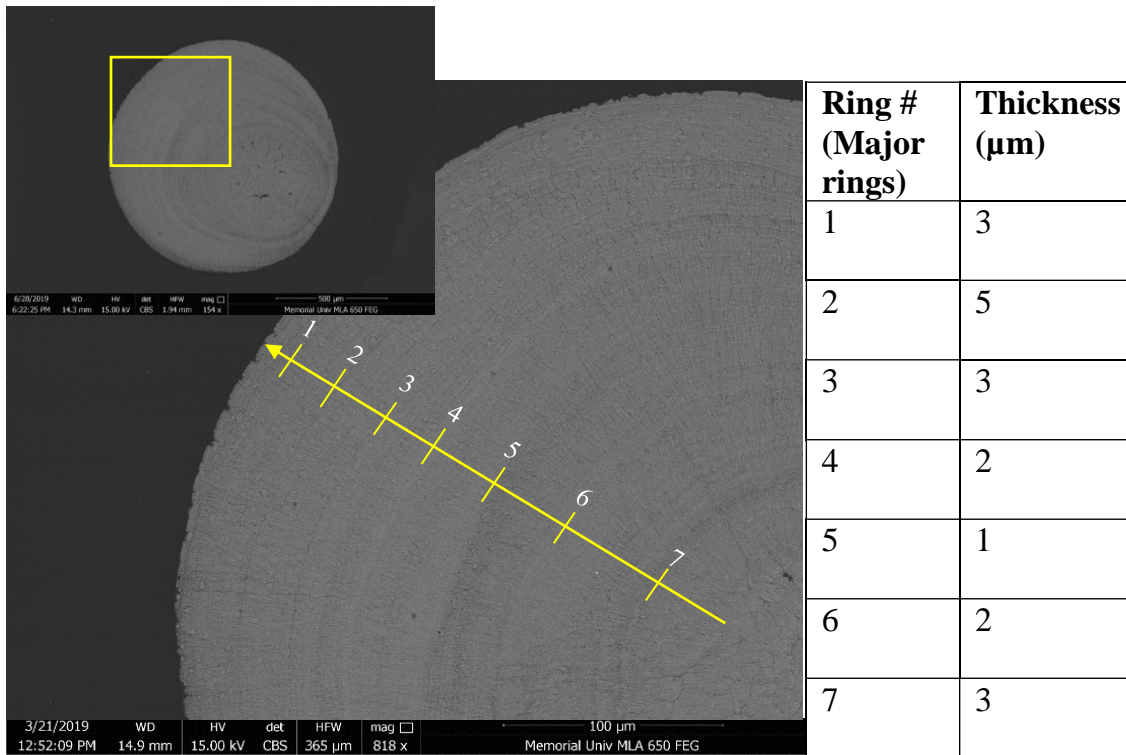


Figure 3-18. Thickness (μm) of each major couplet (indicated by the yellow line) in a colony of *Protoptilum carpenteri* (sample # R2039-3). Number of rings and their thicknesses are shown in the adjacent table. Thickness measured with ImageJ software to the nearest μm .

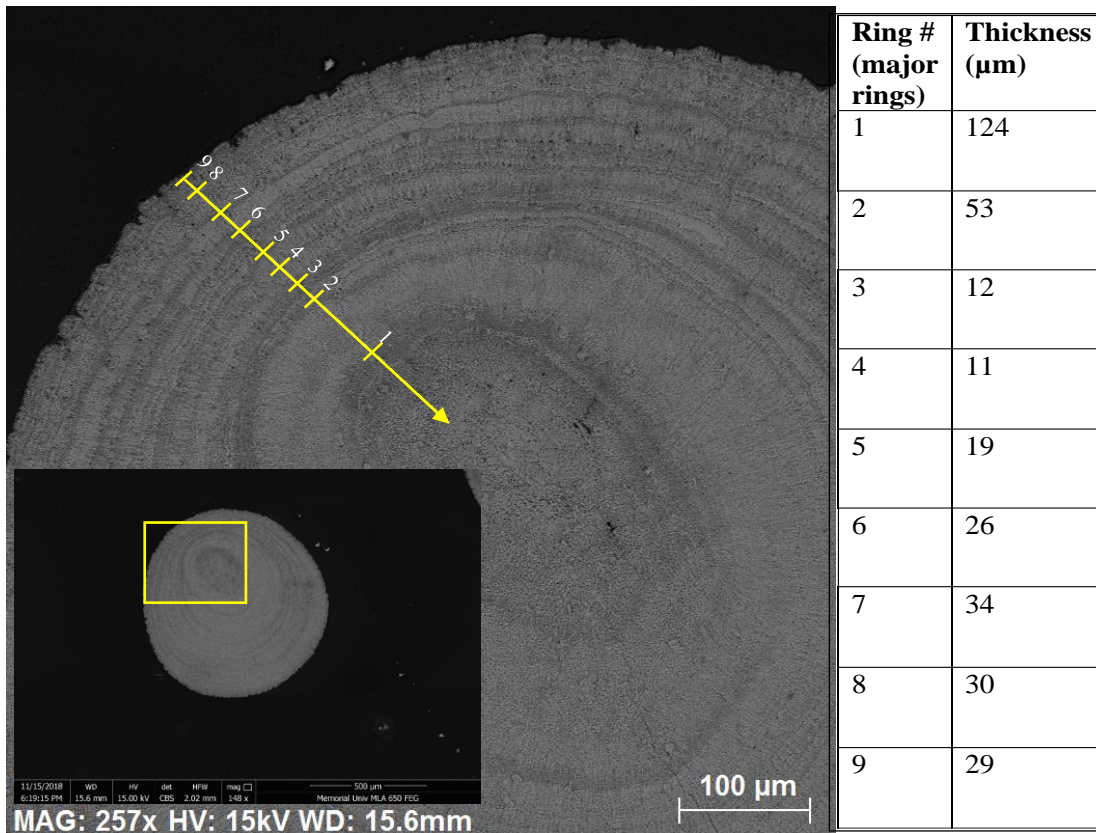


Figure 3-19. Thickness (μm) of each major couplet (indicated by the yellow line) in a colony of *Kophobelemnon stelliferum* (sample # R2041-28). Number of rings and their thicknesses are shown in the adjacent table. Thickness measured with ImageJ software to the nearest μm .

Table 3-3. Summary of sea pen species analyzed in this study and previous studies showing their sample location, age range, radial growth rates and linear growth rates. Standard error was calculated from these values.

Species	Location	Number of rings	Radial growth rates (mm/year)	Linear growth rates (cm/year)	Reference
<i>Anthoptilum</i> spp.	Laurentian Channel MPA	9-22	0.12±0.04	3.1±0.71	This study
<i>P. aculeata</i>	Laurentian Channel MPA	7-15	0.10±0.03	1.4±0.42	This study
<i>F. quadrangularis</i>	Laurentian Channel MPA	6-21	0.08±0.02	3.8±0.86	This study
<i>P. carpenteri</i>	Laurentian Channel MPA	5-7	0.06±0.008	1.9±0.26	This study
<i>K. stelliferum</i>	Laurentian Channel MPA	9-13	0.05±0.005	1.0±0.09	This study
<i>U. encrinus</i>	Eastern Canadian Arctic	8-45	0.067 ± 0.015	4.5 ± 1.2	Neves et al., 2018a
<i>A. grandiflorum</i>	Gulf of St. Lawrence,	5-28	N/A	4.3	Murillo et al., 2018
<i>P. carpenteri</i>	Laurentian Channel	2-21	N/A	1.9	
<i>H. finmarchica</i>	Northwest Atlantic	13-22	0.13 ± 0.0005	4.9 ± 0.06	Neves et al., 2015
<i>H. willemoesi</i>	Bering Sea	6-48	0.121-0.158	3.45-6.54	Wilson et al., 2002

3.4 Discussion

3.4.1 Colony metrics

Relationships between colony metrics and colony length were positive and strong for all species. *P. aculeata* displayed the strongest trends between peduncle length, axis diameter, wet weight and colony length compared to *Anthoptilum* spp. and *F. quadrangularis*. *P. carpenteri* and *K. stelliferum* were not included in these relationships between colony metrics and colony length due to their small sample size, however, their colony metrics were compared to those from the other species. Of the 6 species measured, *F. quadrangularis* was the tallest with the longest peduncle, while *K. stelliferum* was the shortest with the shortest peduncle. Average axis diameter at the transition point between the end of the peduncle and beginning of the rachis was largest in *Anthoptilum* spp., and smallest in *K. stelliferum*. Wet weight in relation to colony length in *Anthoptilum* spp. presented the weakest trend of the three species, calling into question what the cause of this poor relationship was. In a study by Murillo et al., (2018) the relationship between wet weight and colony length in *Anthoptilum grandiflorum* resulted in a strong trend with a few outliers that were heavy for their length (Murillo et al., 2018). While this study also has several outliers, it is possible that the primary difference between the relationship from this study and that from Murillo et al., (2018) is sample size. Murillo et al., (2018) analyzed 1150 specimens of *A. grandiflorum*, while we only analyzed 23 *Anthoptilum* spp., 6 of which were confirmed as *A. grandiflorum*. Another reason the wet weight and colony length relationship in this study was so poor could have to do with differences in colony morphology. There was a variety of *Anthoptilum* spp. colonies collected that were measured to have the same length but differences in polyp density and most likely consisted of multiple species. *F.*

quadrangularis also presented some outliers in the relationship between wet weight and colony length, particularly in the taller colonies. While a higher sample size might improve this relationship, it is possible that slight differences in morphology (i.e. polyp density) caused inconsistencies in their weights. Unfortunately counting or measuring polyp density in sea pen species is beyond the scope of this study.

3.4.2 Longevity and growth rates

Growth ring counting paired with age-growth relationships provided strong support for the longevity and growth rates estimated from major growth ring counts. Determining whether all rings or only major rings were indicative of age in sea pens was one of the primary goals of this study. The strong logistic and Gompertz relationships between major rings and colony length across all species in this study (except for *P. carpetneri* and *K. stelliferum*) show that major rings represent age. Colonies collected for this study were much younger (up to 22 years old) than previous studies that have age dated sea pens (Murillo et al., 2018; Neves et al., 2018a; Neves et al., 2015). In *Umbellula encrinus*, growth rings were assumed to represent years, with the maximum age determined to be 75 years based on correlating the number of trace element ratio peaks to growth rings, and bomb-¹⁴C (Neves et al., 2018a). In *Halipteris finmarchica*, the number of rings counted ranged from 13-26 and were assumed to be annual (Neves et al., 2015). Neves et al., (2015) describes the occurrence of finer rings observed in *H. finmarchica* and *Halipteris willemoesi* that could lead to an overestimation or underestimation of age in these species. Likewise, Murillo et al., (2018) described how counting every visible growth ring in *P. aculeata* resulted in a much higher age estimate (63 years) compared to only counting prominent growth rings (21 years). Even though correlating trace element ratio peaks to the number of growth rings does seem promising for confirming

periodicity, Murillo et al., (2018) emphasized that without evidence of environmental influences on trace element ratios, the age cannot be validated. With this, Murillo et al., (2018) did not confirm or assume growth rings were annual in *A. grandiflorum* or in *P. aculeata*.

Overall, the age range when counting major rings were comparable in each species for this study, ranging from 9-22 for *Anthoptilum* spp., 7-15 for *P. aculeata*, 7-18 for *F. quadrangularis*, 5-7 in *P. carpenteri*, and 9-13 in *K. stelliferum*. Radial growth rates were also comparable between *Anthoptilum* spp. (0.12 ± 0.04 mm/year), *P. aculeata* (0.10 ± 0.03 mm/year), and *F. quadrangularis* (0.08 ± 0.02 mm/year). The radial growth rates in *K. stelliferum* and *P. carpenteri* were 0.06 ± 0.008 mm/year and 0.05 ± 0.005 mm/year; however, the sample size was small ($n < 5$). Linear growth rates varied between these species. The tallest species, *F. quadrangularis* had a linear growth rate of 3.8 ± 0.86 cm/year, followed by 3.1 ± 0.71 cm/year in *Anthoptilum* spp., and 1.4 ± 0.42 cm/year in *P. aculeata*. *K. stelliferum* had linear growth rates of 1.0 ± 0.09 cm/year, and *P. carpenteri* had linear growth rates of 1.9 ± 0.26 cm/year.

Growth rates from this study are comparable to those found in sea pens from previous studies (Murillo et al., 2018; Neves et al., 2018a; Neves et al., 2015) (Table 3-4). The maximum growth rate was estimated to be 4.3 cm/year in *A. grandiflorum*, and 1.9 cm/year in *P. aculeata* (Murillo et al., 2018). In *U. encrinus*, radial growth rates averaged 0.067 ± 0.015 mm/year, and linear growth rates averaged 4.5 ± 1.2 cm/year (Neves et al., 2018a). In *H. finmarchica*, radial growth rates were 0.13 mm/year ± 0.0005 and linear growth rates were 4.9 cm/year. For *U. encrinus*, growth rates are slow due to the limited food availability and cold environment at depth in the Arctic (Neves et al., 2018a). This might also be the case for *H. finmarchica* collected from the Northwest Atlantic (Neves

et al, 2015), as well as *A. grandiflorum* and *P. aculeata* collected from the Gulf of St. Lawrence (Murillo et al., 2018) due to their slow growth rates. However, further research is needed between growth rates and environmental variables to confirm this.

3.4.3 Age estimation from colony size

Growth in *Anthoptilum* spp., *P. aculeata*, and *F. quadrangularis* was best represented by a Gompertz growth curve in which initial growth rates were slow, increasing towards the intermediate stages of growth, and decreasing again once a certain length is reached. Growth ring thicknesses displayed this growth pattern as well in which thick rings occurred closest to the center of the axis (i.e. slow initial growth), thin rings occurred in the middle of the axis (i.e. faster intermediate growth), and thick rings occurred in the outer region of the axis (reduced growth). In this context, *Anthoptilum* spp. began to reduce its growth with age once it reached 60 cm in length, *P. aculeata* around 20 cm in length, and *F. quadrangularis* around 50-60 cm in length. These cut-off lengths limit the interpretations that can be made on these species' population structure based on video surveys. This Gompertz growth pattern was also identified by Murillo et al., (2018) for *A. grandiflorum*, suggesting that the energy used for colony growth was diverted to reproduction after this cut off length. Murillo et al., (2018) estimated a cut off length between 50-70 cm in *A. grandiflorum*, and 30 cm in *P. aculeata*. Wilson et al., (2002) also suggested that energy might be diverted from tissue growth to skeletal growth during the intermediate stages of life. Because these species decrease in growth after a certain age is reached, it would be very difficult if not impossible to accurately determine their ages based on length alone. In response to this, Neves et al., (2018) compared the predicted number of rings based on colony height to the observed number of rings when using 25% of the data, finding that these values were overpredicted in 57% of the

scenarios, underpredicted in 29%, and matched up in 14% of the scenarios. The findings from this study provides further insight into how sea pens grow and their population structure. Based on the data, it is possible to estimate the age of these sea pen species through the enumeration of major growth rings, and it is possible to estimate the maximum ages of these species based on colony length up until a certain length is reached depending on the species.

3.5 Conclusions

These patterns showed that growth is slow initially for smaller colonies, fast for medium sized colonies, and slow for larger colonies that plateau once they reach a certain length despite increasing age, an expected trend found in previous studies on sea pens. Attempts to determine the ages of these species based on their length will prove difficult after this point in their growth, and therefore should be assessed with caution. Analyses of minor rings did not result in a compelling pattern that explained their purpose and further research should be conducted on their occurrences.

3.6References

- Andrews A.H., Cailliet G.M., Kerr L.A., Coale K.H., Lundstrom C., DeVogelaere A.P.,
2005. Investigations of age and growth for three deep-sea corals from the Davidson
Seamount off central California. *Cold-Water Corals and Ecosystems* pp. 1021-1038.
- Aranha R., Edinger E., Layne G., Piercey G., 2011. Growth rate variation and potential
paleoceanographic proxies in *Primnoa pacifica*: insights from high-resolution trace
element microanalysis. Memorial University of Newfoundland, St. John's NL.
- Aranha, R., Edinger E., Layne G., Piercey G., 2014. Growth rate variation and potential
paleoceanographic proxies in *Primnoa pacifica*: Insights from high-resolution trace
element microanalysis. *Deep Sea Research Part II: Topical Studies in Oceanography*
99: 213-226.
- Baillon, S., J. Hamel & A. Mercier, 2014. Protracted oogenesis and annual reproductive
periodicity in the deep-sea pennatulacean *Halipteris finmarchica* (Anthozoa,
Octocorallia). *Marine Ecology* 36: 1364-1378.
- Barnes D.J., Lough J.M., 1993. On the nature and causes of density banding in massive coral
skeletons. *Journal of Experimental Marine Biology and Ecology*, 167, pp. 91-108.
- Birkeland C. 1974. Interactions between a sea pen and seven of its predators. *Ecological
Monographs* 44:211–232. doi:10.2307/1942312
- Fuller S.D., Murillo Perez F.J., Wareham V., Kenchington E., 2008. Vulnerable marine
ecosystems dominated by deep-water corals and sponges in the NAFO convention
area. NAFO SCR Document No. 22, Serial No. N5524. 24 pp.

- Marschal C., Garrabou J., Harmelin, J., Pichon, M., 2004. A new method for measuring growth and age in the precious red coral *Coallium rubrum* (L.). *Coral Reefs* 23:423-432.
- Murillo F., Durán Muños P., Altuna A., Serrano A., 2011. Distribution of deep-water corals of the Flemish Cap, Flemish Pass, and the Grand Banks of Newfoundland (Northwest Atlantic Ocean): Interaction with fishing activities. *ICES Journal of Marine Science* 68:319-332.
- Kenchington E, Murillo FJ, Lirette C, Sacau M, Koen-Alonso M, Kenny A, et al. (2014) Kernel Density Surface Modelling as a Means to Identify Significant Concentrations of Vulnerable Marine Ecosystem Indicators. *PLoS ONE* 9(10): e109365.
<https://doi.org/10.1371/journal.pone.0109365>
- Marschal C., Garrabou J., Harmelin J., Pichon M., 2004. A new method for measuring growth and age in the precious red coral *Corallium rubrum* (L.). *Coral Reefs* 23:423-432.
- Murillo F.J., Duran Munoz P., Altuna A., Serrano A., 2011. Distribution of deep-water corals of the Flemish Cap, Flemish Pass, and the Grand Banks of Newfoundland (Northwest Atlantic Ocean): interaction with fishing activities. *ICES Journal of Marine Science*, 68(2), 319-332.
- Murillo F.J, MacDonald B.W., Kenchington E., Campana S.E., Sainte-Marie B. & Sacau M., 2018. Morphometry and growth of sea pen species from dense habitats in the Gulf of St. Lawrence, eastern Canada. *Marine Biology Research*, 14:4, 366-382.
- Neves B., Edinger E., Wareham V., Layne G., 2018a. Size metrics, longevity, and growth rates in *Umbellula encrinus* (Cnidaria: Pennatulacea) from the Eastern Canadian Arctic. *Arctic Science* 00: 1-28.

- Neves B., Edinger E., Wareham V., 2018b. Morphology and composition of the internal axis in two morphologically contrasting deep-water sea pens (Cnidaria: Octocorallia). *Journal of Natural History*, 52:11-12, 659-685.
- Neves B., Edinger E., Layne G., Hayes V., 2015. Decadal longevity and slow growth rates in the deep-water sea pen *Halipterus finmarchica* (Sars, 1851) (Octocorallia: Pennatulacea): Implications for vulnerability and recovery from anthropogenic disturbance. *The International Journal of Aquatic Sciences, Hydrobiologia* 759: 147-170.
- Roark E.B., Guilderson T.P., Flood-Page S., Dunbar R.B., Ingram B.L., Fallon S.J., McCulloch M., 2005. Radiocarbon-based ages and growth rates of bamboo corals from the Gulf of Alaska. *Geophysical Research Letters* Vol 32.
- Roark E.B., Guilderson T.P., Dunbar R.B., Lynn Ingram B., 2006. Radiocarbon-based ages and growth rates of Hawaiian deep-sea corals. *Mar Ecol Prog Ser* Vol. 327: 1-14.
- Roark E.B., Guilderson T.P., Dunbar R.B., Fallon S.J., Mucciarone D.A., 2009. Extreme longevity in proteinaceous deep-sea corals. *PNAS* 106: 5204-5208.
- Robinson L., Adkins J., Frank N., Gagnon A., Prouty N., Roark B., Flierdt T., 2014. The geochemistry of deep-sea coral skeleton: A review of vital effects and applications for palaeoceanography. *Deep-Sea Research II* 99: 184-198.
- Rollion-Bard C., Blamart D., Cuif J.-P., Juillet-Leclerc A., 2003. Microanalysis of C and O isotopes of azooxanthellate and zooxanthellate corals by ion microprobe. *Coral Reefs* 22:405-415.
- Sherwood, O., Heikoop, A., Sinclair, J.M., Scott, D.J., Shearer C., and Azetsu-Scott, K., 2005a. Skeletal Mg/Ca in *Primnoa resedaeformis*: relationship to temperature.

Friewald A, Murray JM (eds) *Cold-water corals and ecosystems*. Springer, Berlin, p. 1061-1079.

Sherwood O., and Edinger E., 2009. Ages and growth rates of some deep-sea gorgonian and anthipatharian corals of Newfoundland and Labrador. *Can. J Fish. Aquat. Sci.* 66: 142-152.

Urban H.J., 2002. Modeling growth of different developmental stages in bivalves. *Mar Eco Prog Ser* Vol. 238:109-114.

Wilson M., Andrews A., Brown, A., Cordes E., 2002. Axial rod growth and age estimation of the sea pen, *Halipteris willemoesi* Kolliker. *Hydrobiologia* 471:133-142.

4. General conclusions

4.1 Growth band characteristics

Cross sections taken in each species' axis presented defined growth bands of thick and thin light and dark couplets. These couplets differed in shape amongst each species depending on the shape of their axes. Dark growth bands were abundantly filled with large voids while light growth bands had fewer, smaller voids. Voids varied in size and shape within each colony and were loosely dispersed within the light growth bands. Cross sections taken at the transition point between the end of the peduncle and the beginning of the rachis resulted in an uneven distribution of growth bands in most species in which single growth bands combined in one region but separated in another. We believe that differences in growth rates caused this uneven distribution of growth bands in which a shift in the currents and thus in the direction of food cause one side of the axis to be favored in growth band construction at that time (Barnes 1993). If this is the case, a lack of food availability could explain the need for voids within the growth bands in which the specimen can continue to grow despite the lack of energy available. If this is not the case, it is possible that these voids could have been filled with water or organic matter prior to collection as previous studies on sea pens have found a significant portion of organic material in their skeletons (Neves et al., 2018a). Overall, growth bands were most visible in *Anthoptilum* spp., *P. aculeata*, and small colonies of *F. quadrangularis*. *P. carpenteri*, *K. stelliferum*, and tall colonies of *F. quadrangularis* presented growth bands that were almost too faint to distinguish from one another.

4.2 Growth band elemental analysis

Visually-dense light growth bands and visually-less dense dark growth bands did

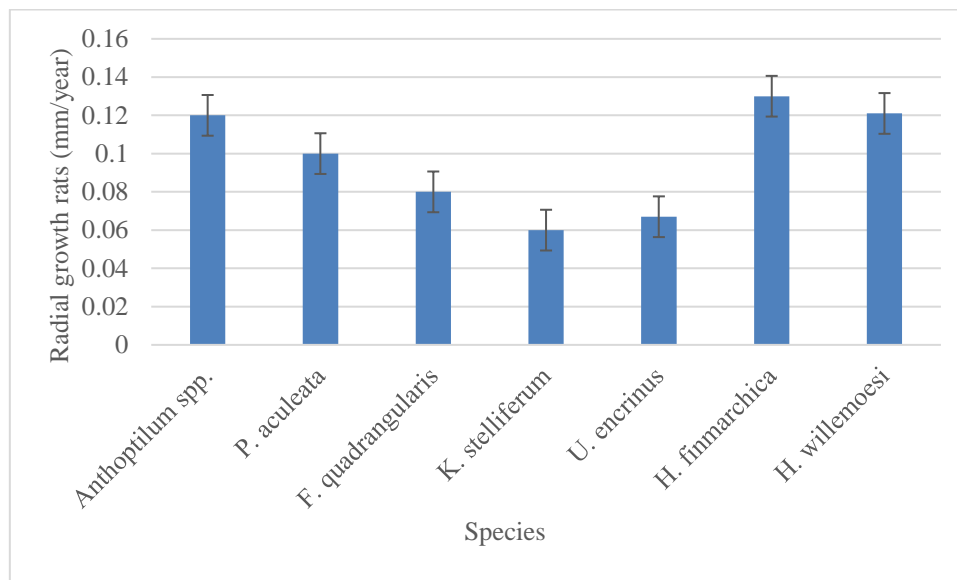
not differ much in their composition when analyzed with SEM-EDX spot analyses. Both types of bands presented relatively low counts of Na, Al, S, P, Si, Cl, Sr, and Ba, and relatively high counts of Mg and Ca. Spot analyses conducted on the dark growth bands presented similar results due to the spot diameter (~5 μm) and the large spatial diameter (~10 μm) that caused the surrounding skeleton to be measured. Despite this, EDX spectrum spot analyses showed a lack of skeletal material found in the dark bands compared to the light bands. Measuring the composition from the center of stem formation to the outermost region of the cross section presented little to no change, suggesting that these species utilize the same methods of growth band and skeletal construction throughout their growth. Unusual growth features were found within the growth bands and the center of each species, each differing in shape and size. We believe some of these features are a result of siphonozoids, however further research is necessary (Baillon et al., 2015).

4.3 Colony metrics, age, growth rates and longevity

Logistic relationships between colony metrics (peduncle length, axis diameter, wet weight) and colony length were strong in *P. aculeata* and *F. quadrangularis*, but weak for *Anthoptilum* spp. These relationships were not assessed for *P. carpenteri* and *K. stelliferum* due to their low sample numbers ($n < 5$). Logistic functions were used in these relationships due to the hypothesis that biological organisms have slow initial growth, grow faster during their intermediate stages of growth, and slow down again until a certain height is reached in which the organism no longer needs to grow with age to survive and reproduce.

Relationships between number of growth rings (major rings vs all rings) and colony length for all six species were shown through logistic and Gompertz growth

curves. It was well supported through these growth curves that major rings (most prominent, thick growth bands) were shown to best represent annual periodicity in all six species of sea pen, while counting all rings (all visible growth bands) did not. Previous studies on sea pen growth have utilized these growth curves to better interpret the pattern of growth experienced by these species when it comes to determining which growth bands are annual (Murillo et al., 2018). Minor rings have been identified in previous studies (Neves et al., 2018a; Murillo et al., 2018; Neves et al., 2015; Wilson et al., 2002), however more research is needed to understand why they occur.



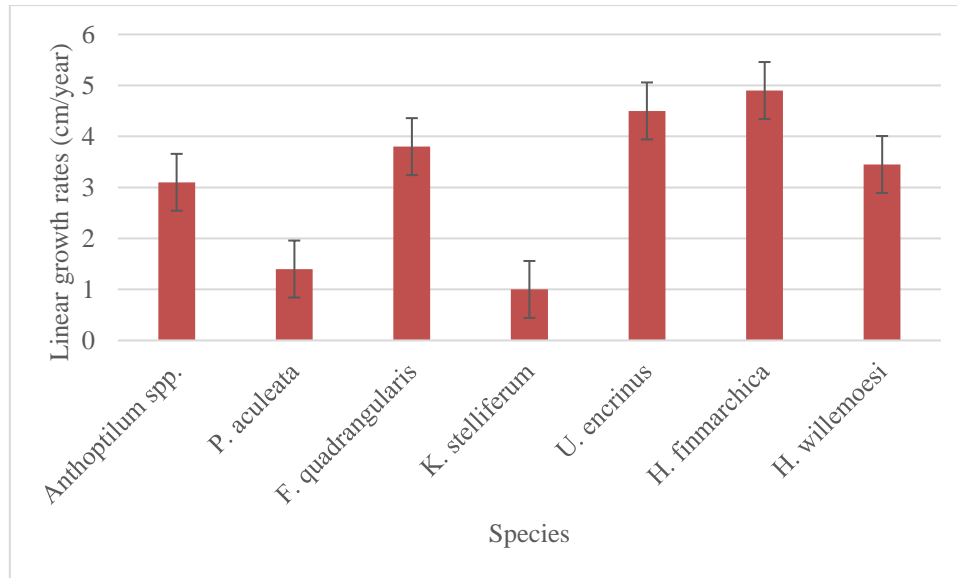


Figure 4-1. Bar graphs showing radial growth rates (A) and linear growth rates (B) for *Anthoptilum* spp., *P. aculeata*, *F. quadrangularis*, and *K. stelliferum* from this study, and *U. encrinus*, *H. finmarchica*, and *H. willemoesi* from previous studies.

4.4 Future work

From this thesis, sea pens have proven to have a complex biomineralization process in which their growth band periodicity and mechanisms of construction remain a mystery. Advancements in deep-sea ROV equipment and analytical technology continue to provide us with more knowledge on the vulnerability of these essential deep-water species, enabling proper protection to be established. While this thesis does not provide all the answers to the basic questions regarding the growth and geochemistry of sea pens, it is building crucial evidence that can be implemented in future studies. In order to further augment our understanding of sea pen and general deep-sea coral skeletal growth, answers to the following questions need to be answered:

I) **What do minor bands represent?**

Thus far, research on what minor bands represent with regards to deep-sea coral growth

has been minimal. Further research on the relationship between environmental factors and growth bands is necessary to determine why these bands are constructed and what purpose they serve.

II) Do environmental factors influence growth band construction?

Studies on what mechanisms deep-sea corals like sea pens use to construct their growth bands are necessary to assess their vulnerability. Previous studies have interpreted growth band construction to be related to food flux and environmental factors, however more environmental data is required to confirm these relationships.

III) Does morphology influence growth band formation?

Studies on deep-sea coral morphology and how it relates to skeletal structure is necessary to understand how these species grow. Previous studies have correlated skeletal formation to the coral's ability to collect food particularly when encountering hydrodynamic forces (Mortensen & Buhl-Mortensen, 2005). If a coral's morphology allows it to collect more food, more energy can be allotted to growth band formation.

4.5 References

- Buhl-Mortensen, P., Buhl-Mortensen L., Gorgon Jr D.C., 2005. Distribution of deep-water corals in Atlantic Canada. *International Coral Reef Symposium*, 1832-1848.
- Baillon S., English M., Hamel J.F., Mercier A., 2015. Comparative biometry and isotopy of three dominant pennatulacean corals in the Northwest Atlantic. *Acta Zoologica (Stockholm)* 00: 000-000.
- Barnes D.J, Lough J.M., 1993. On the nature and causes of density banding in massive coral skeletons. *Journal of Experimental Marine Biology and Ecology*, 167, pp. 91-108.
- Marschal C., Garrabou J., Harmelin, J., Pichon, M., 2004. A new method for measuring growth and age in the precious red coral *Coallium rubrum* (L.). *Coral Reefs* 23:423-432.
- Murillo F., Durán Muños P., Altuna A., Serrano A., 2011. Distribution of deep-water corals of the Flemish Cap, Flemish Pass, and the Grand Banks of Newfoundland (Northwest Atlantic Ocean): Interaction with fishing activities. *ICES Journal of Marine Science* 68:319-332.
- Murillo F.J, MacDonald B.W., Kenchington E., Campana S.E., Sainte-Marie B. & Sacau M., 2018. Morphometry and growth of sea pen species from dense habitats in the Gulf of St. Lawrence, eastern Canada. *Marine Biology Research*, 14:4, 366-382.
- Neves B., Edinger E., Layne G., Hayes V., 2015. Decadal longevity and slow growth rates in the deep-water sea pen *Halipteris finmarchica* (Sars, 1851) (Octocorallia: Pennatulacea): Implications for vulnerability and recovery from anthropogenic disturbance. *The International Journal of Aquatic Sciences, Hydrobiologia* 759: 147-170.

- Neves B., Edinger E., Wareham V., Layne G., 2018a. Size metrics, longevity, and growth rates in *Umbellula encrinus* (Cnidaria: Pennatulacea) from the Eastern Canadian Arctic. *Arctic Science* 00: 1-28.
- Neves B., Edinger E., Wareham V., 2018b. Morphology and composition of the internal axis in two morphologically contrasting deep-water sea pens (Cnidaria: Octocorallia). *J Nat Hist*, 52:11-12, 659-685.
- Risk M.J., Heikoop J.M., Snow M.G., Beukens R., 2002. Lifespans and growth patterns of two deep-sea corals: *Primnoa resedaeformis* and *Desmophyllum cristagalli*. *Hydrobiologia* 471: 125-131.
- Robinson L., Adkins J., Frank N., Gagnon A., Prouty N., Roark B., Flierdt T., 2014. The geochemistry of deep-sea coral skeleton: A review of vital effects and applications for palaeoceanography. *Deep-Sea Research II* 99: 184-198.
- Wilson M., Andrews A., Brown, A., Cordes E., 2002. Axial rod growth and age estimation of the sea pen, *Halipteris willemoesi* Kolliker. *Hydrobiologia* 471:133-14

